Microfluidic synthesis of drug-loaded block copolymer nanoparticles and its effect on drug delivery

by

Yimeng Cao
B.Sc., Nankai University, 2014

A Thesis Submitted in Partial Fulfillment
of the Requirements for the Degree of

MASTER OF SCIENCE

in the Department of Chemistry

University of Victoria

Supervisory Committee

Microfluidic synthesis of drug-loaded block copolymer nanoparticles and its effect on drug delivery

by

Yimeng Cao
B.Sc., Nankai University, 2014

Supervisory Committee

Matthew G. Moffitt, (Department of Chemistry)
Supervisor

Fraser Hof, (Department of Chemistry)
Departmental Member

Abstract

Supervisory Committee
Matthew G. Moffitt, (Department of Chemistry)
Supervisor
Fraser Hof, (Department of Chemistry)
Departmental Member

In this thesis, I used a two-phase gas-liquid segmented microfluidic platform to synthesize drug-loaded block copolymer nanoparticles. In Chapter 2 and 3, the anti-cancer drug 7-ethyl-10-hydroxycamptothecin (SN-38) was physically encapsulated in poly(6-methyl-caprolactone-*co*-ε-caprolactone)-*block*-poly(ethylene oxide) (P(MCL-*co*-CL)-*b*-PEO) nanoparticles with various drug-to-polymer loading ratios, under different flow conditions. The effects of chemical and flow conditions on the size, morphology, drug loading efficiency, *in vitro* release and cytotoxicity of the nanoparticles were determined. For various loading ratios, the intermediate total flow rate (Q = 200 µL/min) produced the smallest nanoparticle sizes and pure spheres. The various nanoparticle preparation conditions showed flow-variable release rates and cytotoxicities against MCF-7 cancer cell line. Specifically, we found that release half times of SN-38 from the nanoparticles were from $\tau_{1/2}$ = 0.8 to 3.3 h as the total flow rate increased from Q = 50 to 200 µL/min. We also found that most conditions of SN-38 formulations generated stronger cytotoxicity than free SN-38. As well, at short and intermediate incubation time (48 and 72 h), the cytotoxic potency of microfluidic nanoparticles prepared at Q = 200 µL/min were slightly higher than nanoparticles prepared using a conventional bulk method, while potencies of microfluidic nanoparticles prepared at higher and lower flow rates were slightly lower than the bulk control. In Chapter 4, in order to pursue even higher shear rate and increased throughput, we switched the microfabrication material to silicon/glass from polydimethylsiloxane (PDMS) used in earlier chapters, maintaining the gas-liquid microfluidic reactor design. A comparison between the two microfluidic reactor materials at constant liquid flow rate showed that channel material affected both flow behaviour and the resulting nanoparticle morphologies. A new, single-phase microfluidic strategy was also proposed in order to generate high shear, in which variable high and low shear would arise from periodic changes in channel dimensions. However, issues regarding clogging of the more narrow microchannels require future work of improvements in either reactor design or the microfabrication process.

Table of Contents

List of Tables

List of Figures

Acknowledgments

First, I would like to give my sincere gratitude to my supervisor, Dr. Matthew Moffitt, for the tireless assistance, encouragement, and constant proposal of challenging new ideas. I am also grateful to him for providing me opportunities to interact with other excellent researchers in different fields.

I also appreciate all my brilliant co-workers, Abby, Aman, Alex, who trained me on different kinds of techniques and generously shared their ideas and experience on microfluidics or drug delivery; Amy, who is not only a good scientist but also a sweet friend of me; Brain, Fraser, and Sun for all the fun we had during the past two years.

I also express my appreciation to Dr. David Sinton in University of Toronto for providing me the opportunity to work in his lab; and all excellent engineers in Sinton group for helping me solve all the problem, especially Jason, who offered so many amazing ideas on high-shear chips.

In addition, I would like to thank Dr. Jeremy Wulff for training me on the skills of cell culture and cytotoxicity assay; Andrew MacDonald for fixing the instruments; Hof group and Van Veggel group for sharing the instruments and helping me solve problems on them.

Last but not the least, I would like to thank my family and friends who gave me numerous encouragement when I met challenges in research or in life. Without your support and company, I have no chance to make it.

Chapter 1. General Introduction

1.1 Background and Goal

Controlled drug delivery has been developed since 1952 with the invention of the first sustained release formulation, and gained more and more attention in recent years due to its significance on pharmacotherapy and human health. Controlled drug delivery is a technology that can control the release rate of pharmaceutical agents, the site and duration of their action and subsequently the side-effect profile, by loading them into vehicles or other nanocarriers, providing a desired concentration level of the drug.[2] One of the promising approaches to achieve this is to encapsulate the drug into nanoparticle-based carriers, including polymer micelles, lipids, chitosan, and dendrimers, since nanoparticles have enormous surface area that can increase the dissolution rate of poorly soluble drugs. [3]Among all these materials, colloidal systems based on polymers have superior advantages over the others, such as the flexibility and diversity in terms of composition and chemical properties.[4] Block copolymer nanoparticles, as a member of the family of polymer-based nanoparticles, enjoys an increasing interest. After the initial idea of Ringsdorf's group to use block copolymers in drug delivery,[5] both Kabanov's group[6] and Kataoka's group[7] have expanded the scope of such applications. In recent years, it becomes a tremendous field where a wide range of polymers are used to deal with different kinds of drug using innovative ideas.[8,9,10,11] Individual block copolymers with hydrophobic and hydrophilic blocks can form amphiphilic micelles, in which hydrophobic cores provide a microenvironment for the encapsulation of hydrophobic drugs, while the hydrophilic shell stabilizes the interface between the core and the aqueous medium. Researchers have been devoted to improving characteristic of this system, including size, size distribution, morphology, loading efficiency, release kinetics, stability and cell toxicity by optimizing polymer composition,[12,9] polymer concentration,[13,14] micelle preparation method,[15] water content,[16] choice of organic solvent,[17,18] etc.

Microfluidics is an important and developing manufacturing method of drug delivery vehicles, which is a top-down approach to control the self-assembly process parameter, in order to simply and efficiently tune physical and chemical properties of materials. Because in microfluidic device, reactions are carried out within microchannels, which lead to rapid heat and mass transfer that can produce nanoparticles in a robust manner with improved yield, controllability, reproducibility and size distribution, compared to conventional bulk methods.[19,20]

In this thesis, I applied an advanced microfluidic platform for the controlled synthesis of block copolymer nanoparticles and pursued to encapsulate an anti-cancer drug 7-Ethyl-10-hydroxycamptothecin (SN-38) into poly(methyl-ε-caprolactone-*co*-caprolactone)-*block*-poly(ethylene oxide) (P(MCL-*co*-CL)-*b*-PEO) nanoparticles and release it into a phosphate buffered saline (PBS) medium. Half maximum inhibitory concentration (IC_{50}) of SN-38 loaded micelles on MCF-7 breast cells was also studied. SN-38 is a prominent and efficacious anticancer drug. As an active metabolite of irinotecan (CPT-11), SN-38 is 100-1000 times more potent than irinotecan and effective against many malignancies.[21] The hydroxyl group at C_{10} and ethyl group at C_7 stabilize SN-38 in physiological environments, making it more potent than other CPT analogues.[22] However, due to various chemical and pharmacological limitations, it is only commercially available by slow intravenously injection into a vein, in which case most of administrated CPT-11 may not be able to transform to the active metabolite SN-38. Therefore, development of SN-38 delivery strategy becomes an essential challenge. Currently, there are two formulations in

Phase 2 clinical stage. One uses NK-012 micelles, where SN-38 is loaded in PEO-poly(glutamic acid) micelles through chemical conjugation,[23] the other is EZN-2208, which is a water-soluble, polyethylene glycol drug conjugate of SN-38.[24] Both of them are categorized as prodrug approaches, since each of them has a moiety covalently attached to the drug molecule. However, this approach is obviously a little tedious since the preparation of the conjugates need multiple chemical reactions, giving rise to the concern of stability and product yield.

Our study focuses on physical encapsulation of SN-38 into amphiphilic block copolymer without any modification of the drug. The microfluidic technology used is a gas-liquid segmented microreactor in which the high-shear provides control over the size and morphology of drug-loaded nanoparticles and allows optimization of drug loading efficiency, *in vitro* release kinetics, and cytotoxicity.

In order to further explore the role of high shear in polymer nanoparticles' characteristics as well as increase the rate of nanoparticle output, we would like to greatly enhance flow rates on chip. Silicon/glass chips which can resist to the high pressure induced by high flow rate were made for polymer nanoparticle preparation. Comparison between microfluidic reactors with two different materials and identical channels were also conducted to study the influence of surface properties, inner pressure and gas-liquid pattern on the formation of nanoparticles. This may give some insight of synthesis mechanism and inspiration for some new design. Furthermore, we explored new design of single-phase microreactor in which high-shear can be achieved without introducing gas, by adding extreme narrow channels between relatively wide channels periodically. This can avoid the difficulty of viewing bubbles and precise control of the gas pressure.

The future goals of follow-up studies might focus on two issues. 1) pharmacokinetic study of SN-38 loaded polymer nanoparticles 2) development of targeted delivery of SN-38 towards target site and into the tumor core; this would greatly improve the therapeutic effect and minimize the toxicity of the drug.[25] It may be helpful to giving some thoughts on the tumor's special environmental aspects such as pH and hypoxia.

1.2. Introduction to Specific Topics

1.2.1. Polymers

Polymers are macromolecules consisting of a large number of regularly repeated chemical units (or monomers) linked by covalent bonds. Polymers can be classified in many ways. Based on the chain architecture, polymers are categorized into linear, branched and network polymers, as shown in Figure 1-1.[26] Based on the arrangement of monomers, there are also different types. When a polymer is comprised of two or more types of monomers, it is called copolymer. According to properties, there are thermoplastics, elastomers or thermosets, among which, thermoplastics form the majority in use.[27] They are either linear or branched and they soften above the melting temperature, $T_{m.}$ In the molten state, they consist of a tangled mass of dynamic molecules. Upon cooling, they may form a glass below glass transition temperature, $T_{g,}$ or they may crystallize below the melting temperatures. The crystallization is only partial with the remaining polymer in an amorphous liquid-like state. Polymers like this are said to be semicrystalline.[28]

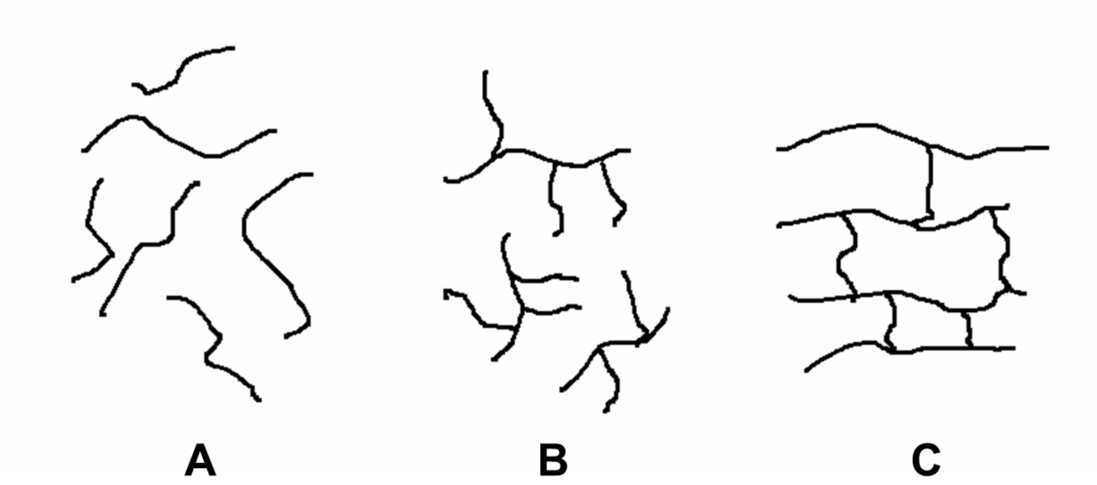

Figure 1- 1. Schematic representations of linear (A), branched (B) and network polymers (C).[26]

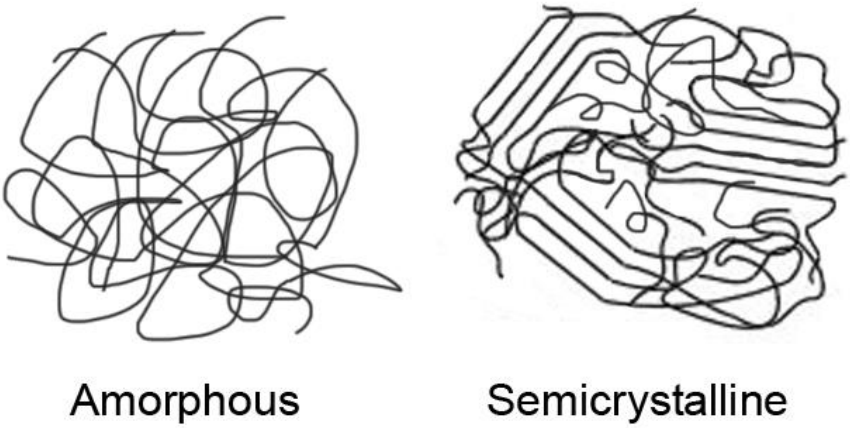

Figure 1- 2. Schematic representations of an amorphous and a semicrystalline polymer.

Crystallization is a first-order phase transition characteriazed by alignment and close-packing of molecular chains in an extended linear state. The glass transition is a second-order transition which leads to a change in chain dynamics but not a change in structure. Below T_g, chains only have vibrational motions, leading to hard and glassy polymer. At T_g, the polymer starts to soften and becomes rubbery, the modulus significantly drops. As the temperature further increases, the polymer will experience rubbery plateau, act like rubbery flow and viscous flow (Figure 1-3).

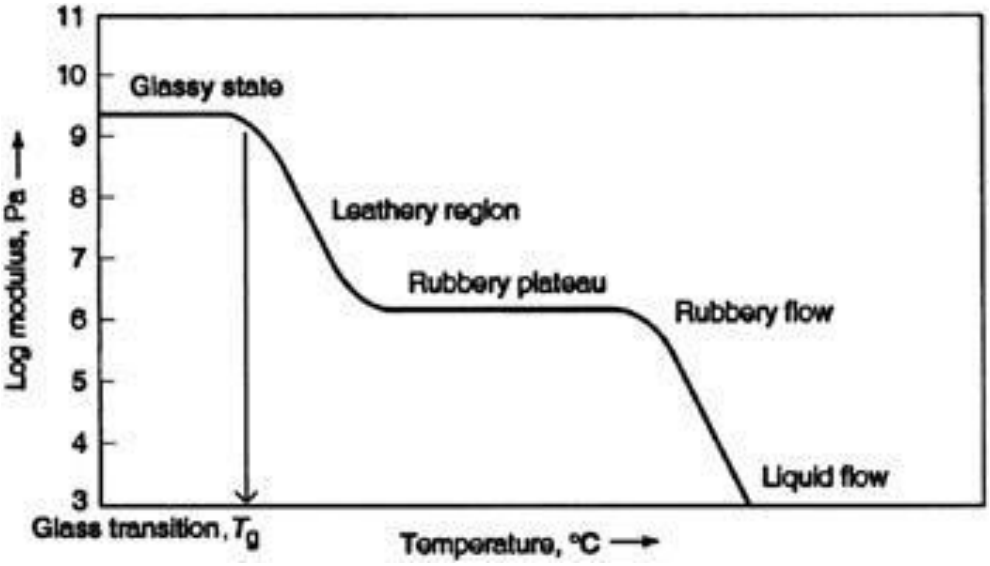

Figure 1- 3. Young's modulus of a typical polymer material versus temperature.[29]

1.2.2. Block Copolymers

Block copolymers are macromolecules containing two or more blocks of dissimilar polymers connected via covalent bonds. There's a wide range of architectures like linear diblock (AB), triblock (ABA), multiblock $(AB)_n$ and branched copolymers. When a third monomer is added, linear triblocks can be prepared, and also three-armed stars.[30] The reason why considerable attention has been focusing on block copolymers is their self-assembly can result different nanostructures with a variety of applications.[31] By changing the molecular weight and structure of monomers or selecting polymers for each block, the size, morphology, functionality and properties of self-assembled block copolymer nanostructures can be controlled precisely.[32]

Block copolymer with two thermodynamically incompatible blocks can spontaneously self-assemble upon addition of a selective solvent that is a good solvent for one block and precipitant for the other. The process is very similar to the well-known formation of small molecule surfactant. The critical concentration at which the micelle starts to form is called the critical micelle concentration (CMC), which is much lower in the case of block copolymers than small molecule amphiphiles.[33] If the self-assembly occurs in a solvent mixture containing a polar organic solvent and water, it occurs only when the water content exceeds the critical water content (CWC).

In this thesis, we deal with the situation that block copolymer self-assembles in a mixture of the polar organic solvent *N*, *N*-dimethylformamide (DMF) and water. Eisenberg's group studied the thermodynamics of micellization of polystyrene-block-poly(acrylic acid) (PS-*b*-PAA).[34] Results showed that the process could be either enthalpy-driven or entropy-driven. When the water content is low (< 5 wt% water), the energetically unfavourable polymer/solvent interactions take place of favourable polymer/polymer and solvent/solvent interactions upon micellization, resulting in a decrease of enthalpy. When the water content is high (> 15 wt% water), there are stronger hydrophobic interactions between the polymer chains and water molecules, in which case increased entropy derived from hydrophobic effect (micelle formation and the hydrophobic effect) drives the micellization.

Block copolymer self-assemblies have a wide spectrum of different morphologies. This is governed by three factors to the free energy: the degree of core-forming blocks' stretching, the interfacial tension between the core and the solvent outside, and the interaction among corona-forming chains.[35] Eisenberg's group first reported the control of multiple morphologies of the crew-cut aggregates from PS-*b*-PAA in 1995,[36] by changing the block lengths of the copolymer. These kinds of bottom-up control strategies also include changing polymer concentration, nature of common solvent, water content, presence of additives, etc. Since then, more and more morphologies of different block copolymer micelles have been found. Figure 1-4 shows some morphologies obtained with PS-b-PAA, i.e. spheres, rods, vesicles, large compound vesicles (LCV).[37] Figure 1-5 shows interesting morphologies obtained with PS-*b*-PEO, i.e. LCVs, porous spheres, tube-walled vesicles, "onions", large trapped vesicles.[38]

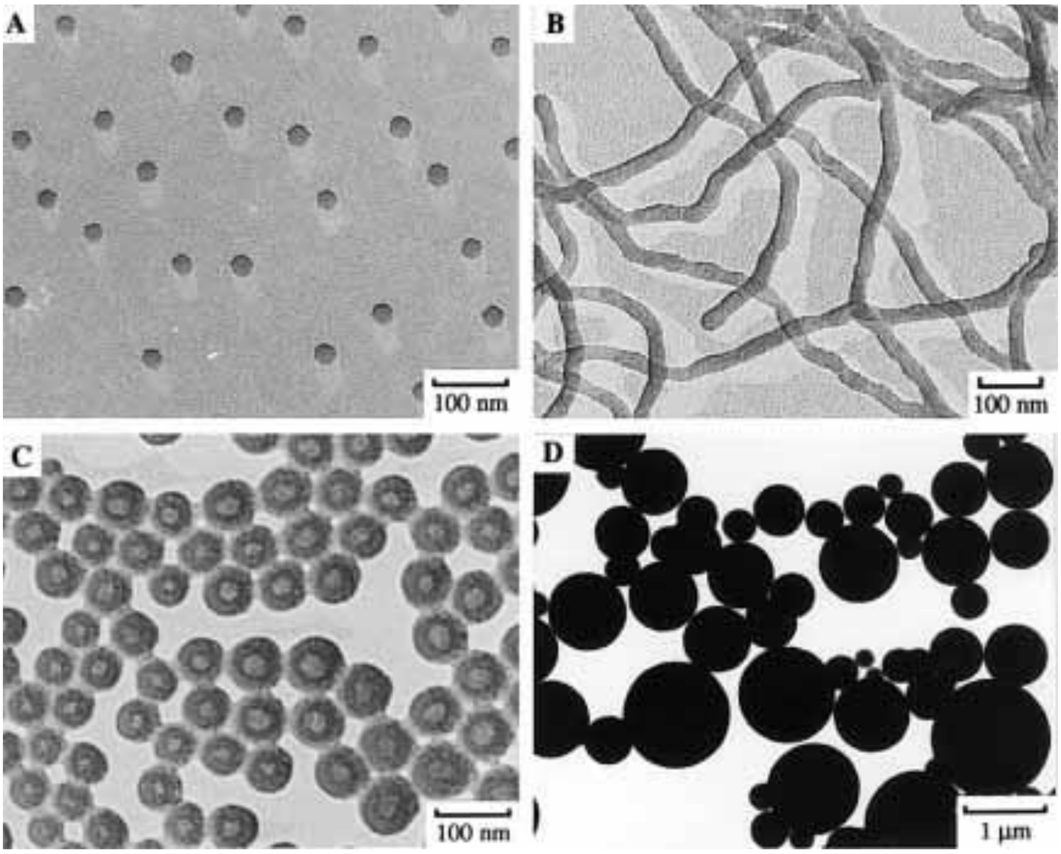

Figure 1- 4. Crew-cut aggregates of PS-*b*-PAA. A. PS(500)-*b*-PAA(58). B. PS(190)-*b*-PAA(20). C. PS(410)-*b*-PAA(20). D. PS(200)-*b*-PAA(4).[37]

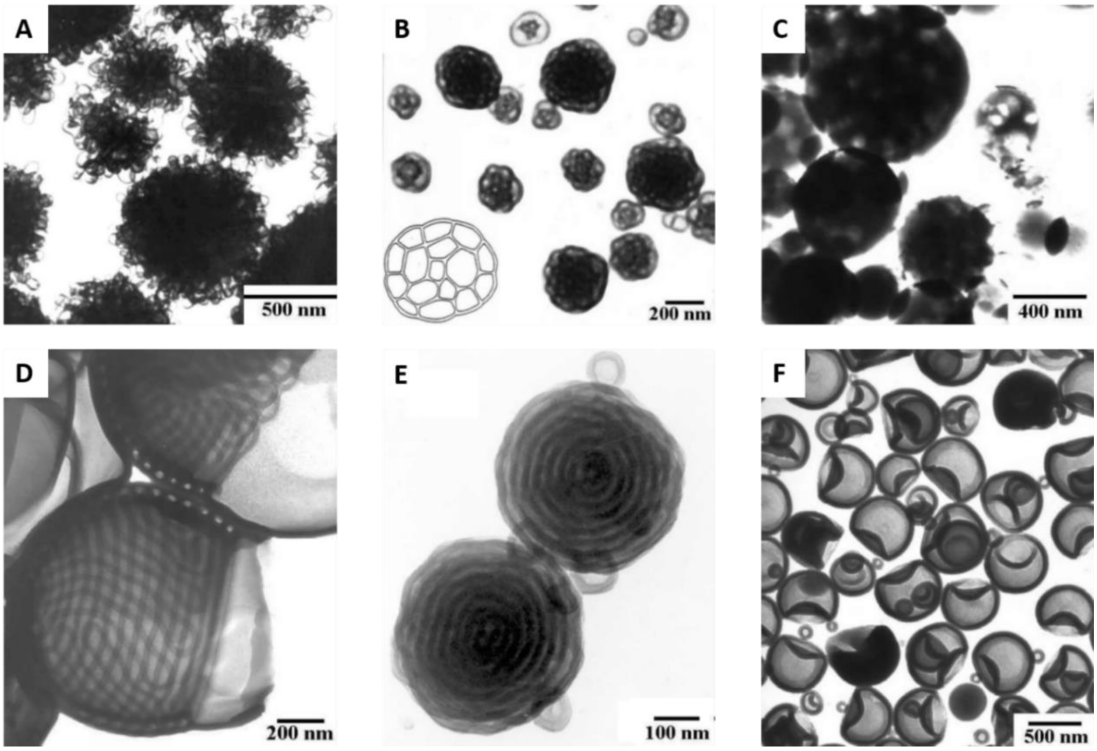

Figure 1- 5. Aggregates of PS-*b*-PEO (A) PS(240)-*b*-PEO(15), (B) PS(410)-*b*-PAA(13), (C) PS(240)-*b*-PEO(45), (D) PS(100)-*b*-PEO(30), (E) PS(410)-*b*-PAA(13), (F) PS(200)-*b*-PAA(20).[38]

1.3. Drug Delivery

1.3.1. Basic Concepts

The development of drug delivery has been pursued vigorously as a new way to release proper dosage through appropriate administration. The aim is to achieve high effectiveness and safety of therapeutic agents as well as compliance of patients.[3]

A wide range of drug delivery systems have been investigated, including liposome,[39] prodrugs,[40] cyclodextrins,[41] and gels,[42] etc. Among these, polymeric nanoparticles are particularly interesting especially biodegradable block copolymer nanoparticles.[4] Block copolymers consist of two blocks which play different roles in forming the drug carrier. The hydrophilic block can increase the solubility in aqueous environment whereas the hydrophobic block protects the drug in the core. Second, they enjoy relatively simple preparations, especially the method of drug loading via physical interaction without any chemical modification of the drug and chemical conjugation.

Several formulations based on polymer nanoparticles have already reached clinical trials for some drugs. One of them is a commonly used medication in treatment of a wide range of cancers, doxorubicin (DOX).[43] The first polymeric micelles incorporating DOX to proceed into clinical trials is named NK911.[44] It initially developed in the late 1980s[45] by using polyethyleneglycol and poly(aspartic acid) conjugated with DOX. DOX was released from the inner core by diffusion and showed stronger toxicity than free DOX against cell lines tested. Another attractive drug is paclitaxel (PAX) for its high clinical efficacy. PAX-loaded polymeric micelles (NK105; Nippon Kayaku, Co.) were constructed using PEG as the hydrophilic block and modified polyaspartate as the hydrophobic block. Carboxylic groups of polyaspartate were engineered for increasing the affinity of the hydrophobic backbone of the copolymer with PAX.[46] This formulation was proved to be able to extend *in vivo* antitumor activity and ruduce neurotoxicity of PAX. And a multi-national Phase 3 study was thus encouraged for comparing NK105 with PAX in patients with metastatic solid tumors as well as recurrent breast cancer.

Cisplatin represents the most significant member of classical platinum complex for its essential role in chemotherapy regimens for various cancers. Kataoka's group[47] developed a polymeric micelles incorporating cisplatin via the polymer metal complex formation between cisplatin and poly(ethylene glycol)-poly(aspartic acid) block copolymers (PEG-P(Asp)). These micelles exhibit enhanced stability, prolonged blood circulation, and high tumor selectivity. All of these desired preclinical results suggested the translation of cisplatin-loaded micelles into clinical as NC-6004 (Nanocarrier, Co.).[48]

1.3.2 Drug Delivery of SN-38

In this study, the drug we dealt with is an anti-cancer drug 7-ethyl-10-hydroxy camptothecin (SN-38). The reason why we interested in this drug includes the facts that SN-38 has very high *in vitro* potency against different malignancies, such as colorectal, lung and ovarian cancer.[21] However, there are two main limits for the clinical application of SN-38. One is the poor solubility in water (~0.1mg/ml) and any pharmaceutically acceptable solvents, which limits the direct delivery as a free drug. The other is the instability in physiological environments. SN-38 is only stable at $pH<4.5$ and completely convert to its carboxylate form, which has no therapeutic effect, at $pH>9.0$.[49] To solve these inherent problems of SN-38 and achieve effective and safe treatment, different drug delivery systems have been investigated.

Within the range of various drug delivery vehicles for SN-38, block copolymers occupy a vital position. These systems have been proved to increase the water solubility, prevent the pH-induced hydrolysis, prolong drug circulation time and augment accumulation in tumor by the enhanced permeability and retention (EPR) effect.[6,50]

Peng and co-workers[51] reported a functionalized micellar delivery system for SN-38. The chlorin-core star-shaped block copolymer was synthesized from chlorin and mPEG-*b*-PCL-COOH. The center of the star that acts like a photosensitizer is for photodynamic therapy (PDT) and the hydrophobic inner core of the micelle encapsulate the drug in it. These SN-38 loaded micelles were prepared using lyophilization-hydration method. They showed high drug loading (81.3 ± 3.6 %) with an optimal size (103.2nm) to achieve promising synergistic therapy. However, the improved cytotoxicity was mainly attributed to the combination with PDT.

After the development of SN-38-incorporating polymeric micelle named NK012 that synthesized from PEG-*b*-PGA,[52] Gu and co-workers[53] combined two different copolymers, Pluronic-F-108 and PCL-*b*-PEG, as a nanocarrier to encapsulate SN-38. F-108 is a commercial name of poly(ethylene glycol)-*block*-poly(propylene glycol)-*block*-poly(ethylene glycol), which is used to increase the solubility of micelle in water. The PCL-*b*-PEG has equal molecular weight of two blocks, which assists in trapping the hydrophobic drug. These micelles prepared by a modified film hydration method successfully improve SN-38 loading, with a loading efficiency of 83.83 ± 1.32 %, as well as *in vitro* cytotoxicity and cellular uptake.

An amphiphilic triblock copolymer poly(acrylic acid)-poly(ε-caprolactone)-poly(acrylic acid) (PAA_{13}-PCL_{35}-PAA_{13}) was also used to prepare micelles as novel carrier for SN-38 in Goracinova’s group.[54] The PAA segments are polyelectrolytes and are pH-responsive and PCL provides the hydrophobic core. The “solvent displacement” nanoprecipitation method used in this study is much more efficient and convenient than traditional methods mentioned above in micelle formation. In that approach, the organic phase containing the polymer and drug was added dropwise to the non-solvent aqueous phase. Upon agitation, a colloidal suspension was formed and then nanoparticles started to form.[55] As a result, the micelles with diameter of 120-140 nm, negative zeta potential and content drug loading exhibited increased growth inhibition effect on SW-480 cell lines compared to free SN-38.

1.4 Microfluidics

Microfluidics is a technology that precisely manipulates fluids at the scale smaller than 1 mm. It can be applied in various areas including chemical synthesis, biological analysis, optics and information technology.[56]

1.4.1 Useful Microfluidic Concepts

1.4.1.1 Laminar Flow vs. Turbulent Flow

The Reynolds number (Re) is defined as:

$$\mathrm{Re} = \frac{\rho v d}{\mu}$$

ρ is density of the fluid, v is velocity of the fluid, d is the diameter of the channel, and μ is dynamic viscosity of the fluid. This demonstrate the ratio of inertial to viscous forces in a fluid. When the Re is high (~2000), fluids can be characterized as turbulent flow whose motion fluctuates randomly. In microfluidic systems, Re can be as low as 100, even less than 1, in which regime, flow is completely laminar, thus it is very orderly with all particles moving in straight lines. Laminar flow can make molecules be transported in a relatively ordered and predictable manner through microchannels.[56]

1.4.1.2 Pressure-driven Laminar Flow (Poiseuille Flow)

If the velocity profile that implicates the distribution of molecules within the channel is parabolic, the flow can be treated as pressure driven flow. In which condition, the fluid velocity is maximum in the center and zero along the wall (Figure 1-6). This is usually achieved by positive displacement pumps. The advantages of pressure-driven flow are relatively low expense and high reproducibility when fluids are pumped into microfluidics device, as well as the possibility to be amenable to miniaturization.[1]

1.4.2 Microfluidics for Nanoparticle Synthesis

The reason why microfluidics becomes an attractive field for both engineers and scientists in recent years is various advantages of microfluidics over conventional batch technology for the production of nanoparticles. For example, microfluidic can provide tremendous potential for the controllable and tunable synthesis nanoparticles. It can also separate the nucleation and growth process by specific designs of microchannels, to achieve some promising sizes and morphologies of nanoparticles.

In the past decade, different kinds of inorganic nanomaterials have been produced using microfluidic reactors, including metallic and silica nanoparticles, quantum dots, etc., with tuneable size, size distribution, and crystal structure.

This undoubtedly gives plenty of possibilities on production of organic nanoparticles and colloidal systems, which can be used as innovative pharmaceutical formulations to overcome the long-lasting problems, such as low aqueous solubility and poor cell uptake, in biomedical field.

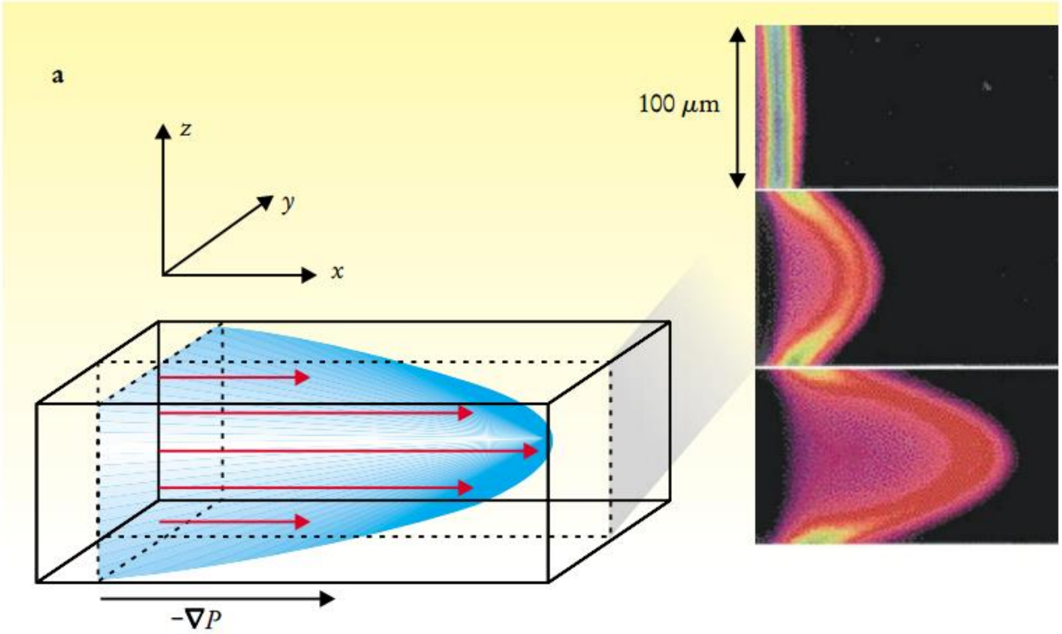

Figure 1 -6. Velocity profile in a Poiseuille flow. A pressure gradient - ∇ P, along a channel generates a parabolic or Poiseuille flow profile in the channel On the right is an experimental measurement of the distortion of a volume of fluid in a Poiseuille flow. The frames show the state of the volume of fluid 0, 66 and 165 ms after the creation of a fluorescent molecule.[1]

1.4.3 Microfluidic Manufacturing of Polymer Particles

Among a large number of interesting organic nanoparticles, block copolymer nanoparticles are promising to have diverse chemical and structural properties by a wide range of controlled polymerization techniques, compared to its popular counterpart, lipid-based system.[32] All these types of polymers can self-assemble into amphiphilic aggregates under certain conditions with multiple morphologies, including spheres, vesicles and cylinders.[37]

Synthesis of biodegradable polymeric nanoparticles have been developed using bulk mixing and nanoprecipitation methods. However, the lack of mixing process control may compromise the properties of resulting nanoparticles. At this point, microfluidic becomes a desired approach to fast mixing, precise control over the process and screening of various production parameters.

Karnick et al.[57] employed hydrodynamic flow focusing microfluidic to synthesis PLGA-PEG nanoparticles with defined size, lower polydispersity and higher drug loading with slower release. Since hydrodynamic flow-focusing can provide the environment in which the central stream is narrowed down by the two adjacent streams and then able to mix rapidly through diffusion. However, it can’t be ignored that hydrodynamic flow-focusing process is always restricted to low Re, namely very low flow rate (<10 μL/min), which limits the possibility of large-scale production. Therefore, Anton and his coworkers[58] applied a new setup of micromixer which is based on impact-jet mixing, to reach a much higher flow rate (1 ml/min). They successfully produce PMMA nanospheres, with a particle size of ~100nm, and a narrow size distribution.

Kucuk et al. synthesized PMSQ polymer nanospheres using a V-shaped microfluidic junction (VMJ) device.[59] Formation of droplets occurs after PMSQ and PFH solutions mixed in the junction. Then the steady continuous stream of droplets goes down through the outlet capillary and can be collected at the exit. These solid polymer nanospheres show promising sizes and structures for drug loading applications.

Another approach to enhance mixing and reduce dispersion in the flow direction is to apply gas-liquid segmented flow reactors. Compared to the other two-phase reactor, liquid-liquid reactors, they can simply separate process of gas from the liquid.[60] Thus, dispersion is limited within the liquid plugs and reactions take place only in these regions, which narrows residence time distribution, in turn, decreases particle size polydispersity. They also have “high-shear” regions in the corner of the liquid plugs, produced by chaotic advection. And this high shear can be utilized to control size and morphology of on-chip production.[61] Our group has pioneered gas-liquid synthesis of polymeric nanoparticles. Wang and co-workers[62] demonstrate PS-*b*-PAA can self-assemble in a gas-liquid segmented microreactor and the unique on-chip shear environment can provide flow-induced variation of sizes and morphologies of nanoparticles.

1.4.4. Different Materials for Microfabrication

Materials for microfluidic chip fabrication vary a lot and matter to applications, for the reason that the surface properties can lead to different characteristics and each material acquires specific microfabrication method.[63] The earliest material used for microfluidic device is silicon or glass. Both two materials possess advantages like solvent compatibility and thermostability. They are normally processed with standard photolithography, which is expensive, time-consuming and requires refined fabrication conditions. Thus, elastomers were developed as an optimal material for microfabrication. The most popular representative is polydimethylsiloxane (PDMS), which is easier and cheaper to prepare than silicon and glass templates.[64] Soft lithography is generally used for PDMS chips fabrication currently. And its high elasticity also opens possibilities of different designs. Despite all the merits, PDMS still has a few drawbacks like incompatibility with some kinds of organic solvents and absorption of hydrophobic molecules onto the inner wall. Other materials like thermoplastic, hydrogels and paper have been widely used in recent years.[63]

1.5. Outline of Thesis

This thesis consists of 5 chapters, the first of which is an introduction. The second chapter is regarding production and characterization of anti-cancer drug SN-

38 loaded P(MCL-*co*-CL)-*b*-PEO nanoparticles by microfluidics. Different drug to polymer ratio, water content and on-chip flow rate were investigated. Size, morphology, loading efficiency and release profile of drug-loaded nanoparticles were characterized. The third chapter deals with *in vitro* study of cytotoxicity of the nanoparticles produced on chip. More specifically, aspects related to flow-induced anti-cancer activity on MCF-7 cancer cell lines were discussed. In Chapter 4, we proposed some new strategies to optimize the chip design as well as to achieve high-shear effect. These include the use of different materials and switching from two-phase to single-phase reactor. PCL-*b*-PEO with different block length were used to test the applicability and effectiveness of new chips. Finally, Chapter 5 covers conclusion generated from the work and outlook for the future work. All in all, this thesis focuses on the effect of microfluidics on nanoparticles size, morphology, drug loading, release and cytotoxicity. The main goal of the thesis is to get insight into microfluidic shear-directed formation of block copolymer nanoparticles for SN-38 drug delivery.

1.5 References

1. Stroock, G. M. W. a. A. D., Flexible methods for microfluidics. *Physics Today* **2001,** *54* (6).

2. Hoffman, A. S., The origins and evolution of “controlled” drug delivery systems. *Journal of Controlled Release* **2008,** *132* (3), 153-163.

3. Park, K., Controlled drug delivery systems: Past forward and future back. *Journal of Controlled Release* **2014,** *190*, 3-8.

4. Kumari, A.; Yadav, S. K.; Yadav, S. C., Biodegradable polymeric nanoparticles based drug delivery systems. *Colloids and Surfaces B: Biointerfaces* **2010,** *75* (1), 1-18.

5. Bader, H.; Ringsdorf, H.; Schmidt, B., Watersoluble polymers in medicine. *Die Angewandte Makromolekulare Chemie* **1984,** *123* (1), 457-485.

6. Kabanov, A. V.; Batrakova, E. V.; Miller, D.; Alakhov, V., Amphiphilic block

copolymers in drug delivery. *Abstracts of Papers of the American Chemical Society* **1997,** *214*, 157-COLL.

7. Kwon, G.; Naito, M.; Yokoyama, M.; Okano, T.; Sakurai, Y.; Kataoka, K., Block copolymer micelles for drug delivery: loading and release of doxorubicin. *Journal of Controlled Release* **1997,** *48* (2-3), 195-201.

8. Topp, M. D. C.; Dijkstra, P. J.; Talsma, H.; Feijen, J., Thermosensitive Micelle-Forming Block Copolymers of Poly(ethylene glycol) and Poly(N-isopropylacrylamide). *Macromolecules* **1997,** *30* (26), 8518-8520.

9. Kim, J. H.; Emoto, K.; Iijima, M.; Nagasaki, Y.; Aoyagi, T.; Okano, T.; Sakurai, Y.; Kataoka, K., Core-stabilized polymeric micelle as potential drug carrier: Increased solubilization of taxol. *Polym. Adv. Technol.* **1999,** *10* (11), 647-654.

10. Torchilin, V. P., PEG-based micelles as carriers of contrast agents for different imaging modalities. *Advanced Drug Delivery Reviews* **2002,** *54* (2), 235-252.

11. Bae, Y.; Jang, W. D.; Nishiyama, N.; Fukushima, S.; Kataoka, K., Multifunctional polymeric micelles with folate-mediated cancer cell targeting and pH-triggered drug releasing properties for active intracellular drug delivery. *Mol. Biosyst.* **2005,** *1* (3), 242-250.

12. Tian, M.; Arca, E.; Tuzar, Z.; Webber, S. E.; Munk, P., Light scattering study of solubilization of organic molecules by block copolymer micelles in aqueous media. *Journal of Polymer Science Part B: Polymer Physics* **1995,** *33* (12), 1713-1722.

13. Xing, L.; Mattice, W. L., Strong solubilization of small molecules by triblock-copolymer micelles in selective solvents. *Macromolecules* **1997,** *30* (6), 1711-1717.

14. Gadelle, F.; Koros, W. J.; Schechter, R. S., SOLUBILIZATION OF AROMATIC SOLUTES IN BLOCK-COPOLYMERS. *Macromolecules* **1995,** *28* (14), 4883-4892.

15. Kabanov, A. V.; Nazarova, I. R.; Astafieva, I. V.; Batrakova, E. V.; Alakhov, V. Y.; Yaroslavov, A. A.; Kabanov, V. A., MICELLE FORMATION AND SOLUBILIZATION OF FLUORESCENT-PROBES IN POLY(OXYETHYLENE-B-OXYPROPYLENE-B-OXYETHYLENE) SOLUTIONS. *Macromolecules* **1995,** *28* (7), 2303-2314.

16. Soo, P. L.; Eisenberg, A., Preparation of block copolymer vesicles in solution. *J. Polym. Sci. Pt. B-Polym. Phys.* **2004,** *42* (6), 923-938.

17. La, S. B.; Okano, T.; Kataoka, K., Preparation and Characterization of the Micelle-Forming Polymeric Drug Indomethacin-lncorporated Polyfethylene oxide)-Poly(β-benzyl L-aspartate) Block Copolymer Micelles. *Journal of Pharmaceutical Sciences* **1996,** *85* (1), 85-90.

18. Kim, S. Y.; Shin, I. L. G.; Lee, Y. M.; Cho, C. S.; Sung, Y. K., Methoxy poly(ethylene glycol) and ϵ-caprolactone amphiphilic block copolymeric micelle

containing indomethacin.: II. Micelle formation and drug release behaviours. *Journal of Controlled Release* **1998,** *51* (1), 13-22.

19. Pissuwan, D.; Niidome, T.; Cortie, M. B., The forthcoming applications of gold nanoparticles in drug and gene delivery systems. *Journal of Controlled Release* **2011,** *149* (1), 65-71.

20. Tran, T. H.; Nguyen, C. T.; Kim, D.-P.; Lee, Y.-k.; Huh, K. M., Microfluidic approach for highly efficient synthesis of heparin-based bioconjugates for drug delivery. *Lab on a Chip* **2012,** *12* (3), 589-594.

21. Bala, V.; Rao, S. S.; Boyd, B. J.; Prestidge, C. A., Prodrug and nanomedicine approaches for the delivery of the camptothecin analogue SN38. *Journal of Controlled Release* **2013,** *172* (1), 48-61.

22. Li, Q.-y.; Deng, X.-q.; Zu, Y.-g.; Lv, H.; Su, L.; Yao, L.; Zhang, Y.; Li, L., Cytotoxicity and Topo I targeting activity of substituted 10--nitrogenous heterocyclic aromatic group derivatives of SN-38. *European Journal of Medicinal Chemistry* **2010,** *45* (7), 3200-3206.

23. Matsumura, Y., Preclinical and clinical studies of NK012, an SN-38-incorporating polymeric micelles, which is designed based on EPR effect. *Advanced Drug Delivery Reviews* **2011,** *63* (3), 184-192.

24. Garrett, C. R.; Bekaii-Saab, T. S.; Ryan, T.; Fisher, G. A.; Clive, S.; Kavan, P.; Shacham-Shmueli, E.; Buchbinder, A.; Goldberg, R. M., Randomized Phase 2 Study of Pegylated SN-38 (EZN-2208) or Irinotecan Plus Cetuximab in Patients With Advanced Colorectal Cancer. *Cancer* **2013,** *119* (24), 4223-4230.

25. Singh, R.; Lillard, J. W., Nanoparticle-based targeted drug delivery. *Experimental and Molecular Pathology* **2009,** *86* (3), 215-223.

26. V. R. Gowariker, N. V. V. a. J. S., *Polymer Science. 1 ed*. New Age International Limited: New Delhi: 1986.

27. Bower, D. I., *An Introduction to Polymer Physics*. Cambridge University Press: New York, 2002.

28. Sperling, L. H., *Introduction to Physical Polymer Science. 4 ed.* John Wiley & Sons, Inc: New Jersey, 2006.

29. Harper, C. A., *Handbook of Plastics, Elastomers, and Composites. 4 ed.* McGraw-Hill: New York, 2002.

30. Lodge, T. P., Block copolymers: Past successes and future challenges. *Macromolecular Chemistry and Physics* **2003,** *204* (2), 265-273.

31. Riess, G., Micellization of block copolymers. *Prog. Polym. Sci.* **2003,** *28* (7), 1107-1170.

32. Mai, Y. Y.; Eisenberg, A., Self-assembly of block copolymers. *Chemical Society Reviews* **2012,** *41* (18), 5969-5985.

33. Moffitt, M.; Khougaz, K.; Eisenberg, A., Micellization of ionic block copolymers. *Accounts of Chemical Research* **1996,** *29* (2), 95-102.

34. Shen, H. W.; Zhang, L. F.; Eisenberg, A., Thermodynamics of crew-cut micelle formation of polystyrene-b-poly(acrylic acid) diblock copolymers in DMF/H2O mixtures. *Journal of Physical Chemistry B* **1997,** *101* (24), 4697-4708.

35. Zhang, L. F.; Eisenberg, A., Multiple morphologies and characteristics of "crew-cut" micelle-like aggregates of polystyrene-b-poly(acrylic acid) diblock copolymers in aqueous solutions. *Journal of the American Chemical Society* **1996,** *118* (13), 3168-3181.

36. Zhang, L.; Eisenberg, A., Morphologies of "Crew-Cut" Aggregates of Polystyrene-poly(acrylic acid) Block Copolymers. *Science* **1995,** *268* (5218), 1728-1731.

37. Zhang, L. F.; Eisenberg, A., Formation of crew-cut aggregates of various morphologies from amphiphilic block copolymers in solution. *Polym. Adv. Technol.* **1998,** *9* (10-11), 677-699.

38. Cameron, N. S.; Corbierre, M. K.; Eisenberg, A., 1998 E.W.R. Steacie Award Lecture Asymmetric amphiphilic block copolymers in solution: a morphological wonderland. *Canadian Journal of Chemistry-Revue Canadienne De Chimie* **1999,** *77* (8), 1311-1326.

39. Zamboni, W. C., Liposomal, nanoparticle, and conjugated formulations of anticancer agents. *Clinical Cancer Research* **2005,** *11* (23), 8230-8234.

40. Rautio, J.; Kumpulainen, H.; Heimbach, T.; Oliyai, R.; Oh, D.; Jarvinen, T.; Savolainen, J., Prodrugs: design and clinical applications. *Nature Reviews Drug Discovery* **2008,** *7* (3), 255-270.

41. Liu, Y. Y.; Fan, X. D., Synthesis, properties and controlled release behaviors of hydrogel networks using cyclodextrin as pendant groups. *Biomaterials* **2005,** *26* (32), 6367-6374.

42. Qiu, Y.; Park, K., Environment-sensitive hydrogels for drug delivery. *Advanced Drug Delivery Reviews* **2001,** *53* (3), 321-339.

43. Nakanishi, T.; Fukushima, S.; Okamoto, K.; Suzuki, M.; Matsumura, Y.; Yokoyama, M.; Okano, T.; Sakurai, Y.; Kataoka, K., Development of the polymer micelle carrier system for doxorubicin. *Journal of Controlled Release* **2001,** *74* (1-3), 295-302.

44. Matsumura, Y.; Hamaguchi, T.; Ura, T.; Muro, K.; Yamada, Y.; Shimada, Y.; Shirao, K.; Okusaka, T.; Ueno, H.; Ikeda, M.; Watanabe, N., Phase I clinical trial and pharmacokinetic evaluation of NK911, a micelle-encapsulated doxorubicin. *British*

Journal of Cancer **2004,** *91* (10), 1775-1781.

45. Yokoyama, M.; Inoue, S.; Kataoka, K.; Yui, N.; Okano, T.; Sakurai, Y., MOLECULAR DESIGN FOR MISSILE DRUG - SYNTHESIS OF ADRIAMYCIN CONJUGATED WITH IMMUNOGLOBULIN-G USING POLY(ETHYLENE GLYCOL)-BLOCK-POLY(ASPARTIC ACID) AS INTERMEDIATE CARRIER. *Makromolekulare Chemie-Macromolecular Chemistry and Physics* **1989,** *190* (9), 2041-2054.

46. Hamaguchi, T.; Kato, K.; Yasui, H.; Morizane, C.; Ikeda, M.; Ueno, H.; Muro, K.; Yamada, Y.; Okusaka, T.; Shirao, K.; Shimada, Y.; Nakahama, H.; Matsumura, Y., A phase I and pharmacokinetic study of NK105, a paclitaxel-incorporating micellar nanoparticle formulation. *British Journal of Cancer* **2007,** *97* (2), 170-176.

47. Nishiyama, N.; Okazaki, S.; Cabral, H.; Miyamoto, M.; Kato, Y.; Sugiyama, Y.; Nishio, K.; Matsumura, Y.; Kataoka, K., Novel cisplatin-incorporated polymeric micelles can eradicate solid tumors in mice. *Cancer Research* **2003,** *63* (24), 8977-8983.

48. Plummer, R.; Wilson, R. H.; Calvert, H.; Boddy, A. V.; Griffin, M.; Sludden, J.; Tilby, M. J.; Eatock, M.; Pearson, D. G.; Ottley, C. J.; Matsumura, Y.; Kataoka, K.; Nishiya, T., A Phase I clinical study of cisplatin-incorporated polymeric micelles (NC-6004) in patients with solid tumours. *British Journal of Cancer* **2011,** *104* (4), 593-598.

49. Thakur, R.; Sivakumar, B.; Savva, M., Thermodynamic Studies and Loading of 7-Ethyl-10-hydroxycamptothecin into Mesoporous Silica Particles MCM-41 in Strongly Acidic Solutions. *Journal of Physical Chemistry B* **2010,** *114* (17), 5903-5911.

50. Gong, J.; Chen, M. W.; Zheng, Y.; Wang, S. P.; Wang, Y. T., Polymeric micelles drug delivery system in oncology. *Journal of Controlled Release* **2012,** *159* (3), 312-323.

51. Peng, C. L.; Lai, P. S.; Lin, F. H.; Wu, S. Y. H.; Shieh, M. J., Dual chemotherapy and photodynamic therapy in an HT-29 human colon cancer xenograft model using SN-38-loaded chlorin-core star block copolymer micelles. *Biomaterials* **2009,** *30* (21), 3614-3625.

52. Koizumi, F.; Kitagawa, M.; Negishi, T.; Onda, T.; Matsumoto, S.; Hamaguchi, T.; Matsumura, Y., Novel SN-38-incorporating polymeric micelles, NK012, eradicate vascular endothelial growth factor-secreting bulky tumors. *Cancer Research* **2006,** *66* (20), 10048-10056.

53. Gu, Q. R.; Xing, J. Z.; Huang, M.; He, C.; Chen, J., SN-38 loaded polymeric micelles to enhance cancer therapy. *Nanotechnology* **2012,** *23* (20).

54. B. Djurdjic, S. D., N. Geskovski, M. Petrusevska, V. Gancheva, G. Georgiev, P. Petrov and K. Goracinova, Synthesis and self-assembly of amphiphilic poly(acrylicacid)–poly(e-caprolactone)–poly(acrylicacid) block copolymer as novel

carrier for 7-ethyl-10-hydroxy camptothecin. *Journal of Biomaterials Applications* **2015,** *29* (6), 867-881.

55. Mora-Huertas, C. E.; Fessi, H.; Elaissari, A., Polymer-based nanocapsules for drug delivery. *International Journal of Pharmaceutics* **2010,** *385* (1-2), 113-142.

56. Whitesides, G. M., The origins and the future of microfluidics. *Nature* **2006,** *442* (7101), 368-373.

57. Karnik, R.; Gu, F.; Basto, P.; Cannizzaro, C.; Dean, L.; Kyei-Manu, W.; Langer, R.; Farokhzad, O. C., Microfluidic platform for controlled synthesis of polymeric nanoparticles. *Nano Letters* **2008,** *8* (9), 2906-2912.

58. Anton, N.; Bally, F.; Serra, C. A.; Ali, A.; Arntz, Y.; Mely, Y.; Zhao, M. J.; Marchioni, E.; Jakhmola, A.; Vandamme, T. F., A new microfluidic setup for precise control of the polymer nanoprecipitation process and lipophilic drug encapsulation. *Soft Matter* **2012,** *8* (41), 10628-10635.

59. Kucuk, I.; Edirisinghe, M., Microfluidic preparation of polymer nanospheres. *Journal of Nanoparticle Research* **2014,** *16* (12).

60. Hessel, V.; Angeli, P.; Gavriilidis, A.; Lowe, H., Gas-liquid and gas-liquid-solid microstructured reactors: Contacting principles and applications. *Industrial & Engineering Chemistry Research* **2005,** *44* (25), 9750-9769.

61. Schabas, G.; Yusuf, H.; Moffitt, M. G.; Sinton, D., Controlled self-assembly of quantum dots and block copolymers in a microfluidic device. *Langmuir* **2008,** *24* (3), 637-643.

62. Wang, C. W.; Sinton, D.; Moffitt, M. G., Flow-Directed Block Copolymer Micelle Morphologies via Microfluidic Self-Assembly. *Journal of the American Chemical Society* **2011,** *133* (46), 18853-18864.

63. Ren, K.; Zhou, J.; Wu, H., Materials for Microfluidic Chip Fabrication. *Accounts of Chemical Research* **2013,** *46* (11), 2396-2406.

64. deMello, A. J., Control and detection of chemical reactions in microfluidic systems. *Nature* **2006,** *442* (7101), 394-402.

Chapter 2.

Manufacturing and Characterization of SN-38-Loaded P(MCL-*co*-CL)-*b*-PEO Nanoparticles

2.1 Introduction

Amphiphilic block copolymers self-assemble into various nanostructures termed polymeric micelles that have been used in a wide range of applications, among which drug delivery using biocompatible block copolymer has attracted a tremendous amount of interest from researchers.[1-4] Block copolymers can be modified and functionalized to increase biocompatibility and permit encapsulation of specific therapeutic agents, and they have intrinsic robustness and exhibit a wide range of self-assembled morphologies.[2] All of these features make them attractive in the field of drug delivery.

SN-38 is an anticancer drug with very high potency. The main limitations of the direct delivery of SN-38 are the poor solubility in water and most pharmaceutically acceptable solvents. Currently, the prodrug of SN38, irinotecan (CPT-11), is approved for chemotherapy. Macromolecular prodrug, EZN-2208 is in Phase 2 clinical stage. However, the prodrug approaches instability in the physiological environment and enzymatic or chemical cleavage, etc. Nanomedicine formulations based on nanoemulsions, liposomes, and polymeric micelles have been developed more recently to improve the delivery of SN-38.[18]

PCL-*b*-PEO nanoparticles have been extensively investigated for drug delivery systems because of their biodegradability and biocompatibility, especially for anticancer drugs.[3-5] PCL is a biodegradable and semi-crystalline polymer with a relatively polar ester group and five non-polar methylene groups in its repeat unit. It shows more resistance to chemical hydrolysis than other polyesters.[4] PEO, a hydrophilic and non-toxic semicrystalline polymer becomes an ideal hydrophilic block in copolymers with PCL because of its absence of immunogenicity, as well its stealth-like nature due to its hydration, high mobility and thus protein repulsion.[5] In aqueous dispersions of PCL-*b*-PEO, PCL forms the hydrophobic core and PEO forms the hydrophilic corona. These nanocarriers enhance the water solubility of hydrophobic drugs, facilitate passive targeted delivery to solid tumors *via* the enhance permeation and retention (EPR) effect, and provide increased kinetic stability,[6] enhanced pharmacokinetics and long blood circulation times.[7,8]

However, there are still some disadvantages of PCL-*b*-PEO as drug delivery vehicles, which includes poor drug loading efficiency and slow degrading rate *in vivo*. Poor drug loading efficiency may originate from the high crystallinity of the PCL block and the lack of amorphous regions in which the drug molecules can solubilize.[10] Longer PCL blocks may increase the loading efficiency and thermodynamic stability of the micelle, since the main driving force for physical encapsulation is the hydrophobic interaction between the PCL block and the drug, and longer PCL blocks lead to higher hydrophobicity. In this case, however, the higher crystallinity may not be favorable for drug loading because only the amorphous PCL phase is likely to accommodate drug molecules.[11] A copolymer micelle with an amorphous core poly(ethylene glycol)-*b*-poly(2-hydroxyethyl methacrylate-*g*-poly(ε-caprolactone)) (PEG-*b*-P(HEMA-*g*-PCL)) was used to encapsulate doxorubicin by Zhang et. al..[12] Although this vehicle exhibits higher loading capacity, faster release of DOX from the micelles was observed. This indicates that a balance between amorphous and crystalline structures within block copolymers as well as a balance between hydrophobicity and crystallinity should enable optimum properties for drug delivery systems.

In order to address the balance described above, we introduced a comonomer methyl caprolactone together with caprolactone within the hydrophobic block of the copolymer poly(6-methyl-caprolactone-*co*-ε-caprolactone)-*block*-poly(ethylene oxide) (P(MCL-*co*-CL)-*b*-PEO). The existence of the methyl group interrupts the tacticity relative to a purely-PCL chain, decreasing the crystallinity of the hydrophobic block without any non-covalent interactions with drug molecule. We hope that the ability to obtain micelles with amorphous cores can thus be facilitated. Furthermore, MCL can decrease the CMC of polymer because the methyl group increase the hydrophobicity of polymer, behaves stronger tendency to self-assemble.[13]

Our group has introduced the use of gas-liquid segmented microfluidic reactors to synthesize various polymeric nanoparticles with size, shape, crystallinity and functionality (loading efficiency, release rates and photoresponsivity) controlled using the flow rate within the reactor microchannels.[14,15,16] This microfluidic approach is a promising “top-down” method to obtain drug delivery nanoparticles for specific therapeutic applications, with processing control provided by the high-shear generated within the microreactor.[9] Of course, the usefulness of this microfluidic platform relies on its applicability to different polymer materials and therapeutic agents. In this study, we investigate the microfluidic loading of SN-38 into nanoparticles of P(MCL-*co*-CL)-*b*-PEO. We study the effect of flow rate and initial drug-to-polymer ratio on the morphologies, hydrodynamic size distributions, loading efficiencies, and *in vitro* release rates for the resulting series of SN-38-loaded polymeric nanoparticles, and compare these results to nanoparticle formed using a more conventional non-microfluidic (bulk) approach. In addition, we compare the loading of SN-38 (microfluidic and bulk) into nanoparticles of P(MCL-*co*-CL)-*b*-PEO with loading into nanoparticles of the more crystalline copolymer PCL-*b*-PEO.

2.2 Experimental

2.2.1 Materials. NaCl (Bio Basic Canada, 99.9%), KCl (Caledon, 99.0%), Na_2HPO_4 (Bio Basic Canada, 98.0%) and KH_2PO_4 (Caledon, 99.0%) were used to prepare phosphate buffered saline (PBS, pH=7.4). *N*, *N*-dimethylformamide (DMF, Caledon, 99.8%), acetonitrile (ACN, Caledon, HPLC grade) were used as received without further purification. 7-ethyl-10-hydroxycamptothecin (≥ 98.0%) was purchased from AK Scientific. PCL_{12k}-*b*-PEO_{5k}, $PCL_{2.1k}$-*b*-PEO_{5k} (where numbers in subscripts denote number-average degrees of polymerization for the respective blocks) were purchased from Advanced polymer materials INC. P(MCL-*co*-$PCL)_{12k}$-*b*-PEO_{5k} were synthesized by Dr. Changhai Lu in Moffitt's lab.

2.2.2 Critical Water Content (cwc) Determination. Critical water contents were determined using light scattering experiments by Zheqi Xu.[17] previously in our group and listed in Table 2-1.

Table 2- 1. Copolymer Characteristics and Critical Water Contents

Copolymer	Composition[a]	*Mn* / $g.mol^{-1}$	cwc / wt%
PCL12k	PCL_{12k}-*b*-PEO_{5k}	17000	5.5 ± 0.1
PCL2k	$PCL_{2.1k}$-*b*-PEO_{5k}	7100	13.1 ± 0.2
PMCLCL	$P(MCL_{0.25}$-*co*-$CL_{0.75})_{5k}$-*b*-PEO_{5k}	10170	8.6 ± 0.2

a) Subscripts refer number-average molecular weights of block and weight fractions of MCL and CL in the hydrophobic block.

2.2.3 Bulk Preparation of SN-38-Loaded Nanoparticles. Nanoparticles of each block copolymer containing various quantities of SN-38 were prepared by the nanoprecipitation method. Specifically, 3 g of 0.33 wt % copolymer solutions in DMF with various drug-to-polymer ratios (w/w), *r* (*r* = 0.25, 0.50 and 0.75) were prepared and stirred overnight. This solution was then added dropwise at a rate of 120 µL/min into a 10 x volume of deionized water with continuous high-speed stirring using a syringe pump. The resulting nanoparticle dispersion in DMF/water was then dialyzed against deionized water for 12 hours with changing of water every hour for the first 4 h (6-8 kD MWCO dialysis membrane, Spectrum Laboratories) to remove DMF. Precipitated drug in the aqueous dispersion was removed by centrifugation at 16,000 g for 18 minutes; the resulting supernatant was decanted into a pre-weighed vial. Deionized water was added to the centrifuge tube in order to rinse the residue and minimize loss of block copolymer nanoparticles during separation of solid precipitate. Vortexing was applied for 5 min to the centrifugation tube in order to break up the pellet and re-suspend the solid residue, followed by another centrifugation step (16,000 g for 18 minutes) and collection of the supernatant. This process of "water addition-vortexing-centrifugation-supernatant collection" was repeated an additional two times. The mass of the final suspension was weighed to determine the concentration of polymer. It was assumed that the mass of polymer added initially remained unchanged during the dialysis and centrifugation processes.

2.2.4 Microfluidic Reactor Fabrication. Silicon wafers (Silicon Materials) were spin-coated with negative photoresist SU-8 100 (Microchem Inc.) at 2000 rpm. Then the wafers were soft baked at 65 °C for 20 minutes and baked at 95 °C for another 50 minutes. A photomask was then applied and exposed to UV light for 100 s. Immediately after exposure, the silicon wafer was heated at 65 °C for 1 min and 95 °C for another 20 min. Finally, the wafer was submerged in SU-8 developer (Microchem Inc.) until all unexposed photoresist was removed.

Microfluidics chips were fabricated from poly(dimethyl siloxane) (PDMS) using a SYLGARD 184 silicon elastomer kit (Dow Corning, Midland, MI). 28.28g elastomer and 4.71g curing agent (7:1 wt/wt) were mixed and degassed under vacuum. The mixture poured over the master chip facing up in a petri dish. Vacuum was applied again until no more bubbles appeared. The PDMS was heated at 85 °C for at least 20 minutes until cured, and then peeled from the negative master; inlet and outlet holes were punched out. A glass substrate was spin-coated using a mixture consisting of 20:1 elastomer and curing agent instead of 7:1. Both the chip and the substrate layer were treated with oxygen plasma for 90s and bonded together. The resulting microfluidic reactor design is shown in Figure 2-1. The channel depth of resulting reactor is 150 µm. The width of the mixing channel and processing channels is 100 µm and 200 µm wide, respectively.

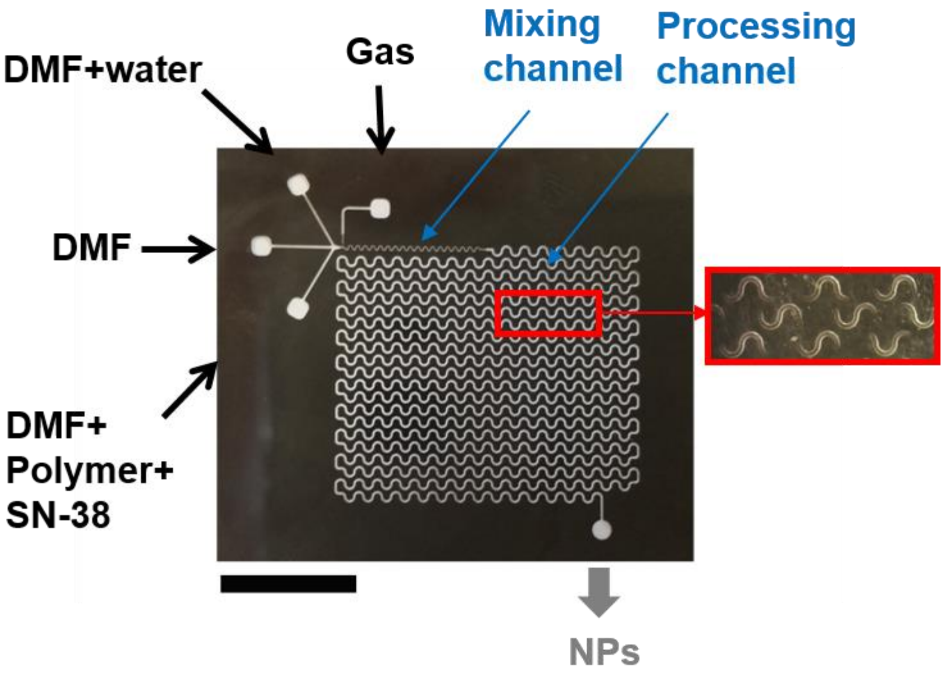

Figure 2- 1. The gas-liquid segmented microfluidic reactor. Scale bar is 1 cm.

2.2.5 Flow Delivery and Control. The microfluidic chip was fitted with 3 injection syringes (Hamilton, Reno, NV) mounted on syringe pumps (Harvard Apparatus, Holliston, MA) via 1/16th-inch (OD) Teflon tubing (Scientific Products and Equipment, ON). The gas inlet was fitted with a 1/16th-inch (OD) / 100-μm (ID) Teflon tube (Upchurch Scientific, Oak Harbor, WA) connected with a downstream regulator (Johnston Controls) for fine adjustments and an Ar tank regulator. The liquid flow rate (Q_{liq}) was programmed via the syringe pumps and the gas flow rate (Q_{gas}) was fine-tuned via the downstream pressure regulator in order to achieve the nominal total flow rates of 50, 100, 200 and 400 μL/min described in the main text. For all experiments, the relative gas-to-liquid flow ratio, $Q_{\mathrm{gas}}/Q_{\mathrm{liq}}$ ~1.

Due to the compressible nature of the gas and the high gas/liquid interfacial tension, discrepancies arise between the nominal (programmed) and actual values of Q_{gas}, $Q_{\mathrm{gas}}/Q_{\mathrm{liq}}$, and the total flow rate (Q_{total}). Therefore, visualization of gas bubbles and liquid plugs within the microchannels was achieved using an upright optical microscope (Omax) with a 3x-objective lens. Images were captured using a 2.07 megapixel PipilCam (Ken-A-Vision) and mean lengths of liquid and gas segments were measured using image analysis software (Image J). Images were taken every time 100 μL of sample has been collected. Actual values of Q_{gas}, $Q_{\mathrm{gas}}/Q_{\mathrm{liq}}$, and Q_{total} for each run were then calculated as described in our previous papers.[16]

2.2.6 Microfluidic Preparation of SN-38-Loaded Nanoparticles. The three syringes connected with liquid inlets contained: (1) 1.0 wt % PMCLCL or PCL12k solution in DMF containing co-dissolved SN-38 in a drug-to-polymer ratio of r = 0.25, 0.5 or 0.75; (2) pure DMF; and (3) a DMF/water mixture containing 40.8 wt % water (for PMCLCL) and 31.5 wt % water (for PCL12k). The flow rates of the three liquid streams were equal, in order to yield steady-state concentrations of 0.33 wt %

copolymer and 13.6 wt % water (for PMCLCL) and 10.5 wt % water (for PCL12k) to yield water contents of cwc + 5 wt % for both copolymers.

For each nanoparticle preparation, colloidal dispersions in DMF/water were collected into pre-weighed vials containing 10 x volume excess deionized water, followed by 12-hour dialysis against deionized water with changing of water every hour during the first 4 h to remove DMF (6-8 kD MWCO dialysis membrane, Spectrum Laboratories). Following dialysis, precipitated drug in the aqueous dispersion was removed by centrifugation at 16,000 g for 18 minutes; the resulting supernatant was decanted into a pre-weighed vial and deionized water was added to the centrifuge tube in order to rinse the residue and minimize loss of block copolymer nanoparticles during separation of solid precipitate. Vortexing was applied for 5 min to the centrifugation tube in order to break up the pellet and re-suspend the solid residue, followed by another centrifugation step (16,000 g for 18 minutes) and collection of the supernatant. This process of “water addition-vortexing-centrifugation-supernatant collection” was repeated an additional two times.

2.2.7 Transmission Electron Microscopy. Transmission electron microscopy (TEM) was performed using a JEOL JEM-1400 TEM, operating at an accelerating voltage of 65 kV and equipped with a Gatan Orius SC1000 CCD camera. Negatively-stained samples for TEM imaging were prepared by depositing one drop of sample on a carbon-coated 300-mesh copper TEM grid followed by one drop of 1 wt % uranyl acetate as a negative staining agent that selectively binds to the hydrophilic blocks, thus giving reverse contrast to the hydrophobic cores. Excess liquid was then removed with a Whatman filter paper. The grid was dried in the air for at least 2 hours.

Due to the high electron density of uranyl acetate, negative staining always influences the visualization of the internal lumen of vesicle structures of block copolymer nanoparticles, which makes it difficult to distinguish spheres from vesicles. Therefore, unstained images were also taken for samples that exhibit spherical-shaped structures.

For each set of nanoparticle formulation conditions (copolymer, flow rate, drug-to-polymer ratio, and water content), morphologies and mean nanoparticle sizes were determined based on triplicate preparations starting with three individually-prepared stock solutions; for each preparation, at least three TEM images were taken in different areas of the grid to characterize the morphology and size of the particles. Identified morphologies and mean dimensions for each copolymer and preparation condition are reported in Table 4-2 for bulk preparations and Table 4-7 for microfluidic preparations.

2.2.8 Dynamic Light Scattering. Effective hydrodynamic diameters of SN-38-loaded nanoparticles were determined using dynamic light scattering (DLS). DLS measurements were carried out using a Brookhaven Instruments correlation spectrometer equipped with a BI-200SM goniometer, a BI-9000AT digital autocorrelator, and a Melles Griot He-Ne Laser (633 nm) with a maximum power output of 75 mW. All DLS measurements of SN38-loaded nanoparticles were performed in pure water and an experimental temperature of 23˚C and at a scattering angle of 90˚.

After overnight dialysis and centrifugation to remove DMF and unincorporated SN-38, drug-loaded nanoparticles were transferred to pre-cleaned scintillation vials. For each preparation, three measurements of the autocorrelation function were taken from which mean effective hydrodynamic diameters and corresponding size distributions were determined using cumulent and CONTIN analysis, respectively.

2.2.9 SN-38 Loading Efficiency Determination. High performance liquid chromatography (HPLC, Ultimate 3000, Thermo Scientific) along with C18 column (Phenomenex Luna 5u C18) and a UV detector set at 265 nm, was used at 25 °C to determine the drug loading efficiencies of SN-38-loaded nanoparticles. The mobile phase, consisting of ACN and water (65:35, v/v) was running at 1 ml/min. The mobile phase was adjusted to pH = 3 by formic acid to ensure SN-38 was in the closed lactone ring form during the assay. After centrifugation of a given sample of SN-38-loaded nanoparticles, all of the water was removed by rotary evaporation at 25 °C; then ACN was used to dissolve the solid (polymer + drug). A volume of 50 µL of sample was then injected automatically by the instrument. A calibration curve was made by analysis of 5 standards consisting of known concentrations of SN-38 in acetonitrile (5, 10, 20, 50, 100 ppm). Quantities of SN-38 in the samples were determined from the calibration curve and loading efficiencies and loading levels were calculated for each sample using the following equations:

$$\text{loading efficiency } (\%) = \frac{\text{mass of encapsulated SN-38 (g)}}{\text{total SN-38 added (g)}} \times 100\% \tag{2-1}$$

$$\text{loading ratio } \left(\frac{\text{w}}{\text{w}}\right) = \frac{\text{total SN-38 added (g)}}{\text{mass of copolymer (g)}} \tag{2-2}$$

$$\text{loading level } \left(\frac{\text{w}}{\text{w}}\right) = \frac{\text{mass of encapsulated SN-38 (g)}}{\text{mass of copolymer (g)}} \tag{2-3}$$

$$\text{loading level} \left(\frac{\text{w}}{\text{w}}\right) = \text{loading efficiency } (\%) \times \text{loading ratio} \left(\frac{\text{w}}{\text{w}}\right) \tag{2-4}$$

2.2.10 *In Vitro* SN-38 Release Kinetics. The following experiments were carried out to monitor the *in vitro* release of SN-38 from drug-loaded nanoparticles. In a typical experiment, a known mass (~2 g) of SN-38-loaded nanoparticles were put into a 5 mL Float-A-Lyzer tube (SpectrumLabs, MWCO 100 kDa) for each predetermined time (t = 1, 2, 4, 8, 12, 18, 24 h). These tubes were then placed in a 5

L-beaker of the release medium, consisting of ~4 L of PBS; throughout release experiments, the release medium was constantly stirred using magnetic stirring and maintained at physiological temperature (37 ± 0.2°C). At each predetermined time (*t* = 1, 2, 4, 8, 12, 18 and 24 h), one of the seven tubes was transferred to a vial and dried by rotary evaporation at 25 °C. Then a known quantity of ACN (0.1-0.3 g depending on release time) was added to dissolve SN-38 and polymer leaving some remaining solid (salts and undissolved polymer).Vortex was applied for 5 min to make sure all the SN-38 was dissolved. The concentration of the resulting solution was measured by HPLC (see previous section for specifications). Percentages of SN-38 released were calculated relative to determined masses of SN-38 in nanoparticles (total mass × loading efficiency) at the *t* = 0 release time. Reported release percentages at each release time are averages determined from triplicate preparations under the specified conditions.

2.3 Results and Discussion

2.3.1 Comparison of SN-38 Loading in PCL-*b*-PEO and P(MCL-*co*-CL)-*b*-PEO Copolymers.

Our initial attempts at loading SN-38 used typical PCL-*b*-PEO copolymers studied previously in our group for loading hydrophobic drugs and probes.[15,16] First, we carried out encapsulation of SN-38 using the bulk microprecipitation method with the copolymer PCL**2**k at three different loading ratio (*r* = 0.05, 0.1, 0.2) and the copolymer PCL12k at the same three loading ratios and also with an additional loading ratio *r* = 0.5. These results are reported in Table 2-2 and Figure 2-2. For PCL2k, loading efficiencies range from 3-7 % and decrease with higher *r* values, indicating that more drug is excluded from the nanoparticle cores as the loading ratio is increased. For PCL12k, higher loading efficiencies from ~3-14 % are obtained and also decrease as the *r* value increases. Loading level of PCL12k increases from *r* = 0.25 to *r* = 0.5 and stars to plateau at ~0.014 (w/w) while the PCL2k has the same loading level at various loading ratios, which means that longer PCL blocks allow more SN-38 to be encapsulated and shorter blocks limit the loading capacity of polymer nanoparticles.

Table 2- 2. Loading Efficiency and Loading Level of SN38-loaded PCL12k and PCL2k.

	PCL12k		**PCL2k**	
Drug Loading Ratio (*r*)	**Loading Efficiency / wt%**	**Loading Level / $\times 10^{-2}$**	**Loading Efficiency / wt%**	**Loading Level / $\times 10^{-2}$**
0.05	14.0±1.9	0.70±0.10	7.2±2.2	0.36±0.11
0.1	10.6±4.2	1.06±0.42	5.8±3.1	0.58±0.31
0.2	5.9±2.1	1.18±0.42	2.7±1.7	0.54±0.34
0.5	2.7±0.4	1.35±0.20	N/A	N/A

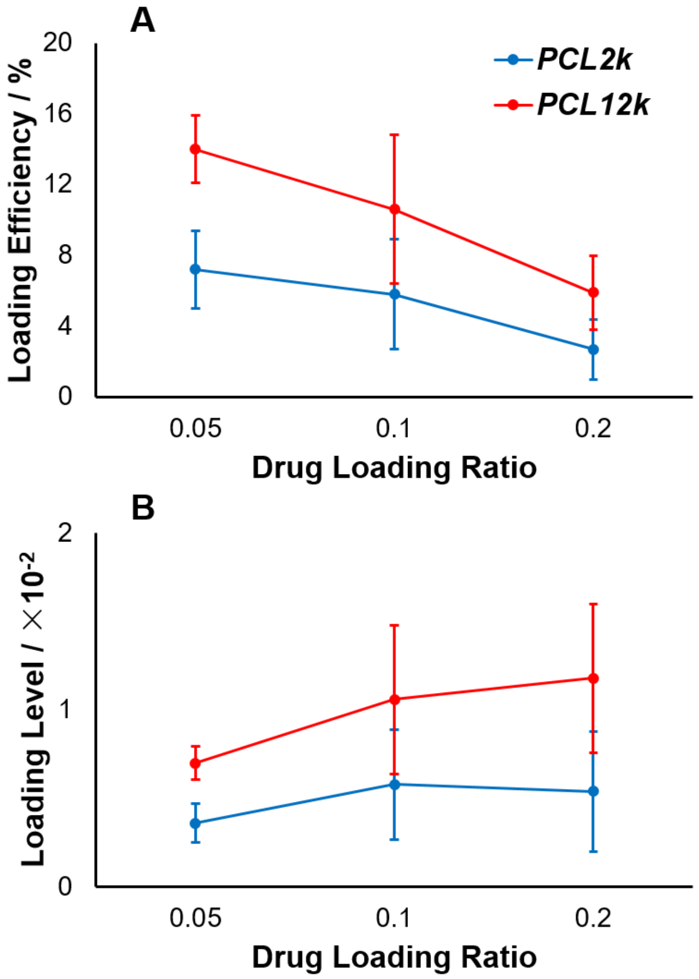

Figure 2- 2. Loading efficiency (A) and loading level (B) of SN-38 loaded nanoparticles prepared in bulk. Error bars are calculated from three separate preparations.

We next tried microfluidic encapsulation of SN-38 using the copolymer PCL12k at a loading ratio of r = 0.5 and a water content of cwc + 5 wt %, in order to determine if on-chip shear effects provided increased encapsulation efficiencies relative to the bulk method. The nanoparticles were prepared at three different flow rates of Q = 50, 100, and 200 μL/min and the resulting loading efficiencies were compared with the bulk-prepared r = 0.5 case (Table 2-3). The resulting microfluidic loading efficiencies were around ~3 % for all three flow rates, similar to the bulk encapsulation method for the same polymer and loading ratio. These result suggested an inherent limitation in the loading of SN-38 into PCL-based copolymers that could not be mitigated by the shear effects in the microfluidic reactor. Possible contributions to the low loading efficiencies of SN-38 in the PCL cores of PCL-*b*-PEO block copolymers include the high crystallinity of PCL and poor thermodynamic solubility of SN-38 in the amorphous phase of PCL.[9] Therefore, we turned to a new block copolymer with a different hydrophobic block being a random copolymer of the monomers caprolactone and methyl-caprolactone: P(MCL-*co*-CL)-*b*-PEO (or PMCLCL). The methyl groups within the hydrophobic cores of the resulting nanoparticles are expected to both increase hydrophobicity and disrupt crystallization relative to PCL.

We compared loading efficiencies for bulk preparations of SN-38-loaded nanoparticles prepared at a loading ratio of $r = 0.5$ using copolymers PCL12k and PMCLCL. As described above, this condition and method gave a loading efficiency of 2.7 ± 0.4 % for PCL12k; in contrast, PMCLCL yielded a loading efficiency of 11 ± 3% under the same conditions. In addition, TEM images of the resulting SN-38-loaded nanoparticles of PCL12k showed a combination of small spheres, long cylinders and large lamellar nanoparticles (Figure 2-3 A), whereas the number of cylinders and platelets decreases and large spheres, possibly vesicles, appear in PMCLCL sample (Figure 2-3 B). Large lamellar nanoparticles are generally not desirable to drug delivery as they can grow to several microns across and tend to gravitationally settle out of colloidal suspensions. Therefore, based on this combination of higher loading efficiencies and more desirable sizes and morphologies in bulk-prepared nanoparticles, we decided to apply the copolymer PMCLCL for the rest of our investigations of microfluidic loading of SN-38.

Table 2- 3. Loading Efficiency of SN38-loaded PCL12k Prepared in Bulk and by Microfluidic at Different Flow Rates. Error bars are calculated from three separate preparations.

	bulk	50 µL/min	100 µL/min	200µL/min
Loading Efficiency / %	2.7 ± 0.4	3.4 ± 2.2	2.7 ± 0.2	2.4 ± 0.7

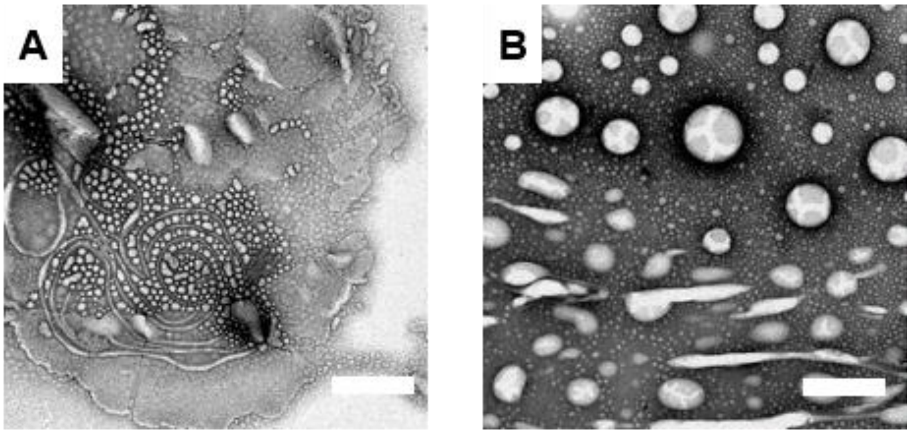

Figure 2- 3. TEM images comparing morphologies from bulk preparations of SN-38-loaded nanoparticles (*r* = 0.5) of PCL12k (A) and PMCLCL (B). Scale bars are 500 nm.

2.3.2 Effect of Drug-to-Polymer Ratio on the Morphologies, Sizes, Loading Efficiencies of SN38-Loaded Nanoparticles of P(MCL-*co*-CL)-*b*-PEO Prepared by the Bulk Method.

We first investigated how drug-loading ratio (*r* = 0.25, 0.5, 0.75) effect SN38-loaded nanoparticles prepared in bulk without influence of on-chip flow rate. Figure 2-4 shows the morphologies and size distribution of these nanoparticles. The main morphologies for all the loading ratios are spheres, along with some short cylinders. Thus, the morphological effect of *r* is negligible. However, the larger size of spheres and cylinders can be observed in the condition of $r = 0.5$, supported by the hydrodynamic size obtained from cumulent analysis of DLS. Loading levels of nanoparticles with higher loading ratio ($r = 0.5, 0.75$) are greater than those with low loading ratio ($r = 0.25$), indicating that as more drug was added initially, the total mass of encapsulated drug was increased. *In vitro* release study was performed at the highest loading ratio ($r = 0.75$). Almost all the SN-38 was released within 24 hours and the release during the first 4 hours is particularly fast.

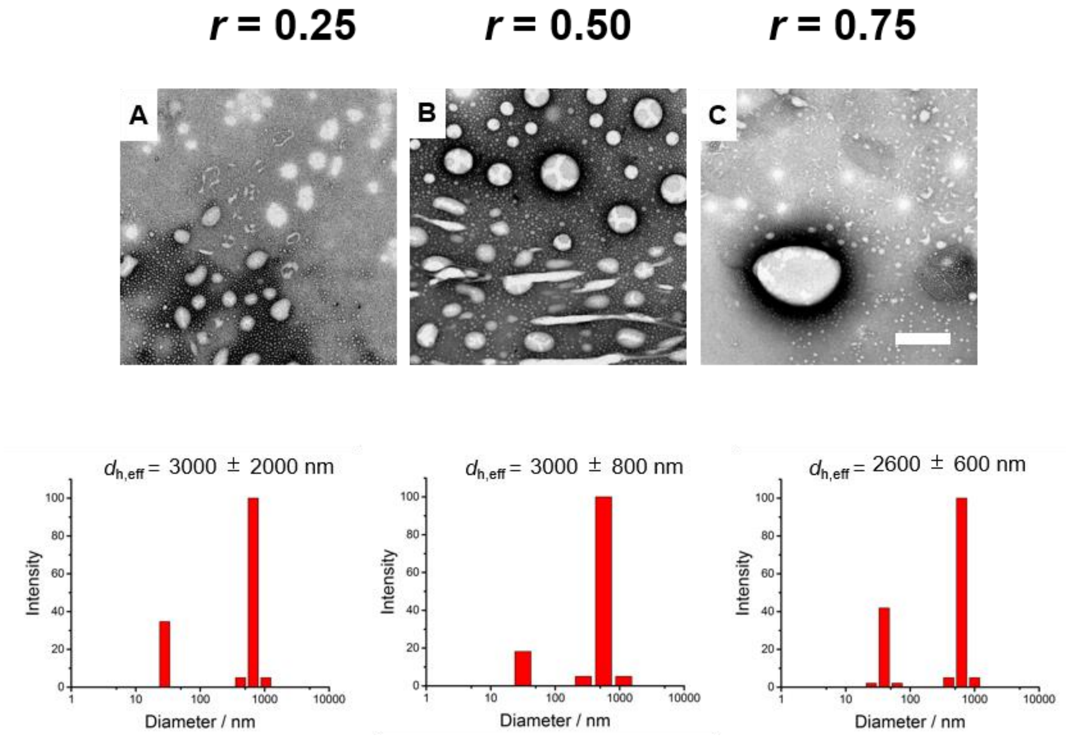

Figure 2- 4. TEM images and size distribution obtained form CONTIM analysis of DLS measurements, along with the mean effective hydrodynamic diameter determined from CUMULENT analysis of PMCLCL nanoparticles synthesized using bulk method with different drug-to-polymer ratio.

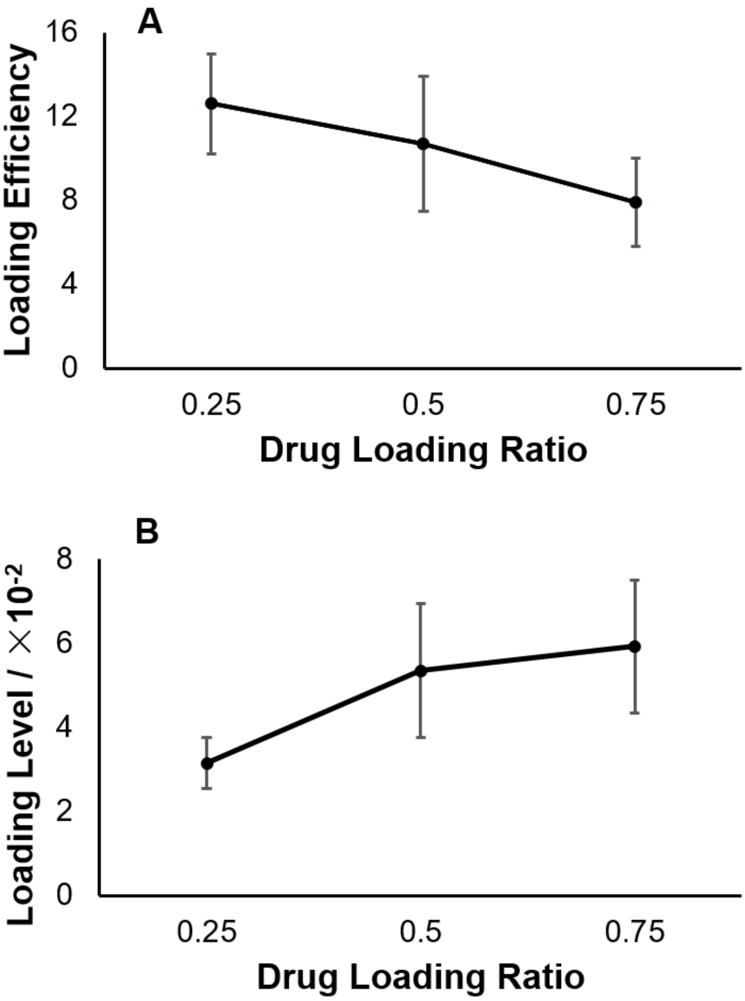

Figure 2- 5. Loading efficiency (A) and loading ratio (B) of bulk-prepared PMCLCL nanoparticles. Error bars are calculated from three separate preparations.

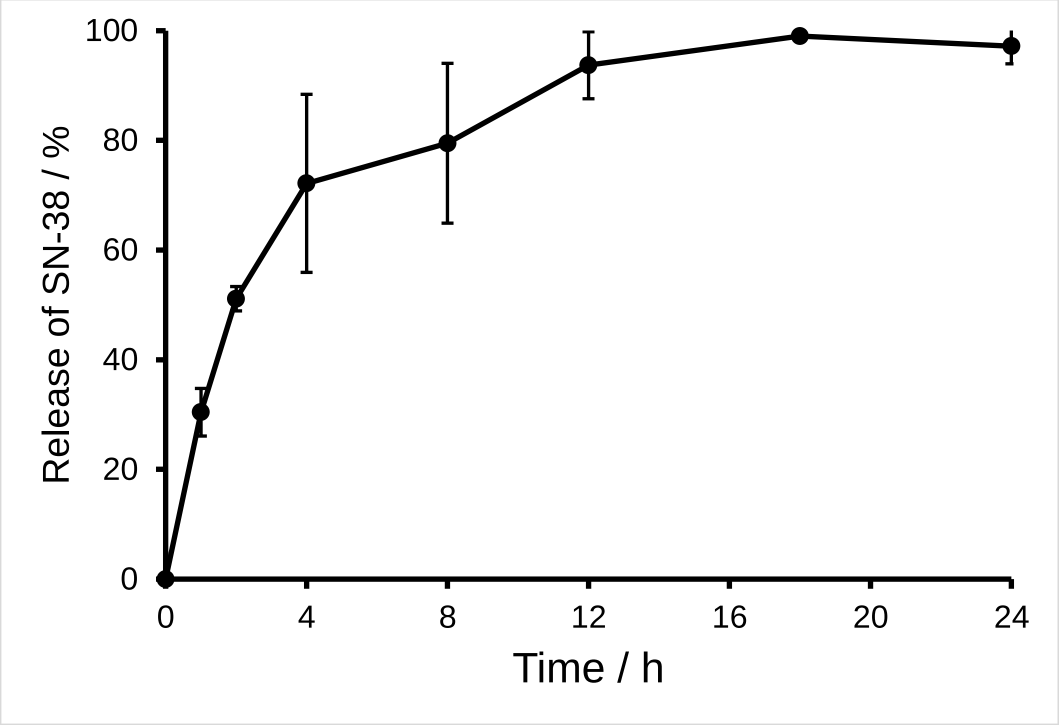

Figure 2- 6. *In vitro* release profile of PMCLCL nanoparticles prepared in bulk at r = 0.75. Error bars are calculated from three separate preparations.

2.3.3 Effect of Drug-to-Polymer Ratio and Flow Rate on Morphologies and Sizes of Microfluidic-Prepared SN38-Loaded Nanoparticles of P(MCL-*co*-CL)-*b*-PEO.

Figure 2-6 shows TEM images of SN-38-loaded nanoparticles synthesized in the gas-liquid microfluidic reactor at different loading ratios and flow rates. TEM images show various combinations of spheres, rods and large lamellae at the different loading ratios and flow rates, although the sizes and specific combinations of morphologies depend on both r and Q. One interesting trend discernable from the TEM images is that for all values of r, large lamellar aggregates are least prominent at the intermediate flow rate of Q = 200 μL/min, and in fact at the two lower loading ratios of r = 0.25 and r = 0.5, only spherical nanoparticles are found at this flow rate (Figure 2-3, G and H).

The corresponding DLS CONTIN size distributions for various loading ratios and flow rates are shown in Figure 2-4, supporting the effects of flow rate drawn from TEM results in Figure 2-6. At the lowest flow rate of Q = 50 μL/min, all loading ratios show three populations centered at ~50 nm, ~1000 nm and ~10000 nm, attributed to small, medium and large aggregates in the dispersions (Figure 2-7, A-C). For all r values, increasing the flow rate to Q = 100 μL/min leads to a disappearance of the largest-sized aggregate population (Figure 2-7, D-F). Then, further increasing the flow rate to Q = 200 μL/min leads to a shift to smaller sizes of both the remaining aggregate populations (Figure 2-7, G-I) compared to the Q = 100 μL/min case. Finally, increasing the flow rate to Q = 400 μL/min results in a shift in the aggregate populations in the opposite direction, toward larger aggregate sizes (Figure 2-7, J-L).

Along with the CONTIN size distributions shown in Figure 2-7, DLS data can also be analyzed using the method of cumulent, which yields mean effective hydrodynamic diameters; these are plotted versus flow rate for the various loading ratios in Figure 2-8. The results are consistent with CONTIN DLS analysis and TEM results described above, showing a similar trend for all loading ratios of decreasing mean particle sizes as flow rate is increased between Q = 50 and 200 μL/min, followed by an increase in mean particle sizes as flow rate is further increased to Q = 400 μL/min.

Previous work in our group on similar two-phase microreactor showed that counter-rotating vortices induced by chaotic advection in the liquid plugs generates extremely high shear (~10^4 to 10^5 s^{-1}) in the corner of gas-liquid interface.[21] For microfluidic manufacturing of nanoparticles, continuous recirculating flow moves micelles in and out of the high-shear corners, resulting in shear-induced micelle coalescence to form larger micelles and shear-induced collision to break up into smaller particles.[22] The resulting particle size is a balance of the relative rates of these processes. The decrease in size from Q = 50 µL/min, to Q = 200 µL/min indicates that the shear-induced break up is dominant in this range of flow rate. As flow rate is further increase to 400 µL/min, the rate of coalescence is increased, to form larger aggregates. Then, due to the kinetic constraints, these aggregates will relax via intraparticle chain rearrangements for form a different morphology which is vesicle in this case. The competing mechanism of on-chip micelle formation leads to size optimization under different chemical conditions, and in this system of SN-38 and PMCLCL, minimum particle sizes of lowest size dispersions are found at Q = 200 µL/min for all loading ratios.

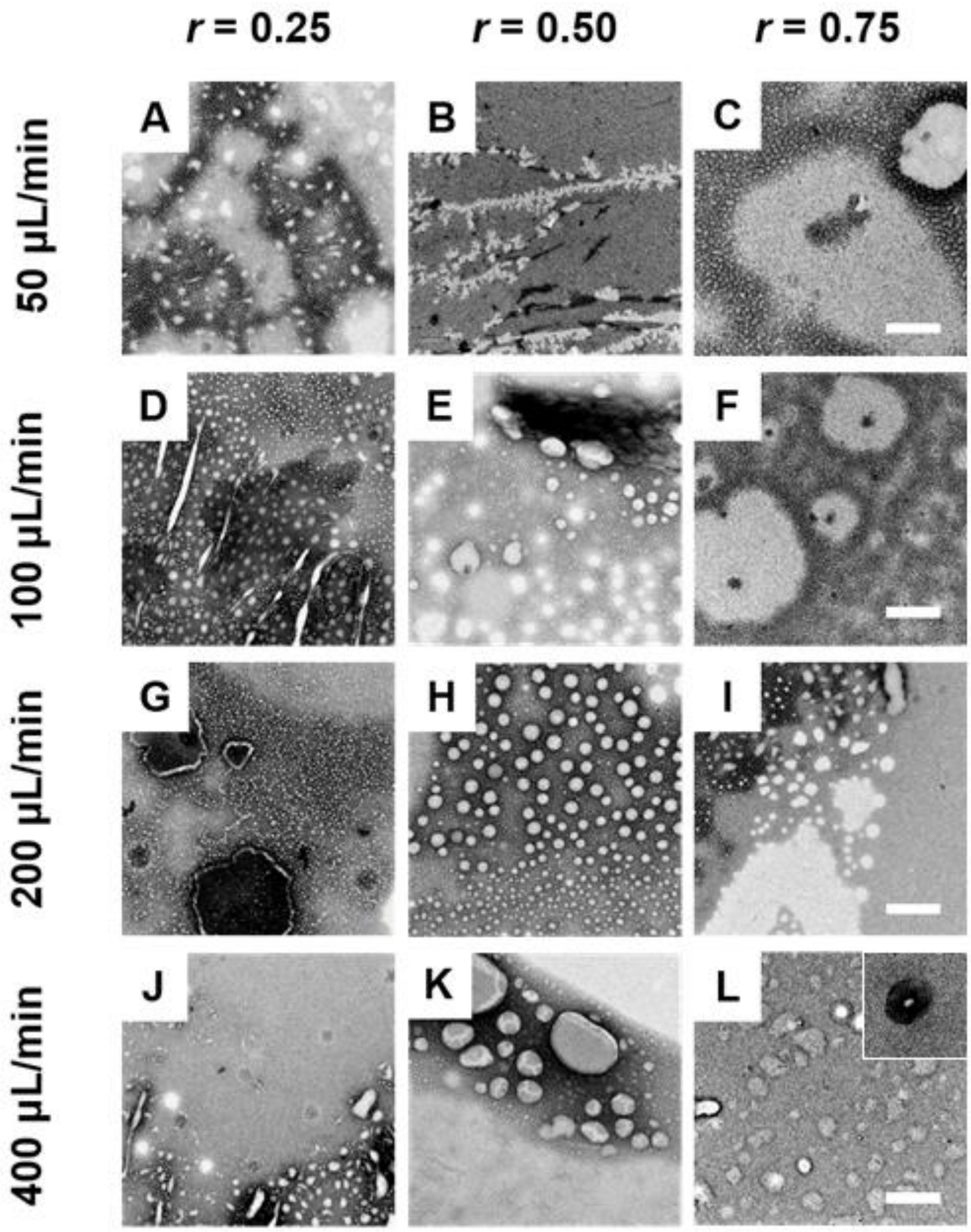

Figure 2- 7. Effect of loading ratio (*r*) and flow rate (*Q*) on PMCLCL nanoparticle morphology through TEM. Inset to L shows unstained image of vesicles. Scale bars are 500 nm.

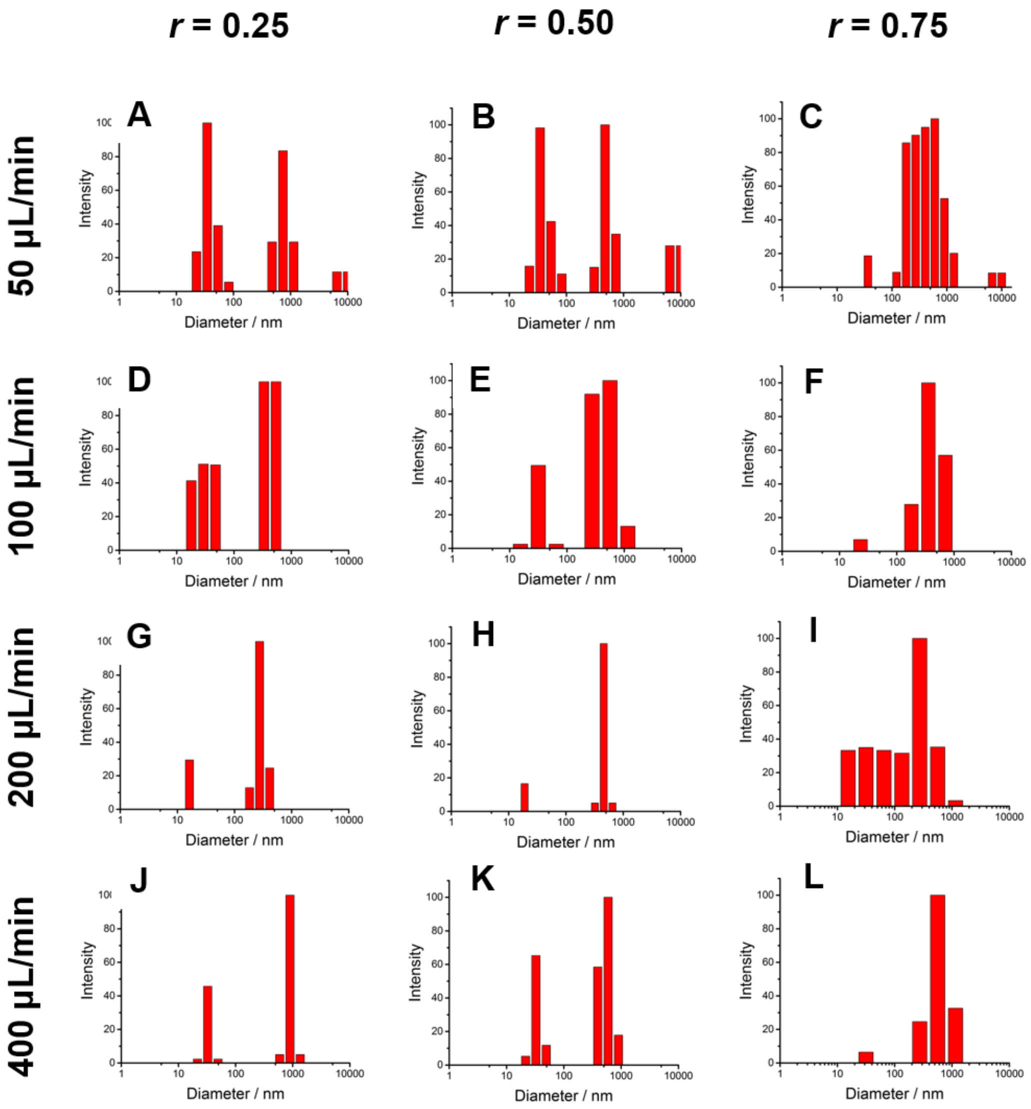

Figure 2- 8. Effect of loading ratio (*r*) and flow rate (*Q*) on size distribution of PMCLCL nanoparticle from CONTIN analysis of DLS autocorrelation function.

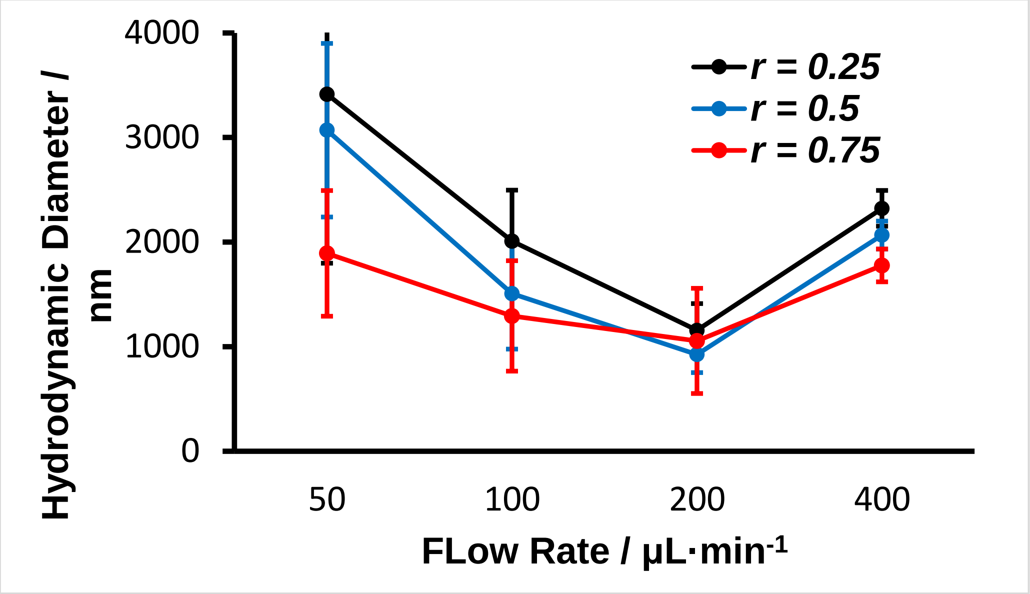

Figure 2- 9. Effect of flow rate (*Q*) on DLS mean effective hydrodynamic diameters of PMCLCL nanoparticles prepared at different drug-to-polymer loading ratios, *r*.

2.3.4 Effect of Drug-to-Polymer Ratio and Flow Rate on Loading Efficiencies of Microfluidic-Prepared SN38-Loaded Nanoparticles of P(MCL-*co*-CL)-*b*-PEO.

For the 12 microfluidics-prepared SN38-loaded nanoparticles (three different loading ratios and four different flow rates), SN-38 loading efficiencies are plotted in Figure 2-9A. Corresponding loading levels (mass encapsulated SN-38 / mass polymer) are plotted in Figure 2-9B. Similar trends were obtained for all loading ratios, where the lowest flow rate (*Q* = 50 µL/min) produces the lowest loading efficiencies, followed by increases in loading efficiencies between *Q* = 50 µL/min and *Q* = 100 µL/min, and no significant change in loading efficiencies at higher flow rates. Compared to bulk loading efficiencies discussed previously (Figure 2-5), microfluidic loading efficiencies at the given loading ratio and at the higher flow rates *Q* > 50 µL/min are either similar or slightly lower than the bulk values.

Although the loading efficiency is decreasing with increasing loading ratio, the loading level which reflects the total amount of encapsulated SN-38 is still increasing (expect for the similar loading level of nanoparticles of *r* =0.25 and *r* = 0.5 at *Q* = 200µL/min). We can reasonably speculate the saturation of the nanoparticles has not been reached at the current highest loading ratio (*r* = 0.75).

The observed increases in loading efficiencies/loading levels when the flow rate exceeds *Q* = 50 µL/min correlates with the disappearance of extremely large lamellar aggregates (Figure 2-6) and loss of the large-particle-size population in the DLS size distributions (Figure 2-7). We speculate that the loss of low-curvature lamellae gives rise to an increase in loading efficiency since the higher surface-to-volume ratio of these structures provides less hydrophobic volume in which SN-38 can dissolve.

We also note that the loading efficiencies of SN-38 in nanoparticles prepared in the microfluidic device are similar or slightly lower than those prepared by the bulk method. This contrasts previous microfluidic-prepared nanoparticle systems explored using this reactor in which loading of PCL-*b*-PEO with PAX showed higher loading efficiencies than the corresponding bulk preparation.[15] In that work, our group reported that changes of both morphology and loading efficiency with flow rate correspond to shear-induced changes of PCL crystallinity.[15] However, in this case, the hydrophobic core of PMCLCL is amorphous,[17] which results in similar morphologies and loading efficiencies for *Q* > 50 µL/min. Yamamoto et al. proposed that drug-incorporation behaviours are governed not only by hydrophobic interactions but also by other factors such as hydrogen bonding, steric configuration and mobility/rigidity of the block copolymer.[23] All of these factors can change the response of the nanoparticles to shear during SN-38 loading, making this current system different from PAX-loaded PCL-*b*-PEO.

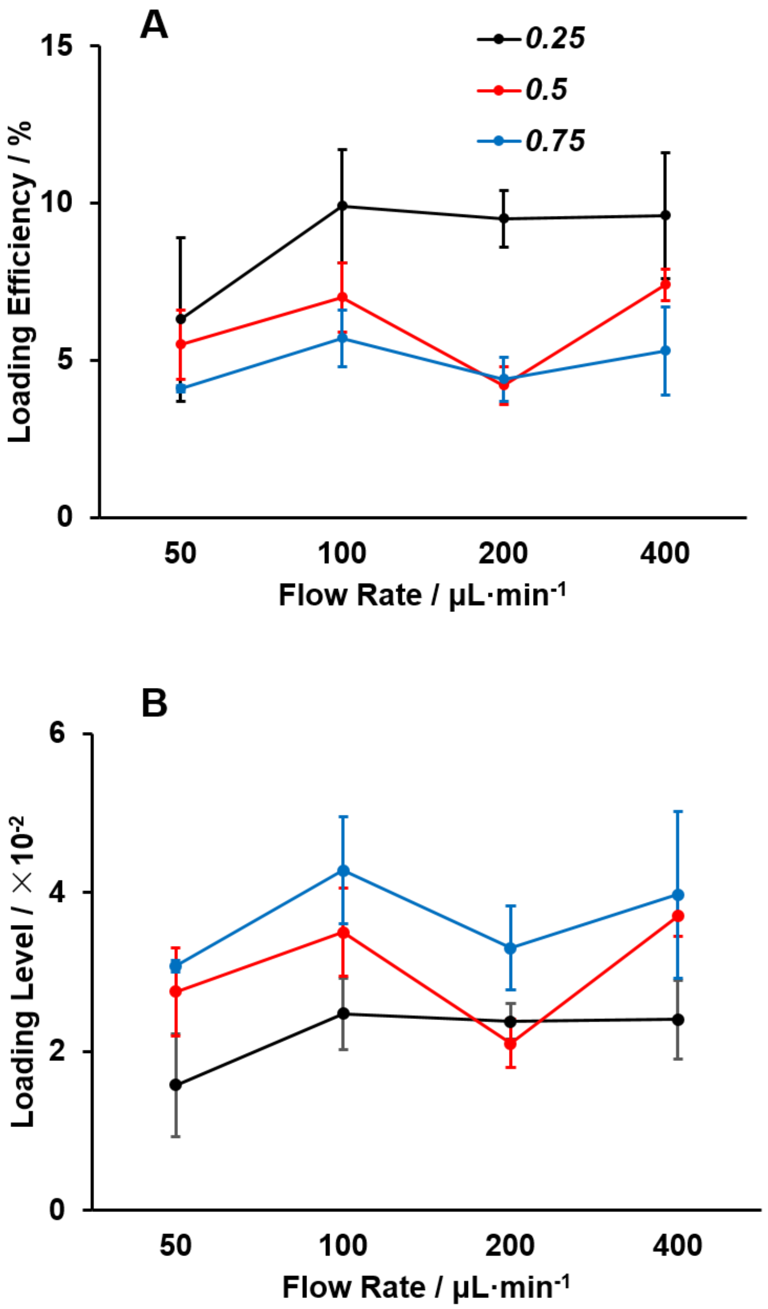

Figure 2- 10. Effect of loading ratio (*r*) and flow rate (*Q*) on the loading efficiency and loading level of PMCLCL nanoparticles. Error bars are calculated from three separate preparations.

2.3.5 Effect of Flow Rate on Release Rates of SN38-Loaded of P(MCL-*co*-CL)-*b*-PEO Nanoparticles.

The *in vitro* release behaviors of SN38-loaded nanoparticles in PBS solution at 37 °C were studied. Figure 2-10 compares SN-38 release profiles of nanoparticles synthesized at a loading ratio of $r = 0.75$ both using the bulk method and using the microfluidic reactor at different flow rates (Q = 50, 100, 200, and 400 μL/min). In general, more than 95% SN-38 was released within 24 hours. A quick release was found in the first 4 hours, followed by slower release.

Based on fits for release profiles, release half time ($\tau_{1/2}$) of microfluidic-prepared nanoparticles under Q = 50, 100, 200 and 400 are found to be 0.77 ± 0.13, 1.36 ± 0.09, 1.71 ± 0.25, 3.32 ± 0.30 h, respectively (Figure 2-12). Comparing the release half time of nanoparticles prepared at different flow rate, the lowest flow rate (Q = 50 μL/min) generates fastest release while the highest flow rate (Q = 400 μL/min) generates the slowest release. A wide range of factors can affect drug release, such as the polymer degradation rate, drug solubility,[24] distribution of the drug within the nanoparticles,[25] nanoparticle size and shape,[26] and crystallinity of the nanoparticle core.[27] In light of the relatively short release time, the degradation of the polymer matrix was not expected to occur.[28] Since we used some amount of drug and polymer with same composition, it is not surprising that all the samples of SN38-loaded nanoparticles demonstrate similar release pattern. Zhang et. al.[29] proposed that larger particles result lower release rate, because it takes longer time for the encapsulated drug to diffuse across the core to the micelle surface and finally into the aqueous medium. In our case, however, the nanoparticles with largest size have the fastest release rate (r = 50 μL/min) and the nanoparticles with smallest size have an intermediate release rate. One assumption of this lack of correlation between particle size and release rate could be that, a portion of drug was located at the region near or within the PEO outer shell and can be released out very quickly without traversing through the core of the micelle. Many researchers found this phenomenon in their study. The hydrophobic core is not the only region for the encapsulation, the core-corona interface can play a role in the solubilization of drug molecule as well. Therefore, slower release in the condition of r = 400 µL/min could be the reason that more drug was encapsulated in the micelle core, which is thought to be induced by fast mixing on chip.

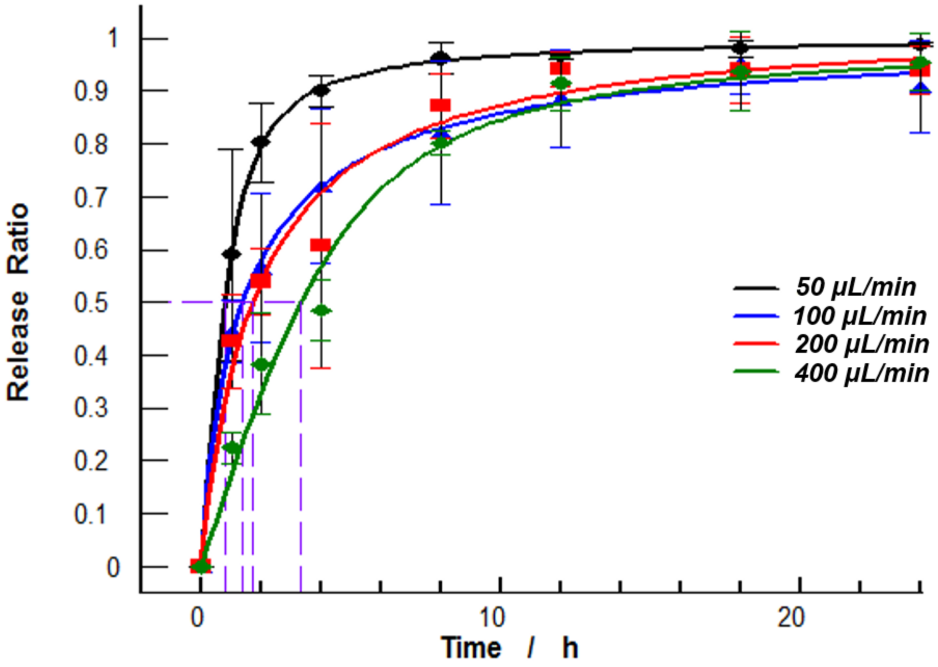

Figure 2- 11. Effect of flow rate (Q) on *in vitro* release of PMCLCL nanoparticles prepared at a loading ratio of r = 0.75. Error bars are calculated from three separate preparations. The fitting method is described in Appendix A.

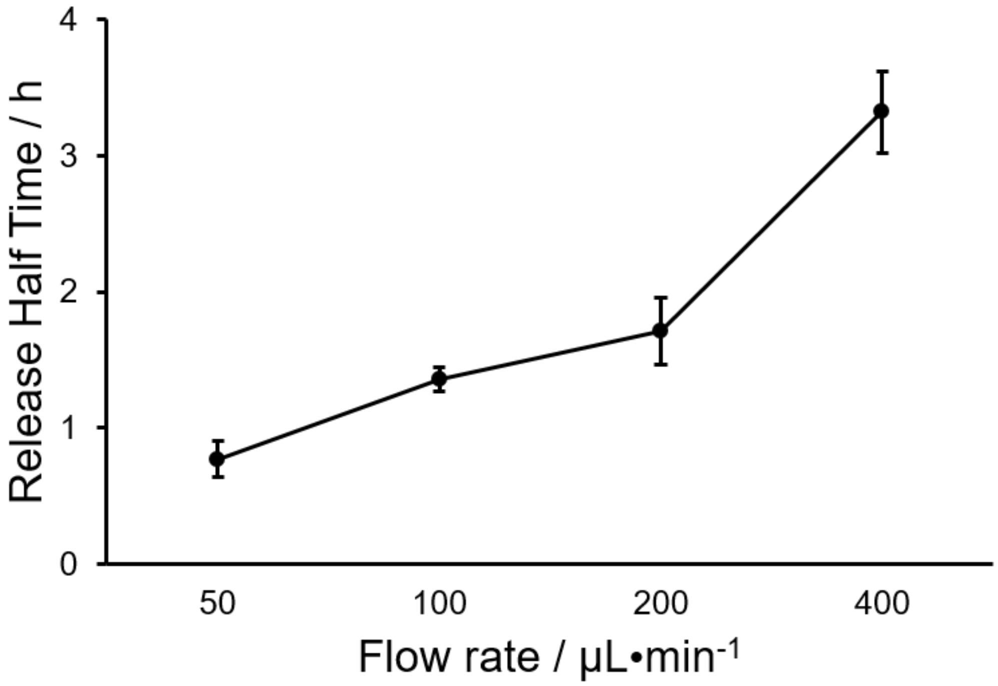

Figure 2- 12. Effect of flow rates on $\tau_{1/2}$ values of microfluidic-prepared nanoparticles (r = 0.75). Error bars are calculated from three separate preparations.

2.4 Conclusion

In this chapter, we first investigated the effect of hydrophobicity and crystallinity of the core-forming block by comparing SN-38 loading in PCL-*b*-PEO and P(MCL-*co*-CL)-*b*-PEO block copolymers. Higher loading efficiency was achieved with the P(MCL-*co*-CL)-*b*-PEO copolymer which is attributed to higher hydrophobicity and lower crystallinity compared to the PCL-*b*-PEO. Next, we used a gas-liquid segmented microfluidic to synthesize SN38-loaded P(MCL-*co*-CL)-*b*-PEO nanoparticles under four different flow rates and three different drug-to-polymer loading ratios, and size, morphology, loading efficiency and *in vitro* release of nanoparticles was studied. Mean particle sizes were found to decrease and then increase with increasing flow rate, with minimum sizes found at Q = 200 μL / min at all loading ratios. Loading efficiencies and loading levels were consistently higher for nanoparticles formed at $Q > 50$ μL / min. At these higher flow rates, microfluidic loading levels were similar to loading levels obtained using the bulk method of SN-38 encapsulation. Comparing *in vitro* release rates for bulk and for microfluidic nanoparticles prepared at different flow rates, release rates decreased in the order of bulk > $Q = 50$ μL / min ≈ $Q = 100$ μL / min ≈ $Q = 200$ μL / min > $Q = 400$ μL / min. Overall, this chapter provides insights into how chemical and processing effects influence the size, structure, loading and release properties of SN-38-loaded polymeric nanoparticles synthesized both in the bulk in and a gas-liquid segmented microfluidic reactor. To further compare the properties of these microfluidic-prepared nanoparticles for drug delivery, we will be studying their cytotoxicity using a cancer cell line in Chapter 3. In addition, the result that slower release can be achieved at higher flow rates provides an impetus to explore even higher on-chip shear rates in Chapter 4.

2.5. Supporting Information

Please see Appendix A for supporting information: TEM images and DLS analysis for bulk-prepared SN38-loaeded PCL-*b*-PEO nanoparticles; Table of actual flow rates; Calibration curve for HPLC; Fits of release data.

2.6 Reference

1. Kabanov, A. V.; Batrakova, E. V.; Miller, D.; Alakhov, V., Amphiphilic block copolymers in drug delivery. *Abstracts of Papers of the American Chemical Society* **1997,** *214*, 157-COLL.

2. Bae, Y.; Jang, W. D.; Nishiyama, N.; Fukushima, S.; Kataoka, K., Multifunctional polymeric micelles with folate-mediated cancer cell targeting and pH-triggered drug releasing properties for active intracellular drug delivery. *Mol. Biosyst.* **2005,** *1* (3), 242-250.

3. Huang, M. H.; Li, S. M.; Hutmacher, D. W.; Schantz, J. T.; Vacanti, C. A.; Braud, C.; Vert, M., Degradation and cell culture studies on block copolymers prepared by ring opening polymerization of epsilon-caprolactone in the presence of

poly(ethylene glycol). *J. Biomed. Mater. Res. Part A* **2004,** *69A* (3), 417-427.

4. Chawla, J. S.; Amiji, M. M., Biodegradable poly(epsilon-caprolactone) nanoparticles for tumor-targeted delivery of tamoxifen. *International Journal of Pharmaceutics* **2002,** *249* (1-2), 127-138.

5. Suk, J. S.; Xu, Q. G.; Kim, N.; Hanes, J.; Ensign, L. M., PEGylation as a strategy for improving nanoparticle-based drug and gene delivery. *Advanced Drug Delivery Reviews* **2016,** *99*, 28-51.

6. Allen, C.; Maysinger, D.; Eisenberg, A., Nano-engineering block copolymer aggregates for drug delivery. *Colloids and Surfaces B-Biointerfaces* **1999,** *16* (1-4), 3-27.

7. Peer, D.; Karp, J. M.; Hong, S.; FaroKhzad, O. C.; Margalit, R.; Langer, R., Nanocarriers as an emerging platform for cancer therapy. *Nature Nanotechnology* **2007,** *2* (12), 751-760.

8. Cabral, H.; Matsumoto, Y.; Mizuno, K.; Chen, Q.; Murakami, M.; Kimura, M.; Terada, Y.; Kano, M. R.; Miyazono, K.; Uesaka, M.; Nishiyama, N.; Kataoka, K., Accumulation of sub-100 nm polymeric micelles in poorly permeable tumours depends on size. *Nature Nanotechnology* **2011,** *6* (12), 815-823.

9. Wang, C. W.; Sinton, D.; Moffitt, M. G., Flow-Directed Block Copolymer Micelle Morphologies via Microfluidic Self-Assembly. *Journal of the American Chemical Society* **2011,** *133* (46), 18853-18864.

10. Karavelidis, V.; Karavas, E.; Giliopoulos, D.; Papadimitriou, S.; Bikiaris, D., Evaluating the effects of crystallinity in new biocompatible polyester nanocarriers on drug release behavior. *International Journal of Nanomedicine* **2011,** *6*, 3021-3032.

11. Gou, J. X.; Feng, S. S.; Xu, H. L.; Fang, G. H.; Chao, Y. H.; Zhang, Y.; Xu, H.; Tang, X., Decreased Core Crystallinity Facilitated Drug Loading in Polymeric Micelles without Affecting Their Biological Performances. *Biomacromolecules* **2015,** *16* (9), 2920-2929.

12. Zhang, W.; Li, Y.; Liu, L.; Sun, Q.; Shuai, X.; Zhu, W.; Chen, Y., Amphiphilic Toothbrushlike Copolymers Based on Poly(ethylene glycol) and Poly(ε-caprolactone) as Drug Carriers with Enhanced Properties. *Biomacromolecules* **2010,** *11* (5), 1331-1338.

13. Zhang, Y.; Li, J. S.; Lang, M. D.; Tang, X. L.; Li, L.; Shen, X. Z., Folate-functionalized nanoparticles for controlled 5-Fluorouracil delivery. *Journal of Colloid and Interface Science* **2011,** *354* (1), 202-209.

14. Xu, Z.; Yan, B.; Riordon, J.; Zhao, Y.; Sinton, D.; Moffitt, M. G., Microfluidic Synthesis of Photoresponsive Spool-Like Block Copolymer Nanoparticles: Flow-Directed Formation and Light-Triggered Dissociation. *Chemistry of Materials* **2015,** *27* (23), 8094-8104.

15. Bains, A.; Cao, Y. M.; Moffitt, M. G., Multiscale Control of Hierarchical Structure in Crystalline Block Copolymer Nanoparticles Using Microfluidics. *Macromolecular Rapid Communications* **2015,** *36* (22), 2000-2005.

16. Bains, A.; Wulff, J. E.; Moffitt, M. G., Microfluidic synthesis of dye-loaded polycaprolactone-block-poly(ethylene oxide) nanoparticles: Insights into flow-directed loading and in vitro release for drug delivery. *Journal of Colloid and Interface Science* **2016,** *475*, 136-148.

17. Xu, Z. Control of Structure and Function of Block Copolymer Nanoparticles Manufactured in Microfluidic Reactors: Towards Drug Delivery Applications. University of Victoria, 2016.

18. Djurdjic, B.; Dimchevska, S.; Geskovski, N.; Petrusevska, M.; Gancheva, V.; Georgiev, G.; Petrov, P.; Goracinova, K., Synthesis and self-assembly of amphiphilic poly(acrylicacid)-poly(epsilon-caprolactone)-poly(acrylicacid) block copolymer as novel carrier for 7-ethyl-10-hydroxy camptothecin. *Journal of Biomaterials Applications* **2015,** *29* (6), 867-881.

19. Du, Z. X.; Xu, J. T.; Fan, Z. Q., Regulation of micellar morphology of PCL-b-PEO block copolymers by crystallization temperature. *Macromolecular Rapid Communications* **2008,** *29* (6), 467-471.

20. Teng, Y.; Morrison, M. E.; Munk, P.; Webber, S. E.; Prochazka, K., Release kinetics studies of aromatic molecules into water from block polymer micelles. *Macromolecules* **1998,** *31* (11), 3578-3587.

21. Schabas, G.; Wang, C.-W.; Oskooei, A.; Yusuf, H.; Moffitt, M. G.; Sinton, D., Formation and Shear-Induced Processing of Quantum Dot Colloidal Assemblies in a Multiphase Microfluidic Chip. *Langmuir* **2008,** *24* (19), 10596-10603.

22. Wang, C.-W.; Sinton, D.; Moffitt, M. G., Flow-Directed Block Copolymer Micelle Morphologies via Microfluidic Self-Assembly. *Journal of the American Chemical Society* **2011,** *133* (46), 18853-18864.

23. Yamamoto, T.; Yokoyama, M.; Opanasopit, P.; Hayama, A.; Kawano, K.; Maitani, Y., What are determining factors for micelle carriers? Consideration stable drug incorporation into polymeric on physical and chemical characters of the micelle inner core. *Journal of Controlled Release* **2007,** *123* (1), 11-18.

24. Gref, R.; Minamitake, Y.; Peracchia, M. T.; Trubetskoy, V.; Torchilin, V.; Langer, R., BIODEGRADABLE LONG-CIRCULATING POLYMERIC NANOSPHERES. *Science* **1994,** *263* (5153), 1600-1603.

25. Huang, X.; Brazel, C. S., On the importance and mechanisms of burst release in matrix-controlled drug delivery systems. *Journal of Controlled Release* **2001,** *73* (2–3), 121-136.

26. Venkataraman, S.; Hedrick, J. L.; Ong, Z. Y.; Yang, C.; Ee, P. L. R.; Hammond, P. T.; Yang, Y. Y., The effects of polymeric nanostructure shape on drug delivery. *Advanced Drug Delivery Reviews* **2011,** *63* (14–15), 1228-1246.

27. Jeong, J. C.; Lee, J.; Cho, K., Effects of crystalline microstructure on drug release behavior of poly(epsilon-caprolactone) microspheres. *Journal of Controlled Release* **2003,** *92* (3), 249-258.

28. Chen, D. R.; Chen, H. L.; Bei, J. Z.; Wang, S. G., Morphology and

biodegradation of microspheres of polyester-polyether block copolymer based on polycaprolactone/polylactide/poly(ethylene oxide). *Polymer International* **2000,** *49* (3), 269-276.

29. Zhang, L.; Hu, Y.; Jiang, X.; Yang, C.; Lu, W.; Yang, Y. H., Camptothecin derivative-loaded poly(caprolactone-co-lactide)-b-PEG-b-poly(caprolactone-co-lactide) nanoparticles and their biodistribution in mice. *Journal of Controlled Release* **2004,** *96* (1), 135-148.

Chapter 3.

In vitro Cell Cytotoxicity Studies and Flow-Directed Anti-Cancer Activity of SN38-Loaded Block Copolymer Nanoparticles Produced by Microfluidics

3.1. Introduction

Although SN-38 is a prominent and efficacious anticancer drug, its clinical application is limited by poor solubility and susceptibility to hydrolysis into the carboxyl form, which has no therapeutic effect. In the previous chapter, we used block copolymer nanoparticles to encapsulate SN-38 using microfluidics and screened multiple chemical and flow parameters including total flow rate, initial drug-to-polymer ratio, water content and copolymer composition. We showed that for a given set of chemical conditions, flow rate provides an experimental handle on controlling the size, morphology, loading efficiency and release rates of SN38-loaded nanoparticles. Specifically, SN38-loaded nanoparticles with various sizes and morphologies were produced in the unique microfluidic environment of flow-variable shear. We showed a decrease of the *in vitro* release rate of SN-38 for nanoparticles synthesized at higher flow-rates. We propose that microfluidic flow rate should also influence the behaviour of the resulting SN-38 nanoparticles against cancer cells.

In this chapter, we will further investigate how microfluidic-prepared drug-loaded nanoparticles influence the cytotoxicity of SN-38 and if the flow rate influences cytotoxicity. The cell line used in this study is a human breast adenocarcinoma cell line, MCF-7. As a cancerous epithelial cell, MCF-7 has high proliferation potential, as well as high resistance to multiple anticancer agents, which make it a good system for cytotoxicity studies.[1] The mechanism by which SN-38 exerts its cytotoxicity is related to its ability to inhibit topoisomerases which are essential enzymes that adjust and regulate the topology of DNA.[2] This kind of DNA damage also procures cell cycle arrest in cancer cells which is not advantageous for killing cancer cells.[3] The cytotoxicity of SN-38 can be affected by various factors including dose and exposure time.

For drug delivery applications of nanoparticles, a variety of considerations may determine the influence of encapsulating nanoparticles on drug cytotoxicity. Cells usually take up particles and macromolecules by two main endocytic mechanisms, phagocytosis and pinocytosis.[4] Large particles (>1 μm) are generally internalized by phagocytosis mechanisms while nanoparticles are more likely to undergo pinocytosis. Recent studies have showed that for different types of tumor cells, the optimal size for cellular uptake varies a lot.[5] In general, particles around 10-100 nm are acceptable for *in vivo* application, because larger particles might be cleared by the immune system and smaller ones are prone to be filtered by kidney. Permeability and extravasation of nanoparticles up to 400 nm through endothelial gaps has been observed in mouse xenograft models of human cancers (enhanced permeation and retention effect, EPR).[6] In addition to size effects, the degree of roughness on nanoparticle surfaces can affect their cytotoxicity by influencing their binding to cells.[7] The local protrusions or depressions on the nanoparticle surface can minimize repulsive forces between cellular and nanoparticle surfaces.[8] The elastic properties of nanoparticles can also play an important role in the pharmacokinetic and biodistribution of particles; more flexible and deformable particles can traverse blood vessels and pores more easily *in vivo*.[9] Due to the variations of size and morphology of SN-38 loaded polymer nanoparticles prepared at different flow rates on chip, we investigated in this chapter if they would exhibit different *in vitro* cytotoxicities against the MCF-7 cancer cell line.

3.2. Experimental

3.2.1 Materials. P(MCL-*co*-CL)$_{12k}$-*b*-PEO$_{5k}$ was synthesized by Dr. Changhai Lu and is described in detail in the previous chapter; it is referred to throughout the thesis as PMCLCL. *N*, *N*-dimethylformamide (DMF, Caledon, 99.8%), acetonitrile (ACN, Caledon, HPLC grade) were used as received without further purification. 7-Ethyl-10-hydroxycamptothecin (≥98.0%, HPLC grade) was purchased from AK scientific. The MCF-7 (human adenocarcinoma breast cancer) cell line was obtained as a generous gift from the BC Cancer agency. The CellTiter-Blue Viability Assay kit (Premega) was used. Dulbecco's Modified Eagle Medium (with the addition of 4.5 g/L D-Glucose, L-Glutamine, 110 mg/L Sodium Pyruvate) was purchased from Life Technologies. Trypsin-EDTA (0.25 % Trypsin / 0.63 mM EDTA) and Fetal Bovine Serum were purchased from Sigma-Aldrich.

3.2.2 Preparation of SN-38-Loaded PMCLCL Nanoparticles. Bulk and microfluidic preparations of SN-38-loaded PMCLCL nanoparticles are described in detail in the previous chapter. Based on results in Chapter 2, we selected a single initial drug-to-polymer ratio of r = 0.75 for bulk and microfluidic preparations of nanoparticles for cytotoxicity studies; for the microfluidic preparations, a single water content of cwc + 5 wt % was selected. Cytotoxicity studies were carried out for four different total flow rates of microfluidic-prepared nanoparticles, Q = 50, 100, 200 and 400 μL/min. The concentrations of SN-38 in samples were determined by high performance liquid chromatography (HPLC, Agilent1100) along with C18 column (Agilent Zorbax SB-C18) and a UV detector set at 265 nm. Specific details can be found in Chapter 2. Three different runs of each condition were conducted for sample preparation of cell line study.

3.2.3 Cell Culture Growth and Cytotoxicity Assays. MCF-7 cancer cell lines were cultured in Dulbecco's modified eagle medium (DMEM) supplemented with 10% fetal bovine serum (FBS). Subsequently, the cell lines were grown at 37 °C in a humidified atmosphere containing 5 % CO_2.

The CellTiter-Blue™ assay was used to evaluate the cytotoxic activity of SN38-loaded nanoparticles. This test is based on the metabolic activity of cells. Viable cells are able to reduce the indicator dye resazurin into the highly-fluorescent resorufin. Nonviable cells with low metabolic activity will result in a low fluorescent signal. In order to perform the cytotoxicity assay, the growing cells were trypsinized, resuspended and centrifuged (4 °C) at low-g (Allegra™ X-12R Centrifuge) to a pellet. The cells were then resuspended, and diluted to 1.0×10^5 cells / mL after determination of concentration using a hemocytometer (Bright Line, 0.1mm deep). A 100 µL/well cell suspension was seeded in 96-well plates and incubated for 24 hours (37 °C, 5 % CO_2 air humidified). 6.5 µL aliquots of either: 1. SN-38-loaded PMCLCL nanoparticles 2. SN-38 solution in DMSO or 3. DMSO (control) were added to 643.5 µL of DMEM media (10% FBS) to obtain the highest working concentration of SN-38. Serial dilutions were conducted to get a range of SN-38 concentrations for analysis. A volume of 100 µL solution of each well was transferred to the corresponding well of sample plates to treat cells (Figure 3-1). The treated cells were incubated for 48, 72 and 96 hours (37 °C, 5 % CO_2 air humidified). After that, 20 µL of CellTiter-Blue™ was added to each well, followed by 4-hours incubation (37 °C, 5 % CO_2 air humidified). Fluorescence absorbance at λ_{ex} = 560 nm, λ_{em} = 590 nm was then determined on a plate reader (SpectraMax M5). IC_{50} (half maximal inhibitory concentration) values of SN38-load nanoparticles against MCF-7 cell line were obtained based on fitted concentration response curves (Figure 3-2).The curves were generated by XLFit (add-in of Microsoft Excel) and fitted using the same model:

$$y = \frac{\mathrm{A}x}{\mathrm{B}+x}\frac{\mathrm{C}x}{\mathrm{D}+x}$$

where y is the %Inhibition and x is the concentration of SN-38. %Inhibition of cells is calculated using the following formula:

$$\%\ \text{Inhibition} = 100 \times (1 - \frac{A_{\text{sample}} - A_{\text{blank}}}{A_{\text{control}} - A_{\text{blank}}})$$

where A_{sample} was the reading of cells + drug + media, A_{blank} was the reading of media alone, and A_{control} was the reading of cells + media (without drug).

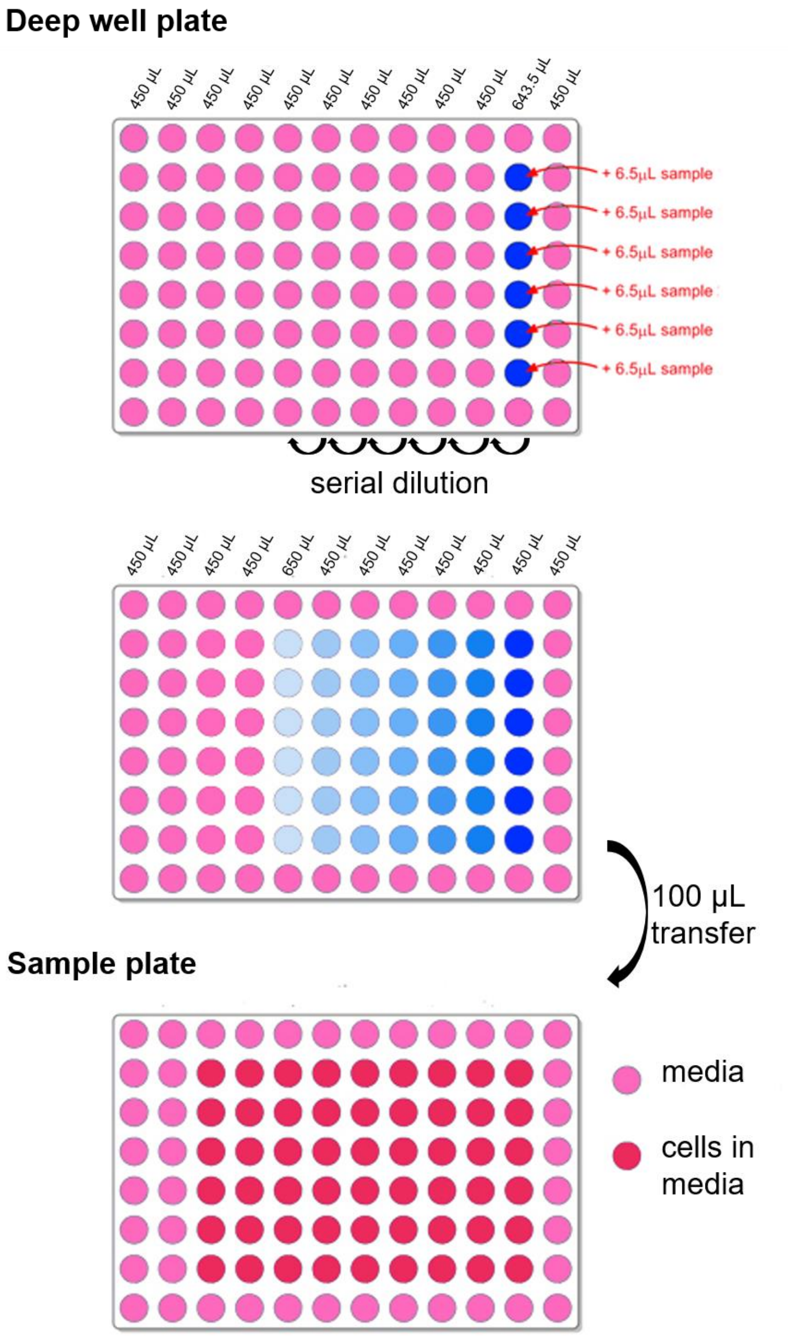

Figure 3- 1. Schematics showing the setup of deep well plates and sample plates.

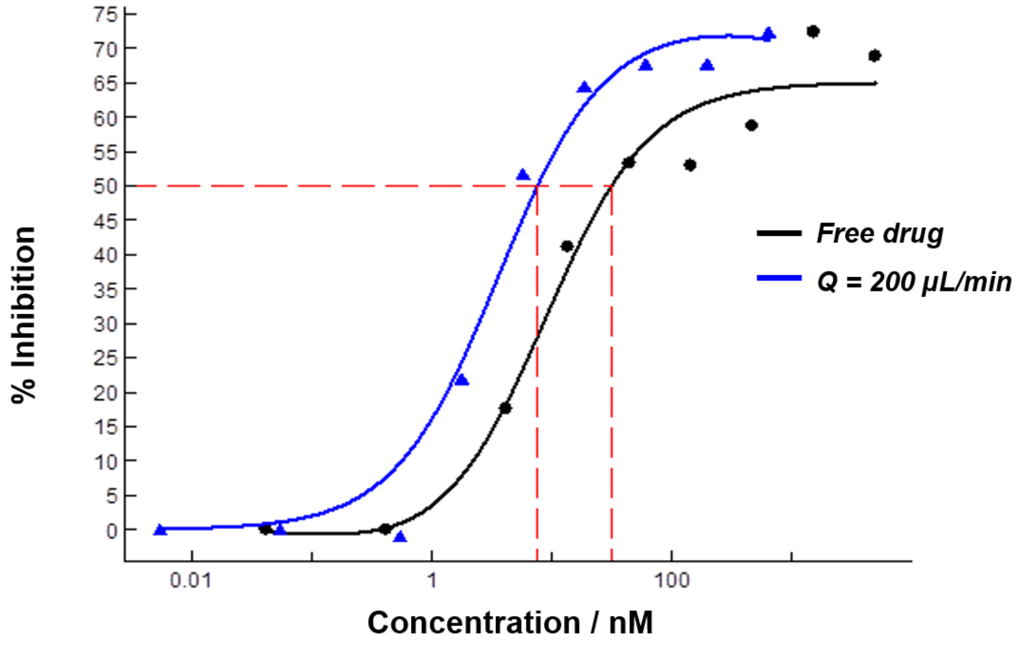

Figure 3- 2. Examples of fitted concentration response curve.

3.3. Results and Discussion

As described in the Experimental section, we investigated cell viability assays for 1 bulk-prepared sample and 4 microfluidic-prepared sample (4 flow rates) of SN-38-loaded PMCLCL nanoparticles. These 5 nanoparticle formulations were compared with assay results for free SN-38 in the absence of nanoparticles. All the samples were used to treat MCF-7 (human breast adenocarcinoma) cell lines for three time periods: 48, 72 and 96 hours. Half maximal inhibitory concentration (IC_{50}) was used to evaluate the cytotoxicity of each samples. The IC_{50} results (Figure 3-3) reveal that all the samples have high toxicity (IC_{50} < 100 nM) against MCF-7, but show different cytotoxicity for different preparation conditions and incubation times.

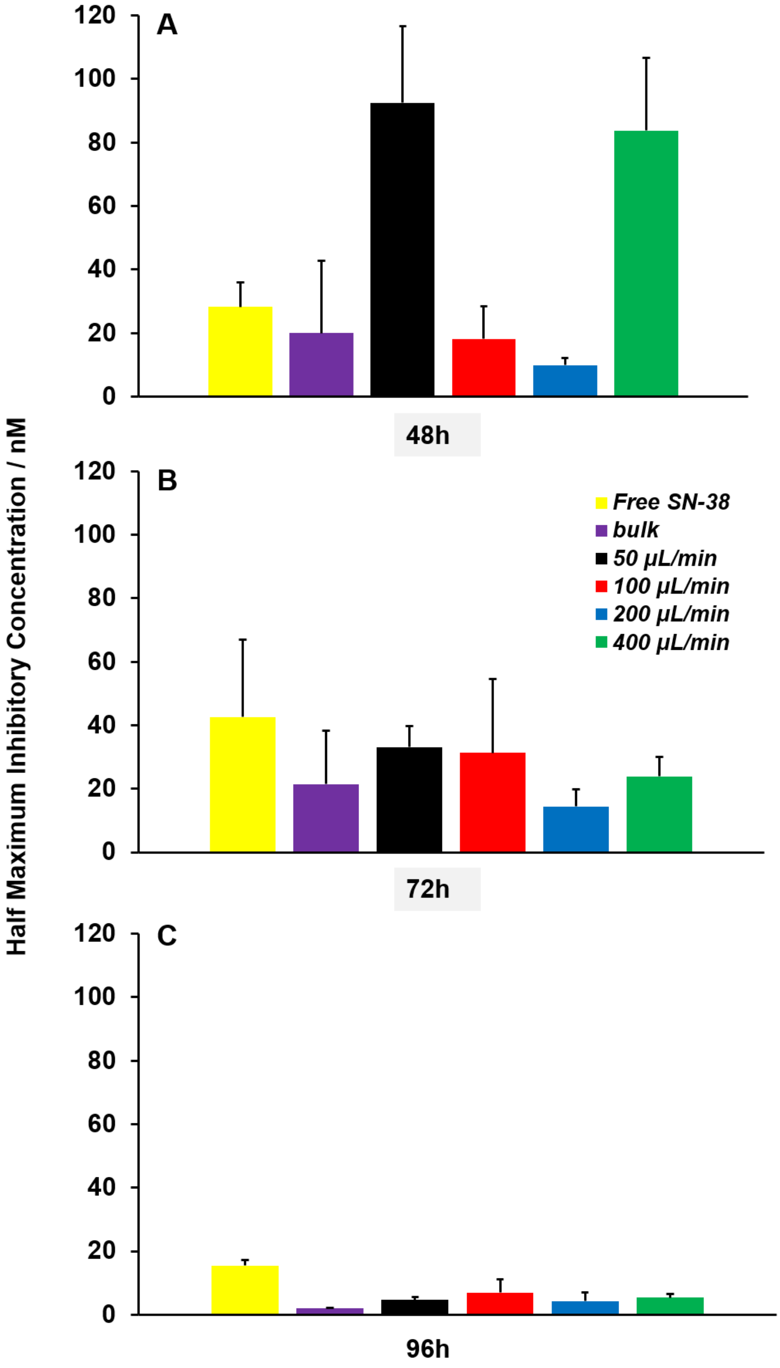

Figure 3- 3. IC_{50} of free SN-38, SN38-loaded P(MCL-*co*-CL)-*b*-PEO nanoparticles prepared in bulk and at 4 different flow rate on chip at 3 different incubation time 48h (A), 72h (B), 96h (C). Error bars are from three separate assays.

3.3.1 Comparison of Cytotoxicities of Free SN-38 and SN38-loaded PMCLCL Nanoparticles at Different Incubation Times.

We first compare the IC_{50} values of free SN-38 with the various SN38-loaded nanoparticles at different incubation times (48, 72, 96h). At 48 h, IC_{50} values of all SN-38 nanoparticles, except microfluidic nanoparticles prepared at Q = 50 and 400 μL/min, are lower than those of the free-drug. At 72 and 96 h, all the SN38-loaded nanoparticles show lower IC_{50} value than the free SN-38. This illustrates that, under most preparation conditions and incubation times, when SN-38 is encapsulated in the PMCLCL nanoparticles it is more potent to kill the cancer cells. As mentioned before, SN-38 is not stable in physiological environments due to its pH sensitivity. We propose that encapsulation of SN-38 increases its activity because the delivery vehicle minimizes contact with the physiological environment which limits its hydrolysis to the therapeutically inactive form. Therefore, more drug is kept intact and active prior to cellular uptake.

In general, most of the investigated SN-38 formulations exhibited similar cytotoxicities (similar IC_{50} values) for 48h and 72 h; the exceptions were free SN-38, which showed decreased cytotoxicity (increased IC_{50} value) at 72 h, and microfluidic nanoparticles prepared at Q = 50 and 400 μL/min, which both showed increased cytotoxicities (decreased IC_{50} values) at 72 h. All of the formulations showed increased cytotoxicities (decreased IC_{50} values) between 72 h and 96 h. It is possible that higher cytotoxicities at 96 h are related to release of SN-38 from the nanoparticles over this period and also the time required for SN-38 to induce apoptosis in MCF-7. The decreasing cytotoxicities between 48 h and 72 h for free drug and for some microfluidic formulations might be related to the rapid growth of MCF-7 and the recovery of cells after the initial dose. In other words, these timedependent results indicate that the incubation time of both free drug and various nanoparticle formulations strongly affects their toxicity to the MCF-7 cell line.

3.3.2 Effect of Preparation Conditions on Cytotoxicities of SN38-loaded PMCLCL Nanoparticles.

At incubation times of 48 and 72 h, similar trends of IC_{50} values were observed for microfluidic-prepared nanoparticles, which is $Q = 50 > 400 > 100 > 200$ μL/min. (IC_{50} for bulk-prepared nanoparticles is within the range.) This surprisingly agrees with the trend of size of these nanoparticles, rather than the *in vitro* release half times (discussed in Chapter 2). Some previous studies proposed that particles in the 40-50 nm range exhibit maximal cellular internalization *in vitro*.[5] In the CONTIN results in Chapter 2 (Figure 2-7), we see the existence of extremely large aggregates around 10 μm at the lowest flow rate ($Q = 50$ μL/min). This portion of nanoparticles are not expected to take up by cells because drug-loaded micelles are more likely internalized into cells via pinocytosis, and the uptake of larger particles are through phagocytosis, which can be only found on professional phagocytic cells, such as macrophages, neutrophils, or dendritic cells.[10] In pinocytosis, otherwise known as cell drinking, small particles are brought into the cell, forming an invagination, and then suspended within small vesicles.[4] The lowest cytotoxicity of nanoparticles prepared at $Q = 50$ μL/min could be attributed to this effect. At $Q = 200$ μL/min, the smallest nanoparticle average sizes and lowest population dispersities were obtained by DLS (Figure 2-7 I, 2-8) and only small spheres were seen by TEM (Figure 2-6 I) which may explain their higher toxicities, since they are more likely to internalize into cell. On the other hand, at incubation time of 96 h, no significant difference can be observed for all the SN38-encapsulated nanoparticles. We hypothesize that by this time most of the drug has been released from the nanoparticles such that cytotoxicity is not influenced by the nanoparticle sizes and morphologies. Cell internalization pathways could be probed in the future, in order to further investigate how nanoparticles internalize with cells.

3.4 Conclusion

In this chapter, we investigated that how preparation methods influence the cytotoxicity of SN38-loaded nanoparticles against MCF-7. In general, for the two shorter incubation time, microfluidic nanoparticles produced at Q = 200 µL/min with pure spherical structures and smallest overall size generates the highest cytotoxicity and those produced at 50 µL/min with large aggregates (> 1 µm) generates the lowest cytotoxicity. However, all the block copolymer formulations improved the activity of the anti-cancer drug, SN-38, regardless of the preparation method. As a matter of fact, to understand the polymer nanoparticle cytotoxic response more deeply, more studies are necessary, such as internalization, cell retrace of cellular uptake, cell recovery assay, DNA fragmentation analysis, etc.

3.5 Supporting Information

Please See Appendix C for supporting information: IC_{50} value for all the conditions.

3.6 References

1. Zhang, F.; Wang, X.; Xu, X.; Li, M.; Zhou, J.; Wang, W., Reconstituted high density lipoprotein mediated targeted co-delivery of HZ08 and paclitaxel enhances the efficacy of paclitaxel in multidrug-resistant MCF-7 breast cancer cells. *European Journal of Pharmaceutical Sciences* **2016,** *92,* 11-21.

2. Bala, V.; Rao, S.; Boyd, B. J.; Prestidge, C. A., Prodrug and nanomedicine approaches for the delivery of the camptothecin analogue SN38. *Journal of Controlled Release* **2013,** *172* (1), 48-61.

3. Yin, M.-B.; Li, Z.-R.; Cao, S.; Durrani, F. A.; Azrak, R. G.; Frank, C.; Rustum, Y. M., Enhanced 7-Ethyl-10-hydroxycamptothecin (SN-38) Lethality by Methylselenocysteine Is Associated with Chk2 Phosphorylation at Threonine-68 and

Down-Regulation of Cdc6 Expression. *Molecular Pharmacology* **2004,** *66* (1), 153-160.

4. Conner, S. D.; Schmid, S. L., Regulated portals of entry into the cell. *Nature* **2003,** *422* (6927), 37-44.

5. Jiang, W.; KimBetty, Y. S.; Rutka, J. T.; ChanWarren, C. W., Nanoparticle-mediated cellular response is size-dependent. *Nat Nano* **2008,** *3* (3), 145-150.

6. Yuan, F.; Dellian, M.; Fukumura, D.; Leunig, M.; Berk, D. A.; Torchilin, V. P.; Jain, R. K., Vascular Permeability in a Human Tumor Xenograft: Molecular Size Dependence and Cutoff Size. *Cancer Research* **1995,** *55* (17), 3752-3756.

7. Hoek, E. M. V.; Agarwal, G. K., Extended DLVO interactions between spherical particles and rough surfaces. *Journal of Colloid and Interface Science* **2006,** *298* (1), 50-58.

8. Nel, A. E.; Madler, L.; Velegol, D.; Xia, T.; Hoek, E. M. V.; Somasundaran, P.; Klaessig, F.; Castranova, V.; Thompson, M., Understanding biophysicochemical interactions at the nano-bio interface. *Nat Mater* **2009,** *8* (7), 543-557.

9. Merkel, T. J.; Jones, S. W.; Herlihy, K. P.; Kersey, F. R.; Shields, A. R.; Napier, M.; Luft, J. C.; Wu, H.; Zamboni, W. C.; Wang, A. Z.; Bear, J. E.; DeSimone, J. M., Using mechanobiological mimicry of red blood cells to extend circulation times of hydrogel microparticles. *Proceedings of the National Academy of Sciences* **2011,** *108* (2), 586-591.

10. Zhao, F.; Zhao, Y.; Liu, Y.; Chang, X.; Chen, C.; Zhao, Y., Cellular Uptake, Intracellular Trafficking, and Cytotoxicity of Nanomaterials. *Small* **2011,** *7* (10), 1322-1337.

Chapter 4. New Microfluidic Strategies for High-Shear Particle Formation: Comparison of Reactor Designs for Manufacturing Polymeric Nanoparticles

4.1. Introduction

As demonstrated in previous chapters, gas-liquid segmented microfluidics provides a top-down method to precisely control the self-assembly process of block copolymers. As a result, the size, morphologies, crystallinity and other physical and chemical properties of nanoparticles can be altered simply and efficiently.

There are two types of microfluidic reactors. One is the single-phase reactor, in which the mixing is dominated by diffusion. The other is multi-phase reactor, which can be divided into liquid-liquid segmented reactors and gas-liquid segmented reactors. In single-phase reactors, previous strategies to enhance mixing include introducing chaotic advection through patterned channel walls[1,2]and mixing through 3D channel networks.[3] The fabrication of these reactors usually involves additional processing steps, and surface profiling and 3D networks may lead to the concern of particles' deposition.

In terms of multi-phase reactors, Ismagilov et al.[4,5] invented a micromixer in which fast mixing was achieved by recirculation within the liquid plugs consisting of multiple solutions of reagents. Jensen et al. proposed a design based on segmented gas-liquid flow.[6] And this type of microreactor was applied to block copolymer self-assembly by Moffitt group, both in this thesis and in previous work from the group.[7,8,9,10] Gas bubbles compartmentalize the liquid flow of reactants into liquid plugs, in which counter-rotating vortices can greatly increase mixing *via* chaotic advection. Numerical modeling has shown that the maximum shear rate on the chip used in both Chapter 2 and Chapter 3 at 25 µL/min is 1×10^5 s^{-1}, which increases linearly with the flow rate.[11] The high-shear "hot spots" can become a control handle on the fabrication of nanoparticles, inducing break-up, coalescence,[7] and crystallization of nanoparticles.[9]

In Chapter 2, we showed that the highest flow rate investigated (Q = 400 µL/min) results in a relatively slow *in vitro* drug release of SN38-loaded P(MCL-*co*-CL)-*b*-PEO nanoparticles compared to other flow rate (Q = 50, 100, 200 µL/min). This inspired us to further explore possibilities of on-chip synthesis of drug-loaded nanoparticles under conditions of even higher flowrate. Another motivation is the requirement of high throughput for drug delivery application, which is enabled by high flow rate. The quest for higher on-chip shear rates led us to consider different materials for microfluidics, which may offer additional advantages over the PDMS used for all microfluidic chips described in previous chapters.

The main advantage of PDMS is its ease and low cost of microfabrication. The major method is soft lithography, which consists of rapid prototyping and replica molding. Other merits of PDMS arise from its high elasticity and gas permeability. Despite its broad use nowadays, there are still some limitations for its application in polymer nanoparticles preparation. For example, its incompatibility with some kinds of organic solvent limits the selection of solvent for polymer and drug (in the case of drug-loaded nanoparticle preparation). The absorption of hydrophobic molecules into PDMS channel walls and their hydrophobic interactions with block copolymers may lead to clogging of the microchannel. Most importantly, the low rigidity of PDMS cannot support a pressure drop higher than ~20 bar within the microsystem without delamination of the chips.[12] Thus, we can't explore much higher shear or achieve higher throughput by greatly increasing the flow rate, since the PDMS chips would fall apart due to the resulting high internal pressures.

To resolve this problem, a microfluidic reactor with an identical design to that described in Chapters 2 and 3, but made of silicon/glass rather than PDMS is fabricated. Glass and silicon, the first generation microfluidic device materials, are perfect for capillary electrophoresis and solvent-involved applications. They are resistant to corrosion from most chemicals except for strong acids. However, both of them also have some drawbacks. Silicon is expensive and opaque in the visible/UV region. Glass is transparent but hard to etch into vertical sidewalls due to the amorphous properties. So combination of silicon and glass can allow for optical access through the glass, investigation of various solvents, high pressure generated by high flow rate and easier cleaning, in order to expand the range of our study on shear-induced manufacturing of drug-loaded nanoparticles.

In addition to new chip materials, we were also interested in exploring a new microfluidic reactor design for enabling high shear that may provide higher shear rates and more convenient running conditions than the reactor described in previous chapters. In our current gas-liquid segmented reactor, precise control of gas and liquid flow rates becomes more difficult as the flow rates are increased to achieve higher shear rates. Therefore, in collaboration with Prof. Dave Sinton’s group, a new single-phase reactor design for the generation of localized high-shear regions without the requirement of gas is proposed.

In this chapter, we explore two new microfluidic strategies for the generation of block copolymer nanoparticles under high shear conditions. In the first case, a silicon/glass chip with the same design as PDMS chip was made and used to synthesize PCL-*b*-PEO nanoparticles with three different block length of PCL, at 4 different flow rates, and collected samples were characterized by TEM and DLS. In the second case, the silicon/glass single-phase reactor was fabricated and the high shear region was calculated to have orders of magnitudes higher shear rate than the two-phase reactor at the same flow rate.

4.2. Experimental

4.2.1 Materials. Poly(caprolactone)-*b*-poly(ethylene oxide) (PCL-*b*-PEO) with constant block length of PCL and different block lengths of PCL were purchased from Advanced Polymer Inc. and used as received: $PCL_{2.1k}$-*b*-PEO_{5k}; $PCL_{6.4k}$-*b*-PEO_{5k}; PCL_{12k}-*b*-PEO_{5k} (numbers in subscripts represent number-average molecular weights of the blocks; theses polymers are referred to simply as PCL2k, PCL6k and PCL12k, respectively). *N*,*N*-dimethylformamide (DMF, Caledon, 99.8%), was used as received without further purification.

4.2.2 Critical Water Content (cwc) Determination. Critical water contents were determined using static light scattering measurements by Aman Bains[13] previously in our group. The cwc values for the 0.33 wt % solutions of PCL2k, PCL6k and PCL12k in DMF are 13.1 ± 0.2 wt %, 6.3 ± 0.2 wt %, 5.5 ± 0.4 wt %.

4.2.3 Design and Rationale of Single-Phase High-Shear Reactor. The single-phase reactor was designed by Dr. Jason Riordan in Prof. David Sinton's group (University of Toronto) and is shown in Figure 4-1 A. Eight sections of narrow channels of *width* × *height* × *length* = 8 µm × 8 µm × 100 µm (one of them is enlarged in the inset of Figure 4-1) are connected in an alternating manner with nine sections of wide channel of 55 µm × 55 µm × 111 cm. Numerical calculations by Jason Riordan showed the shear rate will be higher in the narrow sections of the single-phase reactor than the maximum shear rate in the two-phase reactor at the same flow rate. Since the dwell time would decrease dramatically if the entire channel was narrow, the short, narrow sections were distributed between long, wide sections, leading to period alternating exposure of particles to high and low shear. The design of the inlets (Figure 4-1 A) corresponds to the spacing of holes in the stainless-steel manifold.

4.2.4 Silicon/Glass Microfluidic Reactor Fabrication. Silicon/glass chips were fabricated by Dr. Huawei Li in the Sinton lab (Department of Mechanical & Industrial Engineering, University of Toronto) using the following method. Positive photoresist (S1818) was spin-coated onto a silicon wafer (4’’ diameter, 1 mm thick). Photolithography and deep-reactive-ion-etching (DRIE) were used to etch the desired pattern (Figure 4-1) with the desired depth into the silicon wafer. Holes were drilled through the silicon for inlet and outlet ports. The silicon wafer and borosilicate glass (S.I. Howard Glass, Worcester, MA, USA) were cleaned using Piranha solution (3:1 ratio of H_2SO_4 and H_2O_2) for ~ 1 h. Then, silicon wafer and glass substrates were anodically bonded using a voltage of 600 V, a current of 4 mA at pressure of 10^{-7} bar for ~20 minutes. Finally, the resulting glass-silicon wafers were cut into appropriate sizes for use.

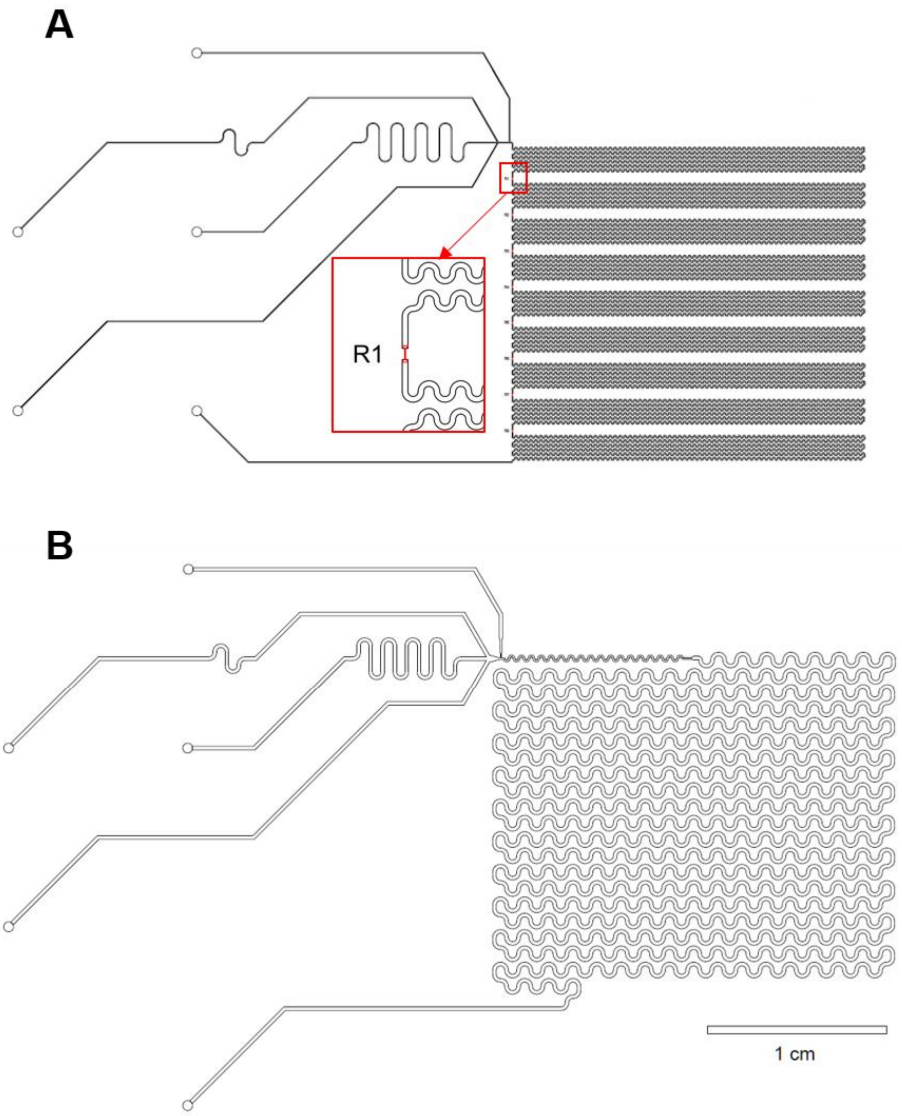

Figure 4- 1. Design of single-phase (A) and two-phase (B) silicon/glass chips.

Before use, the chips were installed on a custom stainless steel manifold (Figure 4-2). O-rings for seals were placed between the chip and the manifold. High-pressure connection components (Swagelok) provided connection to the stainless steel tubing with precise alignment of the connected components.

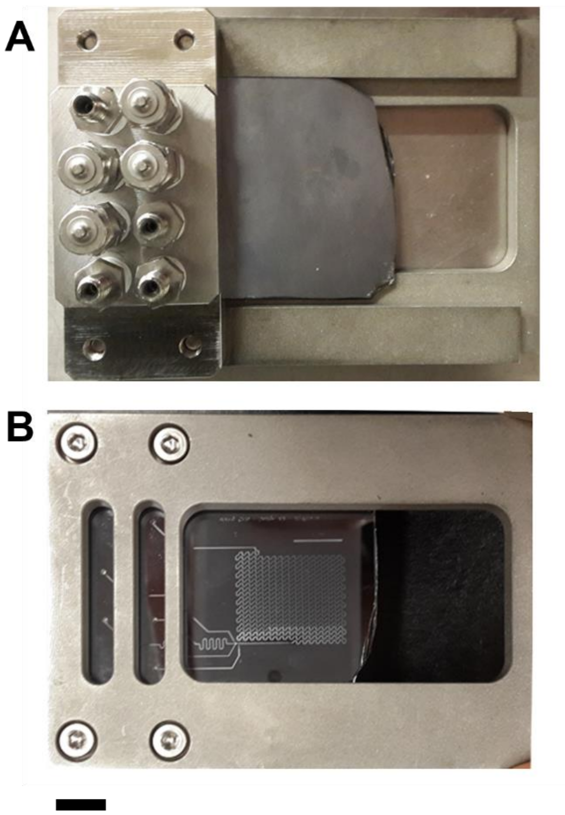

Figure 4- 2. Schematic of a silicon/glass chip installed on a manifold (A) shows the holes for connection to tubing (B) shows the other side of the chip. Scale bar is 1 cm.

4.2.5 PDMS Microfluidic Reactor Fabrication. PDMS chips were fabricated using the same method described in the previous chapter. Briefly, the elastomer and curing agent were mixed at a 7:1 and degassed under vacuum. The mixture was poured over a clean negative master chip (the same one as used in previous chapters) in a Petri dish and further degassed for ~30 minutes. The PDMS was heated at 85 °C for ~30min until hard, and then peeled from the negative master; holes were punched for the insertion of tubing. A glass substrate was spin-coated using a mixture consisting of 20:1 elastomer and cutting agent. Both the chip and the substrate layer were treated with oxygen plasma for 90s and bonded together. Only the two-phase reactor (Reactor B) was fabricated in PDMS and channel dimensions were identical to those of the silicon/glass-fabricated two-phase reactor.

4.2.6 Flow Delivery and Control. Due to the different behavior of flow in silicon/glass chip and PDMS chip (Detailed discussion is in Section 4.3.2), the total flow rates of two chips are difficult to keep the same. Thus, two chips were compared at constant liquid flow rate.

For the gas-liquid silicon/glass chip, an inverted fluorescent microscope (Leica DMLM) was used to image the bubbles in the microchannel with a 10× objective. The images were captured with a high speed camera (model PCO 1200s) at a frame rate of 500 frames per second. The exposure time was 2ms. The manifold was connected to liquid syringes via stainless steel tubing. Gas flow was introduced to the chip via a high-pressure regulator for N_2 tank and a downstream regulator (SMC Pneumatics) for fine adjustment. A valve was put in the middle of two regulators to open/close the gas. The liquid flow rate (Q_{liq}) was set up on syringe pumps (50, 100, 200, 300, 1000 µL/min) and the gas flow rate (Q_{gas}) was tuned via the downstream pressure regulator in order to obtain a stable flow with separated gas and liquid plugs. To begin an experiment, liquid was first introduced into the microchannel through 3 liquid inlets, while the gas inlet was closed by a connected valve. After the chip was filled with liquid, the valve was opened to allow the gas to enter the channel from the gas inlet. Gas bubbles were controlled by precisely adjusting the regulator to form stable gas-liquid segments, corresponding pressure on regulator was 90, 150, 200 and 1000 kPa

For the cases of lower Q_{liq} (50, 100, 200, 300 µL/min), the flow rate of gas can be calculated based on the images taken during the collection of samples. Specifically, the distance travelled by the gas plug in 20 ms can be measured using Image J. The distance was then multiplied by sectional area of the channel and divided by 20 ms to determine the flow rate of the gas plug. Flow rates of three different gas plugs within the same range of the chip were calculated 3 times during each run, in order to get an average gas flow rate. For the case of the highest Q_{liq} (1000 µL/min), due to the limitation of the camera, flow patterns were not able to be monitored.

For the gas-liquid PDMS chip, the visualization of gas and liquid plugs was achieved using and upright optical microscope (Omax) with a 3× objective. Images were captured using a 2.07 megapixel PipilCam (Ken-A-Vision). The exposure time was 1 s. The chip was fitted with 3 liquid syringes via Teflon tubing. Gas flow was introduced to the chip via a downstream regulator (Johnston Controls) for fine adjustments and an Ar tank regulator. The liquid flow rate (Q_{liq}) was set up on syringe pumps (100, 200 µL/min) and the gas flow rate (Q_{gas}) was fine-tuned via the downstream pressure regulator in order to get a flow pattern with same length of gas and liquid plugs. Q_{gas} was calculated based on the relative length of gas plug to the length of liquid plug in the images taken. 3 images were taken during each run. The average value of Q_{gas} was obtained from the same range in 3 images. The detailed method was described in previous papers in our group.[7]

For single-phase silicon/glass chip, due to the high pressure resistance of the chip, the liquid could not be injected into the microchannel directly by syringe pumps. Thus, the liquid was first injected into stainless steel tubing (1/16th-inch OD, 6 ft.) via syringes mounted on syringe pumps. Then the liquid in the tubing was pressurized into the chip by high pressure N_2 controlled by a high pressure regulator.

4.2.7 Nanoparticles Synthesis in Two-phase Segmented Microfluidic Reactor. Three liquid streams were set at equal flow rate using syringe pumps: 1.0 wt% solution of PCL-*b*-PEO (PCL12k, PCL6k, and PCL2k) in DMF; pure DMF; a DMF/water mixture containing 54.3 wt% for PCL12k, 33.8 wt% for PCL6k and 31.5 wt% for PCL2k. Combination of the three liquid streams yielded steady-state concentrations of 0.33 wt% copolymer and water content of cwc + 5 wt%. For each preparation, small amounts of sample were collected into a small vial and used to prepare sample for TEM immediately after collection. Then, colloidal dispersions in DMF/water were collected into vials containing 10 × volume excess deionized water. The quenched samples were ready for DLS measurements.

4.2.8 Attempted Nanoparticles Synthesis in Silicon/glass Single-phase Microfluidic Reactor. Flow was tested by pressurizing pure DMF into the reactor. The flow moved much more slowly inside channel than expectation based on calculation, followed by a full stop of the flow. Then, the channel was carefully checked by fluorescent microscope (Leica DMLM) and clogging was found at the first junction. A several of cleaning methods were applied. First, the outlet of the chip was connected to a high pressure pump (Teledyne Isco) filled with deionized water. The pressure was set up to be 10 MPa, in order to push the obstruction out the front inlet. The chip was submerged in a water bath for safety. Since this method failed to clear the clogging, another method was used. Specifically, the chip was heated at 150 °C under vacuum for 30 min. Then the chip was heated to 650 °C and maintained for 6 h. After cooling down, the chip was treated with vacuum at 200 °C for 1 h. Then, the chip was submerged in HCL and placed in vacuum for 10 min, followed by ultrasound cleaning. Next, the chip was submerged in acetone and placed in vacuum for another 10 min, followed by ultrasound cleaning. At last, the chip was rinsed by submerging it in deionized water and applying vacuum.

4.2.9 Transmission Electron Microscopy. TEM imaging of samples synthesized on the silicon/glass chip was conducted on Hitachi H-7000 equipped with AMT 1K digital camera, operating at voltage of 75kV, whereas TEM of samples synthesized on the PDMS chip was conducted on JEOL JEM-1400 equipped with a Gatan Orius SC1000 CCD camera, operating at voltage of 65 kV.

Negatively-stained samples for TEM imaging were prepared by depositing a drop of sample on a carbon-coated 300-mesh copper TEM grid followed by a drop of 1 wt % uranyl acetate aqueous solution as a negative staining agent. Excess liquid was immediately removed using paper towel, followed by drying of the remaining liquid under ambient conditions.

4.2.10 Dynamic Light Scattering. Effective hydrodynamic diameters obtained from cumulent analysis, intensity-averaged and number-averaged size distribution based on CONTIN analysis were determined using dynamic light scattering (DLS). DLS measurements of samples synthesized on the silicon/glass chip were carried out by Malvern Zetasizer Nano S and those of samples synthesized on the PDMS chip were carried out by a BI-9000AT digital autocorrelator, and a Melles Griot He-NE Laser (633nm) with a maximum power output of 75mW. All DLS measurements were performed in DMF/water mixture and an experimental temperature of 23 °C and at a scattering angle of 90˚. Three measurements were taken from which effective hydrodynamic diameter and corresponding size distributions were determined using cumulent and CONTIN analysis, respectively.

4.3. Results and Discussion

4.3.1. Effect of Flow Rate and Block Copolymer Composition on Sizes and Morphologies of PCL Nanoparticles: Two-Phase Silicon/Glass Microfluidic Reactor.

Figure 4-2 shows TEM images for the polymeric nanoparticles synthesized in the two-phase silicon/glass microfluidic reactor, from three block copolymers of different PCL block lengths and four different flow rates, as well as the corresponding DLS data below each TEM images showing the size distribution of nanoparticles.

If we look at the conditions of three copolymer nanoparticles with different PCL block length, we find that the changes of size and morphology with respect to flow rate are different for different copolymers. For PCL12k, at the lowest flow rate, there are three size populations and large aggregates present (Figure 4-3 A). As flow rate increases to 300 µL/min, samples yield increasing number of spheres and appearance of short rods (Figure 4-3 B) and branched aggregates of short rods (Figure 4-3 C). At the highest flow rate, large lamellae with a broad size distribution appear (Figure 4-3 D). PCL6k demonstrate a more monotonic trend from Q_{liq} = 100 µL/min to Q_{liq} = 300 µL/min. Cylinders become shorter and spheres become smaller, at the same time, smaller particles represent a larger proportion of the overall population with increasing flow rate (Figure 4-3 E-G). However, at the highest flow rate, ring-like aggregates were found, possibly due to coalescence of spheres (Figure 4-3 H). For PCL2k, morphologies like donuts and needles are observed at Q_{liq} = 100 µL/min and 200 µL/min, respectively (Figure 4-3 I and J), while both Q_{liq} = 300 µL/min and Q_{liq} = 1000 µL/min produce bimodal populations of spherical aggregates (Figure 4-3 K and I). At this time, we are not able to tell if they are spheres or vesicles. TEM images without staining of nanoparticles can be checked to determine.

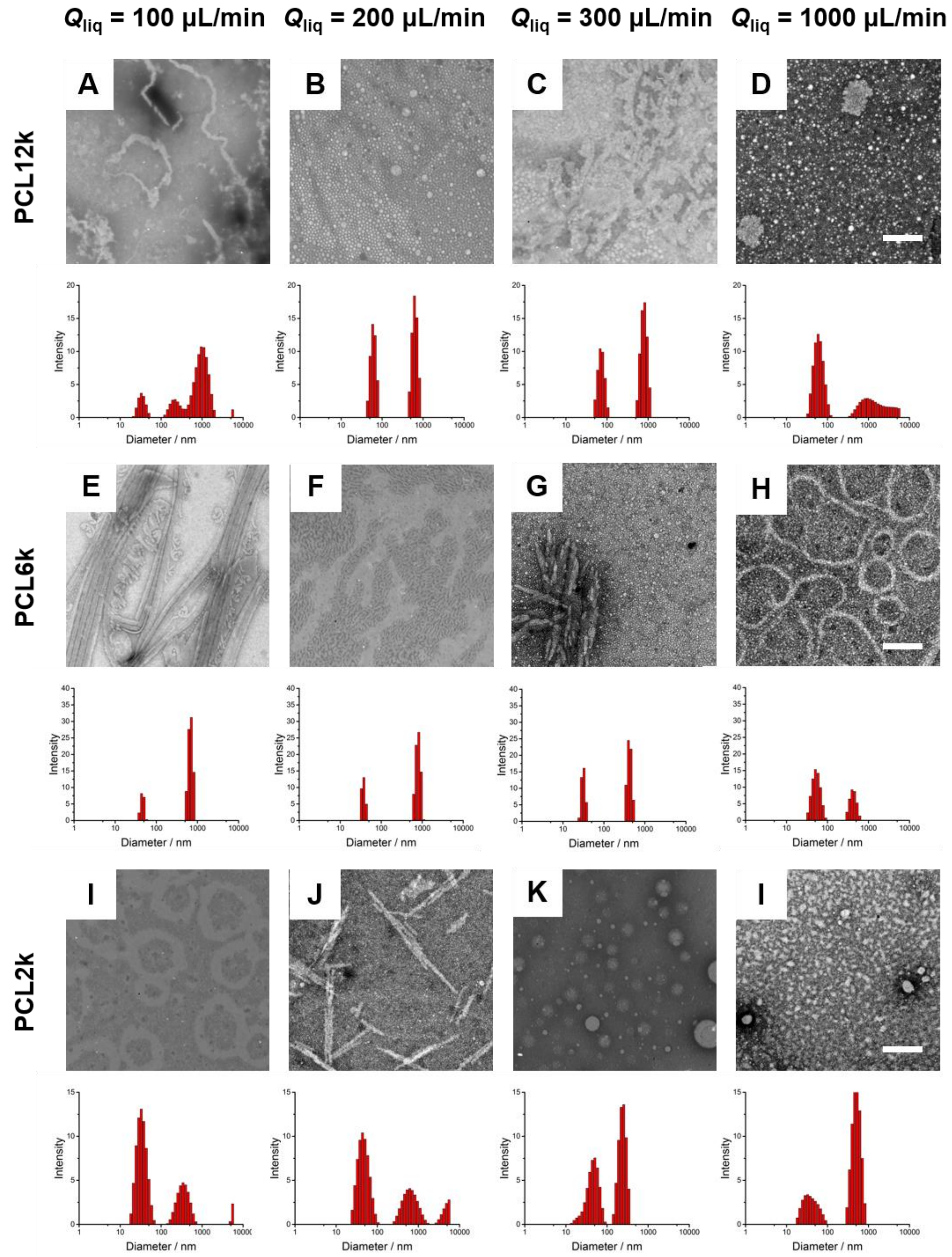

Figure 4- 3. Effect of flow rate and copolymer composition on morphologies from TEM images and size distributions from CONTIN analysis of DLS for PCL-*b*-PEO nanoparticles produced in the two-phase silicon/glass microfluidic reactor. Scale bars are 500 nm.

4.3.2. Comparison of Flow Behavior in Silicon/Glass and PDMS Two-Phase Microfluidic Reactors.

We found that the flow behaviour of gas bubbles and liquid segments were quite different. Specifically, we observed very different relative lengths of gas bubbles to liquid segments in channels made from the different materials at approximately the same gas pressure and liquid flow rate (Figure 4-4). In the PDMS reactor, by tuning the pressure equal lengths of gas bubbles and liquid plugs were easy to obtain, indicating the ~ 1:1 gas:liquid flow ratio. By contrast, gas-liquid segments are hard to generate in the silicon/glass reactor when the regulator was set to a similar pressure. A higher pressure was used to pressurize the gas into the channel, forming much shorter gas segments than liquid plugs. Even if the pressure was increased significantly, the gas segments did not appear to grow larger. As well, a less uniform size distribution of bubbles was obtained in the silicon/glass chip, which may be due to the pressure fluctuation in the channel or the wall roughness caused during deep reactive ion etching. Due to the difficulty in producing ~ 1:1 gas:liquid flow ratio in silicon/glass reactor therefore the different bubble sizes from ones in PDMS reactors, the nanoparticles were synthesized and compared under the same flow rate of liquid. In silicon/glass chip, the gas pressure was same as the stable gas flow was first observed, whereas in PDMS chip, the gas pressure was set to form equal lengths of gas segments and liquid plugs. And we reported flow rate of liquid (Q_{liq}) instead of total flow rate (Q_{tota}), just for easy comparison.

An important difference between silicon/glass and PDMS reactors is the difference in surface energies of the microchannel walls. The piranha solution-treated silicon has a hydrophilic surface whereas PDMS has a hydrophobic surface. This will lead to different wettabilities of the two surfaces. The shape of the droplets transported by the gas flow strongly depends on the wettability of the surface.[14] Also, PDMS is mechanically soft and may experience elastic deformations which will influence the pressure and flow inside the channel. On the other hand, the silicon/glass channels are hard, which may result in different pressure drops compared to the PDMS reactor, leading to different actual flow rates. Therefore, due to the different segment lengths in reactors of these two materials, different mixing and shear effects are expected at the same liquid flow rates. The effects of these differences on particle sizes and morphologies are discussed in the following section. A more specific comparison of flow characteristics in two-phase silicon/glass and PDMS microchannels warrants future simulations and computational studies.

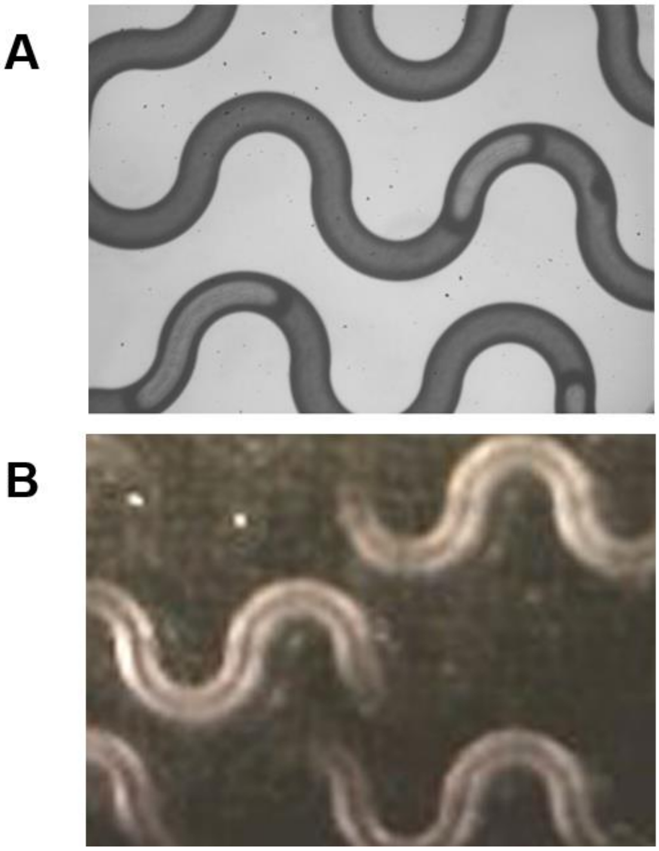

Figure 4- 4. Microscope images of gas-liquid segmented patterns in the silicon/glass chip (A) and the PDMS chip (B). Dark regions represent the liquid segments consisting of polymer solution/water while bright regions represent gas bubbles. Q_{liq} = 100 µL/min.

4.3.3 Comparison of Polymeric Nanoparticles Formed in Silicon/Glass and PDMS Two-Phase Microfluidic Reactors.

According to the previous discussion, even though the design of the reactor is the same, the reactor material affects the flow behaviour of gas bubbles and liquid segments. It has been shown that the mixing in gas-liquid segmented microreactors is induced by chaotic advection inside the liquid plug.[11] Furthermore, high-shear "hot spot" are found in the corners of the liquid plugs,[8] and if liquid plugs are larger relative to the gas bubbles the exposure to the hot spots would decrease. Both the fast mixing and exposure to high shear are crucial to the self-assembly process, and affect the size, morphology and crystallinity of nanoparticles.[7-11] Therefore, it is expected that produced nanoparticles would have different properties in reactors made of the different materials. To make this comparison, we formed PCL-*b*-PEO nanoparticles in both two-phase reactors (silicon/glass and PDMS) under the same chemical conditions and at the same two liquid flow rates (Q_{liq} = 100 and 200 µL/min). The method of pressure control was discussed in the previous section.

Figure 4-5 shows nanoparticle morphologies for the three different copolymers with different PCL block lengths. Each copolymer was self-assembled in either the silicon/glass or PDMS two-phase reactor at the same two liquid flow rates (A: Q_{liq} = 100 µL/min; B: Q_{liq} = 200 µL/min). Based on the calculation of gas flow rates (Q_{gas}) described in the experimental section, the total flow rates ($Q_{\text{total}} = Q_{\text{liq}} + Q_{\text{gas}}$) in the silicon/glass reactor are always smaller than those in the PDMS reactor. Actual values of the total flow rate can be found in Appendix.

In the PDMS reactor at Q_{liq} = 100 µL/min, PCL12k produced more lamellae (Figure 4-5 B), which is similar to morphologies produced by the higher flow rate Q_{liq} = 200 µL/min in the silicon/glass reactor (Figure 4-5 G). PCL6k prepared in both reactors at Q_{liq} = 100 µL/min demonstrate similar morphologies, which include spheres, cylinders and lamellae (Figure 4-5 C and D). PCL2k at Q_{liq} = 100 µL/min produced straight and thin cylinders in the PDMS reactor (Figure 4-5 F), but formed donut-like structures in the silicon/glass reactor (Figure 4-5 E). Interestingly, similar cylindrical structures are found in the silicon/glass chip with same copolymer, but at higher liquid flow rate, Q_{liq} = 100 µL/min (Figure 4-5 K). In the PDMS chip at Q_{liq} = 200 µL/min, cylinders and lamellae formed by PCL12k at Q_{liq} = 100 µL/min are no longer present, resulting in purely spherical structures (Figure 4-5 H). Morphologies of PCL6k are similar at Q_{liq} = 200 µL/min in the two reactors (Figure 4-5 I and J). For nanoparticles of the PCL2k copolymer formed at Q_{liq} = 200 µL/min, the number of lamellae is significantly higher in the PDMS reactor compared to the silicon/glass reactor.

These nanoparticle differences in the two reactors are attributed to the different relative sizes of gas bubbles and liquid plugs. Short mixing times and narrow residence time distributions require short and uniformly distributed lengths of liquid segments. Particles in the PDMS reactor experienced increased shear exposure in the microchannel compared to those in the silicon/glass reactor, due to the increased number of liquid plugs, which explains the different morphologies of synthesized nanoparticles in many of the investigated cases. These results indicate that the flow pattern (regularity and relative sizes of gas and liquid plugs), in addition to the total flow rate, is a predominant factor in determining the sizes and morphologies of nanoparticles formed in two-phase microfluidic reactors.

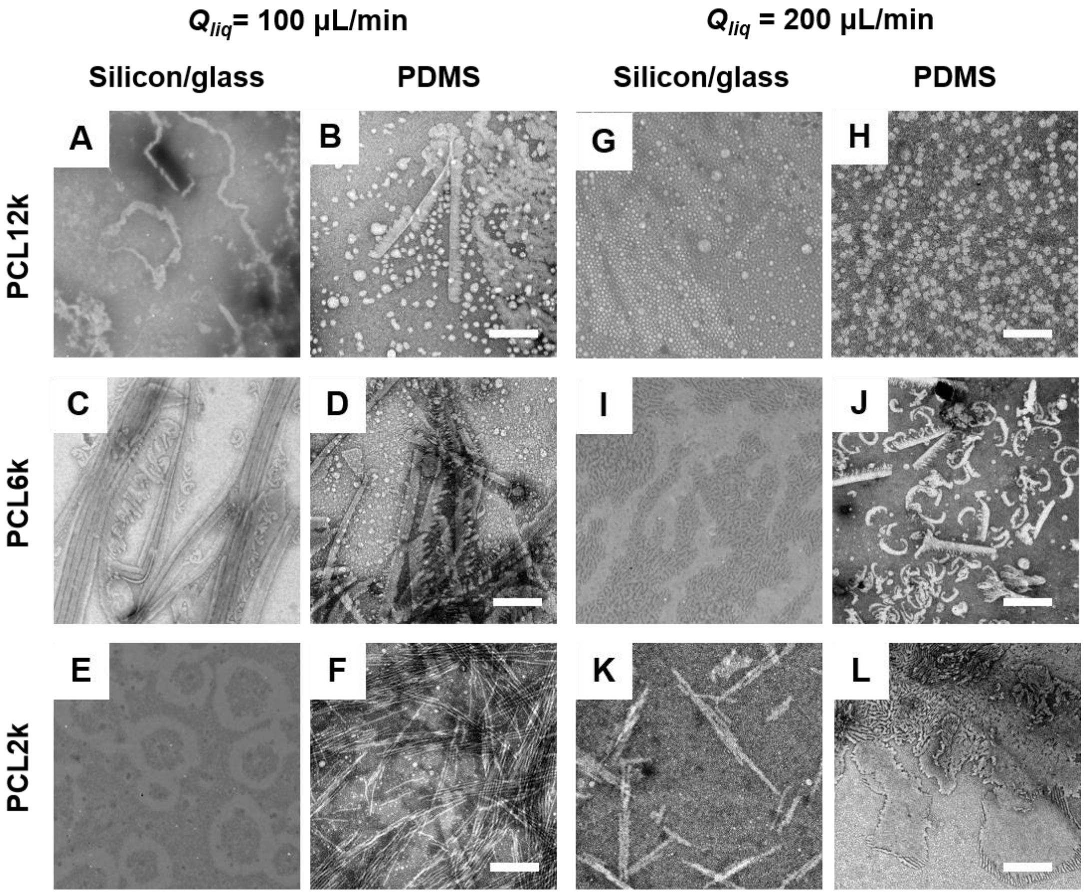

Figure 4- 5. Morphologies of PCL-b-PEO nanoparticles synthesized on the silicon/glass and PDMS two-phase reactors. A: Q_{liq} = 100 µL/min; B: Q_{liq} = 200 µL/min. Scale bars are 500 nm.

4.3.4. Attempted PCL-*b*-PEO Nanoparticle Synthesis in Single-Phase High-Shear Microfluidic Reactor.

Son.[15]proposed a method to calculate the shear rate in a rectangular channel, as follows:

$$\dot{\gamma}= \left(\frac{6Q}{WH^2}\right)\left(1+\frac{H}{W}\right)f^*(\frac{H}{W})$$

in which Q is the flow rate, H and W are the channel height and width, f^* is the aspect ratio correction factor (f^* has different values for different H/W). And a good approximation of the relation between pressure and flow rate is:

$$\Delta\mathrm{p} = \frac{12\mu LQ}{WH^3}\frac{1}{1\text{-}0.63\frac{H}{W}\tan H(1.57\frac{W}{H})}$$

in which Δp is the pressure drop between the two ends of the channel, μ is the fluid viscosity, L is the length of channel.[16]

Based on these equations, one of the most efficient ways to increase shear is to decrease the length of the channel for a fixed pressure drop, thus distributing a large pressure drop over a smaller area. As a result, the time spent by nanoparticles in the channel will decrease. To compensate the dwell time the shear can be distributed periodically at junctions along longer channels. Therefore, a single-phase reactor was designed by Jason Riordan (Figure 4-1 A) possessing narrow high-shear channels with widths of 8 µm located periodically along lengths of low-shear channels with widths of 55 µm at regular intervals. In this manner, nanoparticles formed in the channel will experience high-shear regions periodically, while they are exposed to the “hot spots” randomly by circulating through the plugs in a two-phase reactor. However, the shear rate on this single-phase chip is calculated to be 3 orders of magnitude higher than the two-phase reactor at the same flow rate.

Unfortunately, when we tried to run liquid through this single-phase reactor, the liquid flowed much more slowly than expected, eventually followed by a full stop. This is speculated to be the result of impurities that block the narrow channels as fluid is pushed through. The impurities might be debris generated in the fabrication process. We tried numerous methods to clear out the impurities, including applying ultra-sound, pumping, and baking; however, the problem has not yet been resolved.

4.4. Conclusion

This chapter investigated the size and morphologies of PCL-*b*-PEO nanoparticles synthesized on a gas-liquid segmented microfluidic reactor made of silicon/glass. This reactor shows effective variability of size and morphologies of nanoparticles at different liquid flow rates. We found that the ~1:1 flow ratio applied in the equivalent PDMS rector could not be achieved in the silicon/glass reactor, suggesting that different surface properties and material characteristics can influence the flow dynamics within the microchannels. To further explore the influence of reactor material on nanoparticle formation, we compared the morphologies of nanoparticles synthesized on silicon/glass and PDMS two-phase reactors at the same liquid flow rates and water content. Results show that the reactor material is an important factor in the morphologies of the nanoparticles as the different materials gave rise to different gas:liquid flow ratios at the same inlet gas pressure.

Moreover, a new high-shear single-phase silicon/glass microfluidic reactor was designed and fabricated, in order to achieve even higher shear rates without the requirement of gas bubbles. Although problems of microchannel clogging have thus far prevented successful nanoparticle synthesis in this reactor, it opens the possibility to achieve high shear in a more controlled manner without the complications of gas bubble control and measurement. Some improvements in reactor design and/or fabrication in order to prevent clogging will need consideration before this reactor can be used successfully.

4.5. Supporting Information

Please see Appendix for supporting information: Number-average CONTIN analysis from DLS measurements; Table of actual flow rates.

4.6. Reference

1. Johnson, T. J.; Ross, D.; Locascio, L. E., Rapid microfluidic mixing. *Analytical Chemistry* **2002,** *74* (1), 45-51.

2. Stroock, A. D.; Dertinger, S. K. W.; Ajdari, A.; Mezic, I.; Stone, H. A.; Whitesides, G. M., Chaotic mixer for microchannels. *Science* **2002,** *295* (5555), 647-651.

3. Liu, R. H.; Stremler, M. A.; Sharp, K. V.; Olsen, M. G.; Santiago, J. G.; Adrian, R. J.; Aref, H.; Beebe, D. J., Passive mixing in a three-dimensional serpentine microchannel. *Journal of Microelectromechanical Systems* **2000,** *9* (2), 190-197.

4. Song, H.; Tice, J. D.; Ismagilov, R. F., A microfluidic system for controlling reaction networks in time. *Angewandte Chemie-International Edition* **2003,** *42* (7), 768-772.

5. Tice, J. D.; Song, H.; Lyon, A. D.; Ismagilov, R. F., Formation of Droplets and Mixing in Multiphase Microfluidics at Low Values of the Reynolds and the Capillary Numbers. *Langmuir* **2003,** *19* (22), 9127-9133.

6. Gunther, A.; Jhunjhunwala, M.; Thalmann, M.; Schmidt, M. A.; Jensen, K. F., Micromixing of miscible liquids in segmented gas-liquid flow. *Langmuir* **2005,** *21* (4), 1547-1555.

7. Wang, C. W.; Sinton, D.; Moffitt, M. G., Flow-Directed Block Copolymer Micelle Morphologies via Microfluidic Self-Assembly. *Journal of the American Chemical Society* **2011,** *133* (46), 18853-18864.

8. Schabas, G.; Yusuf, H.; Moffitt, M. G.; Sinton, D., Controlled self-assembly of quantum dots and block copolymers in a microfluidic device. *Langmuir* **2008,** *24* (3), 637-643.

9. Bains, A.; Cao, Y. M.; Moffitt, M. G., Multiscale Control of Hierarchical Structure in Crystalline Block Copolymer Nanoparticles Using Microfluidics. *Macromolecular Rapid Communications* **2015,** *36* (22), 2000-2005.

10. Xu, Z.; Yan, B.; Riordon, J.; Zhao, Y.; Sinton, D.; Moffitt, M. G.,

Microfluidic Synthesis of Photoresponsive Spool-Like Block Copolymer Nanoparticles: Flow-Directed Formation and Light-Triggered Dissociation. *Chemistry of Materials* **2015,** *27* (23), 8094-8104.

11. Schabas, G.; Wang, C.-W.; Oskooei, A.; Yusuf, H.; Moffitt, M. G.; Sinton, D., Formation and Shear-Induced Processing of Quantum Dot Colloidal Assemblies in a Multiphase Microfluidic Chip. *Langmuir* **2008,** *24* (19), 10596-10603.

12. Gothsch, T.; Schilcher, C.; Richter, C.; Beinert, S.; Dietzel, A.; Büttgenbach, S.; Kwade, A., High-pressure microfluidic systems (HPMS): flow and cavitation measurements in supported silicon microsystems. *Microfluidics and Nanofluidics* **2015,** *18* (1), 121-130.

13. Bains, A. S. Microfluidic Synthesis of Block Copolymer Nanoparticles for Drug Delivery. University of Victoria, 2016.

14. S. Hardt, H. P. a. F. J. In *CFD-based Optimization of Gas/Liquid Microreactors with Droplet and Bubble Transport*, Nanotechnology Conference and Trade Show, San Francisco, EM Laudon, B. R., Ed. Computational Publicationscambridge: San Francisco, 2003; pp 254-257.

15. Son, Y., Determination of shear viscosity and shear rate from pressure drop and flow rate relationship in a rectangular channel. *Polymer* **2007,** *48* (2), 632-637.

16. Duan, Z. P.; Yovanovich, M. M.; Ieee, Pressure Drop for Laminar Flow in Microchannels of Arbitrary Cross-Sections. In *Twenty-Fifth Annual Ieee Semiconductor Thermal Measurement and Management Symposium*, 2009; pp 111-120.

Chapter 5. Conclusions and Future Work

5.1. Conclusions

In this thesis, we have applied a gas-liquid segmented microfluidic reactor for the manufacturing of drug-loaded block copolymer nanoparticles. Based on characterization of nanoparticles using TEM, DLS and HPLC, we demonstrated the physical and chemical properties of drug-loaded nanoparticles are significantly influenced by shear rate and rapid mixing on chip, along with other chemical parameters such as copolymer composition and drug loading ratio. Previously, our group has enormously investigated shear-induced self-assembly of polymer nanoparticles, including formulations involving a therapeutic agent, paclitaxel (PAX).[1,2,3] The work in this thesis was aimed to investigate a different drug-polymer system, in which a hydrophobic drug, 7-Ethyl-10-hydroxycamptothecin (SN-38), was physically encapsulated in P(MCL-*co*-CL)-*b*-PEO). The reason why SN-38 is of interest arises from its high potency against a wide range of malignancies and two main limitation of direct delivery which are poor solubility and pH instability. The polymer we used has an amorphous hydrophobic block. The addition of MCL into PCL chain of biocompatible and biodegradable PCL-*b*-PEO tune the core from semicrystalline to amorphous without compromising the hydrophobicity, resulting a higher loading capacity of SN-38 than PCL-*b*-PEO.

The influence of flow-induced shear rate on size, morphology, loading efficiency, and *in vitro* release rate was first explored. The smallest average size and pure spherical structure of nanoparticles were obtained at an intermediate flow rate of 200 µL/min for all the drug loading ratio. For the highest drug loading ratio ($r = 0.75$), vesicles were produced at $Q = 400$ µL/min, which were not observed at other flow rates. Loading efficiencies were consistently higher for nanoparticles from at Q > 50 µL/min. And the slowest release of SN-38 in PBS was found at highest flow rate, Q = 400 µL/min. Next, we continued to investigate how encapsulation of SN-38 and microfluidic preparation under different flow rate would influence the cytotoxicity against MCF-7 cancer cell line. In general, almost all SN38-loaded nanoparticles are more toxic to cells (except for Q = 50 and 400 µL/min at incubation time of 48h) than bare SN-38, which indicates the advantage of drug encapsulation using polymeric nanoparticles. Variations of cytotoxicity among all the preparation conditions (bulk and 4 flow rate) showed that different size, size distribution and morphologies would affect the interaction between SN38-loaed nanoparticles and cells. This provides the possibility to use microfluidic as a control handle on the cytotoxic response of these nanoparticles.

The flow-induced shear on our gas-liquid segmented chip is very attractive in synthesis of block copolymer nanoparticles, by tuning the size, morphology and crystallinity. However, the maximum shear is limited by the flow rate of gas and liquid, due to the limitation of pressure resistance of PDMS as well as the imaging technique which is necessary for the visualization of bubbles in two-phase microreactors. Therefore, in Chapter 4, we switched to silicon/glass chips which are prominent in handling process under high pressure. The one with the same design as previously mentioned PDMS chip was used to synthesize PCL-*b*-PEO nanoparticles, since this polymer is a more general selective for drug delivery application. The investigated liquid flow rate is ranged from 100 to 1000 µL/min. This silicon/glass was proved to have control over the size and morphology of PCL-*b*-PEO nanoparticles with 3 different PCL block length and different polymer generated different response to the shear. Synthesis of same polymer nanoparticles was also conducted on PDMS chip at two lower flow rate of liquid (Q_{liq} = 100 and 200 μL/min) for the purpose of comparison. Different flow patterns were obtained, where the relative length of gas segment to liquid segment is smaller in silicon/glass chip than in the PDMS chip. And for PCL2k and PCL12k, different morphologies were obtained at same flow rate of liquid for both Q_{liq} = 100 and 200 μL/min. This offers some ideas on how the surface property will influence the partition of two phases and their interaction within microchannel, and will eventually lead to different shear-induced behavior of nanoparticles. Another silicon/glass chip we made was designed as a single-phase reactor with narrow and short channels distributing along wide and long channels. Thus, the high shear rate which is 3 magnitudes higher than the two-phase reactor at the same flow rate can be produced in small junctions. Some attempts were done in running the chip. Unfortunately, no sample was successfully collected on this chip due to the clogging issue. The clogging was thought to be caused by the debris left during the fabrication process which could accumulate in small junctions upon flushing liquid inside the channel. If this can be avoided in the fabrication process by improving the cleaning step, we may have chance to test this chip for the synthesis of block copolymer nanoparticles, even the ones loaded with drug. In that case, formation of nanoparticles under high shear could be achieved in a more controlled and simple way.

In conclusion, microfluidic is an efficient and simple way to control the fabrication of materials including polymer nanoparticles and drug-loaded nanoparticles, which makes it a good top-down preparation method for drug delivery vehicles. The on-chip shear rate plays an significant role in effecting the loading and release behaviors of these vehicles. Different types of polymer and drug may experience different mechanism of shear-induced formation. This points us the need to investigate drug-polymer system case by case using microfluidic. In addition, new materials and designs are worth exploring to achieve even higher flow rate without any limitations.

5.2. Future Work

To develop the application of our SN-38 loaded nanoparticles in drug delivery, we need to focus on narrowing the size distribution, especially eliminating large particles which are not optimal for *in vivo* applications, because larger nanoparticles with low curvature may lead to increased interactions of opsonins and faster clearance rates.[4] Block copolymers with different block length as well as different polymer concentration can be investigated to tune the size.

Another important goal to pursue is to increase the loading efficiency and loading level of SN-38. One of the influencing factor is the choice of solvent for nanoparticle preparation. In our case, drug and polymer are dissolved together in an organic solvent initially. Upon mixing with water, drug polymer interaction and the rate of partitioning of the drug between the solidifying micelles core and solvent/water mixture will affect the encapsulation of the drug.[5] Moreover, the type of solvent also plays an important role in microfluidics, especially in manipulating drops and bubbles, by influencing the solid surface/liquid interactions.[6] Thus, solvents with different polarity, viscosity and interfacial tension can be screened for preparation of drug-loaded nanoparticles.

The stability of nanoparticles is also worth investigating, namely the effectiveness of nanoparticles to retain the size, morphology and loading efficiency over a period of time. When SN-38 is encapsulated in the nanoparticles, the probability of them contacting with water and hydrolysis is reduced. However, since there is still a trace amount of water inside the micelle, the percentage of hydrolyzed

SN-38 is unknown. Besides, due to the π-π interactions between SN-38 molecules, they have strong tendency to aggregate. Thus, keeping track of size, morphology and loading efficiency of nanoparticles during storage and release process is necessary. Moreover, our *in vitro* release results show fast release for all conditions ($\tau_{1/2} < 4$ h), which needs to be optimized in our future work. Increasing the stability of SN-38 within the nanoparticles is required.

Different *in vitro* release rates have been found for various on-chip flow rate where the highest flow rate produced the slowest release profile. To deeply understand the mechanism that how rapid mixing and high shear favors the slow release of SN-38, we could investigate the drug distribution in the nanoparticles, since except for the drug actually located in the core, a portion of the drug may be incorporated in the corona or at the core-corona interface and lead to fast release.[7] One approach could be fluorescence quenching.[8] Specifically, a hydrophobic fluorescent dye can be encapsulated into polymeric nanoparticles, followed by the measurement of fluorescence intensity. Then, a quenching agent can be added to remove the fluorescence of unencapsulated dye contacting the solution. Thus, the remaining fluorescence indicates what percentage of hydrophobic dye was in the micelle core. And this number can be compared among samples prepared at different flow rate.

Our *in vitro* cytotoxicity study showed different cytotoxic response against cancer cell line of nanoparticles prepared at different flow rate. Due to the complex nature of the interactions between nanoparticles and cancer cells, more experiments are still required to give better understanding. For example, cellular uptake of SN-38 with time can be traced to obtain a clear knowledge on the amount and location of drug uptake and to evaluate effective intracellular drug delivery. SN38-loaded nanoparticles can be fluorescently labelled to have a better visualization of spatial distribution of the internalized nanoparticles. Cell recovery study can also be conducted to further evaluate the effect of on-chip flow rate on killing cells. Knowing that SN-38 acts through inhibiting DNA topoisomerase I, DNA synthesis and DNA single-strand breaks,[9] we can perform DNA fragmentation study to determine whether the growth inhibition effect of the loaded nanoparticles was due to initiation of apoptosis. All of these *in vitro* cell line study can help us increase the understanding of flow-directed control on cytotoxicity of drug-loaded nanoparticles, in order to set a clear goal for the microfluidic preparation and then seek a pathway to tune the properties of nanoparticles more precisely.

The next step undoubtedly would be turning to *in vivo* study, since the primary objective of drug delivery studies is administering drug into the body and achieve efficient therapy. Systematic pharmacokinetics analysis in xenograft model is necessary, in order to evaluate the drug retention in circulating and antitumor efficacy.

For microfluidic platforms, increasing throughput is always a subject of interest. In Chapter 4, our initial attempt to switch the microfabrication material from PDMS to silicon/glass provides the possibility of high pressure inside the microreactor, which would be caused by high flow rate. However, problem along with the high flow rate on gas-liquid segmented reactor contains limitation of techniques for visualization of bubbles, difficult control of stable flow patterns and the potential of deformation of segments.[10] A new strategy proposed to generate high shear without all these problem is a single-phase reactor with high-shear regions distributed periodically along the channel. Despite the innovative idea, a practical problem arisen from clogging in narrow channel impede us step forward. In the future, some efforts on cleaning the microchannel, improving the microfabrication process and modifying the design of the channel need to be done for the application of this high-shear single-phase reactor in drug delivery vehicles preparation.

5.3. References

1. Bains, A.; Cao, Y. M.; Moffitt, M. G., Multiscale Control of Hierarchical Structure in Crystalline Block Copolymer Nanoparticles Using Microfluidics. *Macromolecular Rapid Communications* **2015,** *36* (22), 2000-2005.

2. Bains, A.; Wulff, J. E.; Moffitt, M. G., Microfluidic synthesis of dye-loaded polycaprolactone-block-poly(ethylene oxide) nanoparticles: Insights into flow-directed loading and in vitro release for drug delivery. *Journal of Colloid and Interface Science* **2016,** *475*, 136-148.

3. Wang, C.-W.; Sinton, D.; Moffitt, M. G., Flow-Directed Block Copolymer Micelle Morphologies via Microfluidic Self-Assembly. *Journal of the American Chemical Society* **2011,** *133* (46), 18853-18864.

4. Vonarbourg, A.; Passirani, C.; Saulnier, P.; Simard, P.; Leroux, J. C.; Benoit, J. P., Evaluation of pegylated lipid nanocapsules versus complement system activation and macrophage uptake. *J. Biomed. Mater. Res. Part A* **2006,** *78A* (3), 620-628.

5. Glover, A. L.; Nikles, S. M.; Nikles, J. A.; Brazel, C. S.; Nikles, D. E., Polymer Micelles with Crystalline Cores for Thermally Triggered Release. *Langmuir* **2012,** *28* (29), 10653-10660.

6. Bianco, M.; Viola, I.; Cezza, M.; Pietracaprina, F.; Gigli, G.; Rinaldi, R.; Arima, V., Microfluidic motion for a direct investigation of solvent interactions with PDMS microchannels. *Microfluidics and Nanofluidics* **2012,** *13* (3), 399-409.

7. Choucair, A.; Eisenberg, A., Interfacial solubilization of model amphiphilic molecules in block copolymer micelles. *Journal of the American Chemical Society* **2003,** *125* (39), 11993-12000.

8. Shen, Y.; Zhan, Y.; Tang, J.; Xu, P.; Johnson, P. A.; Radosz, M.; Van Kirk, E. A.; Murdoch, W. J., Multifunctioning pH-responsive nanoparticles from hierarchical self-assembly of polymer brush for cancer drug delivery. *AIChE Journal* **2008,** *54* (11), 2979-2989.

9. Bala, V.; Rao, S. S.; Boyd, B. J.; Prestidge, C. A., Prodrug and nanomedicine approaches for the delivery of the camptothecin analogue SN38. *Journal of Controlled Release* **2013,** *172* (1), 48-61.

10. Gu, H.; Duits, M. H. G.; Mugele, F., Droplets Formation and Merging in Two-Phase Flow Microfluidics. *International Journal of Molecular Sciences* **2011,** *12* (4),

2572-2597.

Appendix

Appendix A

Supporting Information for Chapter 2

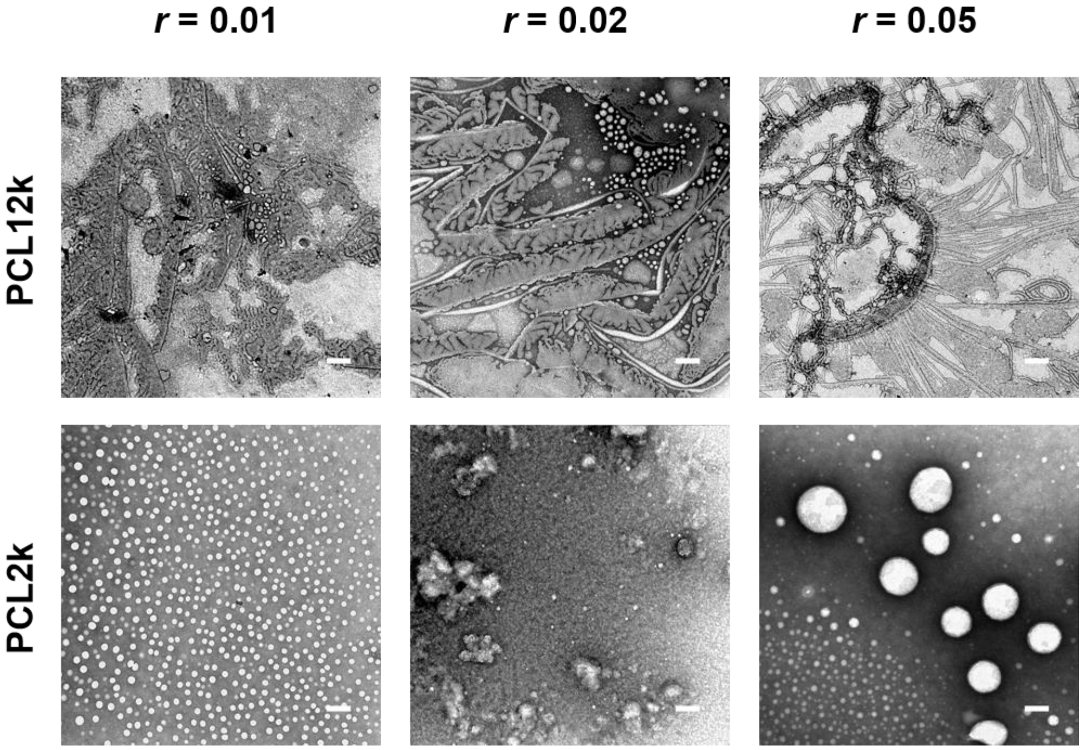

Figure S2-1. TEM images of bulk-prepared SN38-loaded PCL-*b*-PEO nanoparticles. Scale bars are 200 nm.

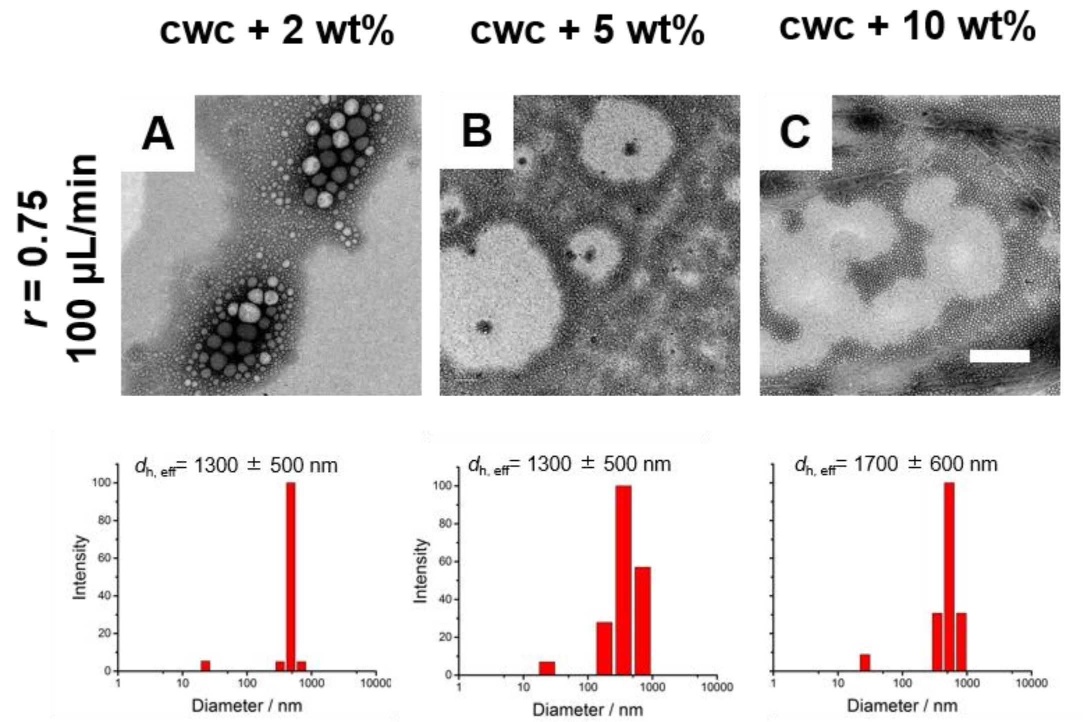

Figure S2-2. Effect of water content on morphology, size distribution and mean effective hydrodynamic diameter of microfluidic-prepared PMCLCL nanoparticles at Q = 100 µL/min (r = 0.75).

Table S2-1. Actual Flow Rates for Various Microfluidic Preparations of PMCLCL Nanoparticles

Nominal Flow Rate	L_{gas} (mm)	L_{liq} (mm)	Q_{gas} (µL/min)	Q_{liq} (µL/min)	Q_{gas}/Q_{liq}	Q_{total} (µL/min)
***r* = 0.25** 50 µL/min						
Prep #1	1.1	1.0	28	25.0	1.1	52
Prep #2	1.2	1.0	30	25.0	1.2	55
Prep #3	1.7	1.4	30	25.0	1.2	55
100 µL/min						
Prep #1	1.3	1.1	59	50.0	1.2	109
Prep #2	1.4	1.5	47	50.0	0.93	97
Prep #3	1.7	1.3	65	50.0	1.3	115
200 µL/min						
Prep #1	2.5	2.3	109	100.0	1.1	209
Prep #2	2.7	2.6	104	100.0	1.0	204
Prep #3	2.6	2.1	124	100.0	1.2	224
400 µL/min						
Prep #1	1.6	1.5	213	200.0	1.1	413
Prep #2	1.6	1.7	188	200.0	0.94	388

Prep #3	1.5	1.3	231	200.0	1.2	431
***r* = 0.5**						
50 µL/min						
Prep #1	1.0	0.9	28	25.0	1.1	53
Prep #2	1.2	0.8	38	25.0	1.5	63
Prep #3	1.5	1.1	34	25.0	1.4	59
100 µL/min						
Prep #1	1.3	1.1	59	50.0	1.2	109
Prep #2	1.5	1.2	63	50.0	1.3	113
Prep #3	1.6	1.5	53	50.0	1.1	103
200 µL/min						
Prep #1	2.4	2.5	96	100.0	0.96	196
Prep #2	2.6	2.7	96	100.0	0.96	196
Prep #3	2.5	2.4	104	100.0	1.0	204
400 µL/min						
Prep #1	1.7	1.6	213	200.0	1.1	413
Prep #2	1.9	1.8	211	200.0	1.1	411
Prep #3	1.5	1.8	167	200.0	0.83	367
***r* = 0.75**						
25 µL/min						
Prep #1	1.6	1.5	27	25.0	1.1	52
Prep #2	1.0	0.9	28	25.0	1.1	53
Prep #3	1.3	1.2	27	25.0	1.1	52
50 µL/min						
Prep #1	1.4	1.3	53	50.0	1.1	104
Prep #2	1.3	1.2	54	50.0	1.1	104
Prep #3	1.6	1.5	53	50.0	1.1	103
100 µL/min						
Prep #1	2.2	2.4	92	100.0	0.92	192
Prep #2	2.7	2.3	117	100.0	1.2	217
Prep #3	2.4	2.1	114	100.0	1.1	214
400 µL/min						
Prep #1	1.6	1.7	188	200.0	0.94	388
Prep #2	1.8	1.9	190	200.0	0.95	390
Prep #3	2.2	2.0	220	200.0	1.1	420

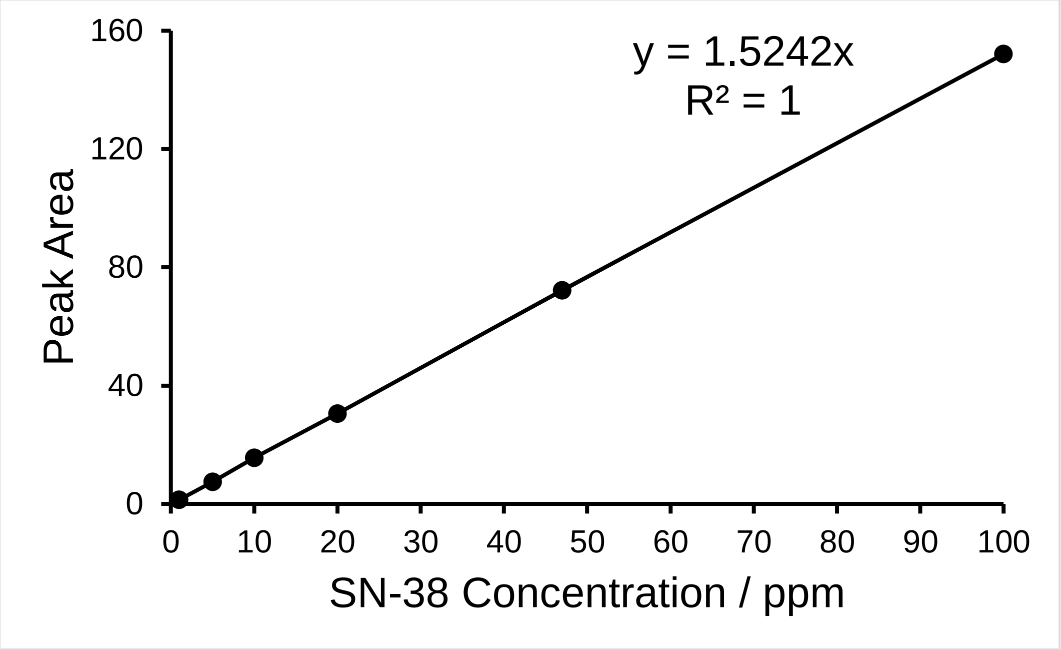

Figure S2-3. Calibration curve of SN-38 in acetonitrile quantified by HPLC with UV-Vis at 265 nm as detector.

The release profiles (Figure 2-11) are fitted using XLFit, an add-in for Microsoft Excel. The fitting model used for all the conditions is:

$$y = \left(\frac{1}{2\mathrm{B}}\right)\left[x+\mathrm{A}+\mathrm{B} - ((x+\mathrm{A}+\mathrm{B})^2 - (4x\mathrm{B})^{0.5}\right]$$

Data is fitted using the Levenburg Marquardt algorithm by the software.

Appendix B

Supporting Information for Chapter 3

Table S3-1. Actual Flow Rates for Various Microfluidic Preparations of PMCLCL Nanoparticles

Nominal Flow Rate	L_{gas} (mm)	L_{liq} (mm)	Q_{gas} (µL/min)	Q_{liq} (µL/min)	$Q_{\mathrm{gas}}/Q_{\mathrm{liq}}$	Q_{total} (µL/min)
***r* = 0.75** 50 µL/min						
Prep #1	1.2	1.1	27	25.0	1.1	52
Prep #2	1.6	1.5	27	25.0	1.1	52
Prep #3	1.7	1.4	30	25.0	1.2	55
100 µL/min						
Prep #1	1.9	1.8	53	50.0	1.1	103
Prep #2	1.4	1.5	47	50.0	0.93	97
Prep #3	1.7	1.3	65	50.0	1.3	115
200 µL/min						
Prep #1	2.3	2.5	92	100.0	0.92	192
Prep #2	2.7	2.6	104	100.0	1.0	204
Prep #3	2.6	2.5	104	100.0	1.0	224
400 µL/min						
Prep #1	1.7	1.6	213	200.0	1.1	413
Prep #2	1.6	1.7	188	200.0	0.94	388
Prep #3	1.5	1.5	200	200.0	1.0	400

Table S3-2. IC_{50} values of free SN-38 and SN38-loaded nanoparticles at different incubation times.

	IC_{50} / nM		
Incubation time /h **Preparation method**	**24h**	**48h**	**96h**
Free SN-38	28.23 ± 7.83	42.57 ± 24.38	15.49 ± 1.77
Bulk preparation	19.98 ± 22.81	21.48 ± 16.91	2.00 ± 0.22
50 µL/min	92.57 ± 24.11	33.13 ± 6.50	4.66 ± 0.89

100µL/min	18.13 ± 10.24	31.35 ± 23.12	6.92 ± 4.15
200µL/min	9.92 ± 3.92	14.45 ± 5.25	4.33 ± 2.65
400µL/min	83.8 ± 22.8	23.83 ± 6.22	5.35 ± 1.07

Appendix C

Supporting Information for Chapter 4

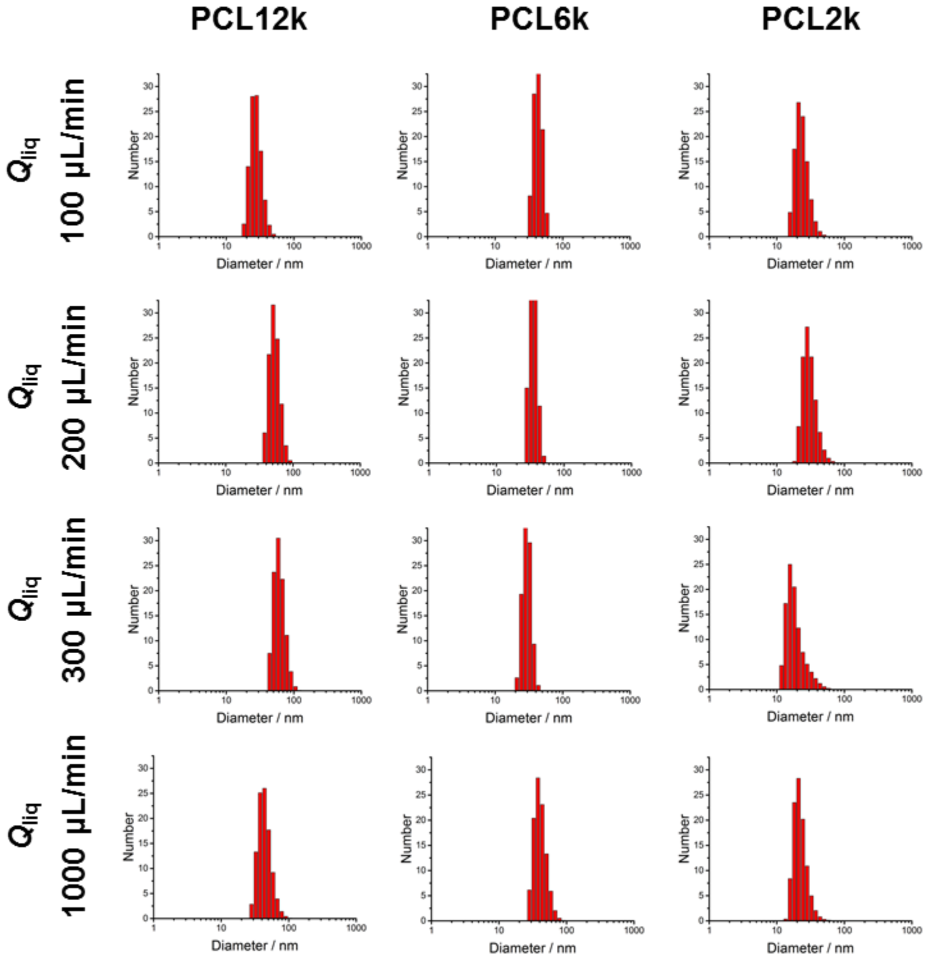

Figure S4-1. Number-Average size distribution from CONTIN analysis of PCL-*b*-PEO nanoparticles synthesized on silicon/glass segmented microfluidic reactor.

Table S4-1. Actual Gas and Liquid Flow Rates for PCL-*b*-PEO Nanoparticles Prepared on Silicon/glass Segmented Microfluidic Reactor.

Copolymer, Nominal Liquid Flow Rate	Q_{gas} (µL/min)	Q_{liq} (µL/min)	Q_{gas}/Q_{liq}	Q_{total} (µL/min)
PCL2k				
100 µL/min	30.8	100	0.308	131
200 µL/min	140	200	0.710	342
300 µL/min	180	300	0.600	480
PCL6k				

100 µL/min	48.5	100	0.485	149
200µL/min	142	200	0.710	342
300 µL/min	190	300	0.633	490
PCL12k				
100 µL/min	38.0	100	0.380	138
200 µL/min	135	200	0.675	335
300 µL/min	160	300	0.533	460

Table S4-2. Actual Gas and Liquid Flow Rates for PCL-*b*-PEO Nanoparticles Prepared on PDMS Segmented Microfluidic Reactor.

Copolymer, Liquidl Flow Rate	L_{gas} **(mm)**	L_{liq} **(mm)**	Q_{gas} **(µL/min)**	Q_{liq} **(µL/min)**	$Q_{\mathrm{gas}}/Q_{\mathrm{liq}}$	Q_{total} **(µL/min)**
PCL2k						
100 µL/min	2.4	2.5	96	100.0	0.96	196
200 µL/min	2.4	2.5	192	200.0	0.96	392
PCL6k						
100 µL/min	2.5	2.7	92	100.0	0.93	193
200 µL/min	2.2	2.3	191	200.0	0.96	391
PCL12k						
100 µL/min	2.8	2.9	97	100.0	0.97	197
200 µL/min	2.0	2.1	191	200.0	0.95	391